Investigating the coordination of cardiac conduction and repolarization in ventricular myocardium

Grace Blair

Dissertation submitted to the faculty of the Virginia Polytechnic Institute and State University in partial fulfillment of the requirements for the degree of:

Doctor of Philosophy

In

Translational Biology, Medicine, and Health

Steven Poelzing

Robert Gourdie

John Chappell

Sunshine Lahmers

April 18, 2023

Roanoke, VA

Investigating the coordination of cardiac conduction and repolarization in ventricular myocardium

Grace Blair

Abstract

Aberrations in conduction or repolarization are established prerequisites for arrhythmogenesis. The following dissertation investigates how reducing either ephaptic (EpC) or gap junctional (GJ) coupling between cardiomyocytes can modulate cardiac conduction, repolarization, or the relationship between these two phenomena. Our lab has previously demonstrated that EpC can be modified in the ventricular epicardium using ionic and osmotic challenges to the Langendorff-perfused heart. In the first series of experiments, we show that reducing EpC via treatment with mannitol or hyponatremia can unmask conduction deficits that are otherwise below the resolution of detection in Scn5a+/- mice. Interestingly, we also observe that combination of the two treatments resolves severe conduction delay due to hyponatremia in the heterozygous animal. These data suggest it may be valuable to pursue the use of mannitol or hyponatremia as novel diagnostics for sodium channel loss of function diseases. The importance of extracellular perfusate is also highlighted by the second investigation, which evaluates how sodium and calcium concentration modulate repolarization in the context of hyperkalemia, a common comorbidity of hospitalized patients that increases the risk of arrhythmia. Calcium may potentially play a role in modulating APD adaptation to pacing rate in the context of this disease state, though more research is needed to clarify the exact mechanism of this effect. Finally, we investigate the relationship between conduction and repolarization in the epicardium, and conclude that this relationship does not appear to be dictated by the degree of cell-cell coupling in the myocardium, but instead is driven by endogenous gradients of action potential duration within the tissue. Taken together, these data demonstrate ways in which both conduction and repolarization are sensitive to modulations of EpC, though we also find that the relationship between these two phenomena is not influenced by such changes in electrical coupling.

Investigating the coordination of cardiac conduction and repolarization in ventricular myocardium

Grace Blair

General Public Abstract

The ability of the heart to function as a pump is dependent on the successful coordination of electrical activity throughout the heart. Disruptions to this intricate electrical system result in cardiac arrhythmias, which in turn prevent the heart from effectively perfusing the body with oxygenated blood. The present dissertation investigates ways in which we can modulate cell-cell communication within the heart, and how this may in turn influence disease states with a high propensity for arrhythmia. We show that reducing electrical coupling between cells using simple interventions like reducing serum sodium or increasing osmolarity may be a viable technique for diagnosing “concealed” disease states (i.e. disease states that are asymptomatic for much of a patient’s life). We then explore ways in which elevated serum potassium, known as hyperkalemia, may alter the heart’s ability to recover from electrical activation (repolarization). Finally, we show that the relationship between cardiac activation and repolarization is not as dependent on cell-cell communication as was once thought.

Taken together, this dissertation provides evidence that transiently disrupting cell-cell communication may hold promise for development of diagnostics for some congenital cardiac diseases, and yet does not appear to disrupt the relationship between electrical conduction and repolarization across the heart.

Acknowledgements

Without the mentorship, support, and unwavering optimism of Steve Poelzing, this dissertation would not have come to fruition. I am fortunate to have had such a thoughtful advisor, and appreciate both the guidance and independence you've granted me throughout graduate school.

I would also like to thank the members of my dissertation committee, as well as each of the members of the Poelzing lab, past and present, who have offered their time and energy to help me develop the following projects. Thank you to Xiaobo Wu, who has been particularly instrumental in helping me complete these experiments over the past year.

Finally, I am deeply grateful for the boundless support of my family, who recognized when to ask about research progress and when to ask about something else. And, of course, I am forever thankful to my loving partner, Patrick, who makes me grateful every day that I chose the path to PhD rather than MD, and to baby Neal, for being our greatest collaboration.

Glossary of Abbreviations

AP	Action Potential
APD	Action Potential Duration
AT	Activation Time
BDM	2,3 Butanedione monoxime
BrS	Brugada Syndrome
Ca^{2+}	Calcium
CaMKII	Calcium/Calmodulin-dependent protein kinase II
CBX	Carbenoxolone
CV	Conduction Velocity
CVL	Longitudinal Conduction Velocity
CVT	Transverse Conduction Velocity
ECG	Electrocardiograph
EpC	Ephaptic Coupling
GJc	Gap Junctional Coupling
gNa	Sodium Channel Conductance
K^+	Potassium
Na^+	Sodium
$Na_v1.5$	Voltage-Gated Sodium Channel (Cardiac isoform)
RMP	Resting Membrane Potential
Wp	Perinexal Width

Table of Contents

Chapter 1

Introduction

Investigating the coordination of cardiac conduction and repolarization in ventricular myocardium

The propagation of action potentials across the myocardium is crucial for proper coordination of contractility of the heart to successfully pump oxygenated blood throughout the body. Cardiac arrhythmias disrupt this coordinated contraction and may lead to sudden cardiac death. Development of an arrhythmia requires (1) abnormal conduction, (2) a substrate, often the result of abnormal repolarization, and (3) an ectopic beat. The following dissertation investigates the first two of these prerequisites, and the present chapter provides a brief introduction to cardiac conduction, repolarization, and the interaction of the two. Next, we explore how ionic and osmotic changes in serum composition may unmask otherwise concealed phenotypes in congenital conduction diseases, such as Brugada Syndrome and Lev Lenegre's Disease. This is followed by a brief foray into the mechanism by which hyperkalemia modifies repolarization, and how serum calcium may in turn modify this behavior. Finally, the phenomena of conduction and repolarization are both assessed in a series of experiments designed to investigate the role of electrical communication in the relationship between activation time and action potential duration. We will conclude with hypotheses about the translational implications of these studies and discuss what may or may not be justified avenues of further scientific pursuit.

1. Cardiac Conduction

The cardiac action potential

The coordinated propagation of an electrical wavefront across the billions of cells that comprise the myocardium is pivotal to the heart's function as a pump, directing deoxygenated blood to the lungs and providing reoxygenated blood to the rest of the body. Electrical activation of the cardiomyocyte takes the form of an action potential (AP), a transient rise in the membrane potential of the cell that is dependent on the intricate choreography of inward and outward currents via ion channels. The cardiac AP proceeds as follows: at rest, the cardiomyocyte is most permeable to potassium[1] and the cell

therefore typically sits at a resting membrane potential near the equilibrium potential of potassium, around -90 mV [2]. An initial inward current to the cardiomyocyte is provided by either an external stimulus or ion flow from the previous cell. This local depolarization of the membrane activates the cardiac isoform of the voltage gated sodium channel $Na_v1.5$, flooding the cell with sodium and rapidly depolarizing the cell. This is referred to as AP phase 0. Sodium channel gating is time-dependent and the channels generally inactivate within 1ms and no longer conduct[3,4]. Transient outward potassium channels then can create a dominant repolarizing current during phase 1, often referred to as the AP notch. Phase 2, the AP plateau, is established by a balance of inward calcium currents (I_{CaT}, I_{CaL})[5] and outward potassium currents (I_{Ks}, I_{Kr})[6]. The delayed rectifiers I_{Ks} and I_{Kr} persist and are paired with inward rectifying potassium current (I_{K1}) to complete repolarization during phase 3[7]. Pumps and exchangers (such as the sodium-calcium exchanger and the sodium-potassium ATPase) also maintain homeostasis as the cell returns to baseline potential. Notably, some of these currents are species-dependent, and therefore result in unique AP morphology, as depicted in Figure 1. This concept will be further discussed below in "Cardiac Repolarization".

Cardiomyocyte structure and conduction

Cardiomyocytes are brick-like structures with dimensions of approximately 150x20 uM[8]. As is so often the case in biology, structure begets function in the myocardial cytoarchitecture. For example, the transverse edges contain invaginations that house ion channel dyads pivotal to contraction-excitation coupling[9,10]. More salient to this thesis is the structure of the lateral ends that connect cells to one another, known as the intercalated disc (ID, Figure 3A). This domain is home to a variety of scaffolding proteins that ensure intercellular adhesion, as well as numerous ion channels and pumps for electrical communication. One protein that straddles the line between structural and electrical connection is the gap junction protein connexin 43 (Cx43). Gap junctions are intercellular channels that, when paired between cells, hold apposing membranes ~2nm apart, while acting as a conduit for molecules up to

1KDa in molecular weight[11]. Such molecules may be ions, metabolic byproducts, or second messengers. While it's clear that gap junctions play a key role in cellular communication, studies using mice heterozygous null for Cx43 have reported conflicting results regarding whether this mutation results in conduction slowing relative to the wild type (WT) mouse. Some groups concluded that >50% reduction in Cx43 would be necessary to slow conduction[12–16], while others reported measurable conduction slowing with only 50% Cx43 loss[17–19]. Further investigation determined that this phenomenon may have been due to experimental differences between the groups, and subsequent experiments revealed that small changes in extracellular ion composition can modulate electrical coupling to a measurable extent and thereby unmask deficits in conduction[20]. Such findings correspond to the predicted effects of ephaptic coupling, the mechanism of which will be outlined in the next section.

Another structure of note within the ID is the perinexus, a nanodomain that lies directly adjacent to gap junction plaques in the interplicate region of the ID. This region was identified relatively recently by Gourdie and Rhett[21], and noted as a possible setting for ephaptic coupling. The perinexus is a narrow cleft between two cells, approximately 30-100nm in width, surrounded by a variety of ion channels and pumps, including $Na_v1.5$[22], $K_{ir}2.1$[23], $Ca_v1.2$ (Hoeker, unpublished), NKA[24], and likely others. While we do not yet have the tools to sample the extracellular fluid within a 20nm wide space, mathematical models and functional optical mapping data together suggest that the composition of this fluid is distinct from that of the bulk extracellular fluid and is regulated in such a way as to modulate electrical activity via ephaptic coupling.

Ephaptic Coupling

Ephaptic coupling is a form of electrical coupling that complements gap junctional coupling and is dependent on the generation of electric fields between two excitable cells. Elegantly summarized by Dr. Sperelakis[25], the theory proposes that removal of positive ions (i.e. sodium) from this extracellular space

will exacerbate the potential difference across the cell membrane, making the cytosolic side relatively depolarized and thereby activate voltage sensitive ion channels (i.e. $Na_v1.5$). In this way, conduction may proceed without complete dependence on gap junctional coupling. Ephaptic coupling is therefore highly dependent on the width, ion channel expression, and extracellular ion composition of this small extracellular region known as the perinexal cleft. While most experimental evidence for ephaptic coupling exists within the field of neural electrophysiology and considers nanodomains between coupled neurons, recent studies from our group have provided insight into ephaptic coupling within cardiac tissue as well[20,22,23,26–30]. Briefly, these studies suggest that manipulation of the width or ionic composition of the perinexal cleft can result in measurable changes to conduction velocity and/or action potential duration (a metric of repolarization) in *ex vivo* guinea pig and mouse heart preparations.

Disease in Cardiac Conduction

The sodium channel $Na_v1.5$ is critical for initiating and propagating conduction, so it is unsurprising that loss of function (LOF) $Na_v1.5$ variants are associated with a number of conduction disease states. What's less intuitive is the concealed nature of some of these diseases, wherein patients may exist asymptomatically for decades, though the LOF variant is present from birth. Lenegre's Disease and Brugada Syndrome are two examples of concealed conduction diseases, as the average age of symptom onset is in the third-fourth decade of life[31,32]. This suggests that even a 50% loss of Nav1.5 alone is not sufficient for the disease state, though it is an important contributor. Rather, a combination of homeostatic imbalance and aging combine to unmask the underlying conduction deficit present in these patients. In chapter 2, we explore two conditions that may unmask this disease phenotype, with the intention of bringing to light possible triggers of arrhythmia in Nav1.5 LOF patients.

2. Cardiac Repolarization

Potassium channel diversity and species specificity

Repolarization is often measured using action potential duration (APD), the amount of time between the upstroke of the action potential and return of the membrane potential to its resting value. As described in the AP outline above, repolarization is predominantly dictated by outward current via potassium channels. While $Na_v1.5$ is largely responsible for excitation of the ventricular myocardium, there is much greater diversity in the potassium channels responsible for cardiac repolarization. Voltage gated potassium channels may be broadly categorized as transient outward K^+ currents (I_{to}), delayed outward rectifiers (I_{KR} and I_{KS}), or inward rectifying potassium currents (I_{K1}). The transient outward current is responsible for the early, sharp repolarization in phase 1 of the action potential, while the outward rectifying currents contribute to phase 3, and the inward rectifying current determine phase 3 and 4. It should be noted that there is distinct species variation in the expression and biophysical properties of these channels, which predisposes some animal models to be better suited for study of repolarization than others. In particular, mouse ventricular myocytes express two forms of I_{to} (fast and slow), with I_{tof} being largely responsible for the abrupt repolarization of the mouse action potential[33]. In contrast, I_{to} in larger mammals contributes to the early phase of repolarization and the plateau of phase 2, with the exception of guinea pigs and ungulates, which do not express I_{tof} and therefore lack an AP notch[34]. More rapid reuptake of cytosolic calcium in the mouse[35,36], as well as three delayed rectifier K currents distinct from I_{Kr} and I_{Ks}[33] yield an AP morphology that is dramatically triangulated relative to the AP of larger mammals. These differences make mice poorly suited for experimental investigation into repolarization. For these reasons, as well as the strong historical precedent for use of guinea pigs in arrhythmia research, the Hartley guinea pig is the model selected to investigate phase 2-4 repolarization in this dissertation.

Potassium current regulation

As elegantly summarized in the voltage gated potassium channel review by Yang and Nerbonne[37], potassium currents are post-translationally regulated by a plethora of factors including phosphorylation, glycosylation, sumoylation, palmitoylation, and more. Most pertinent to the present investigation is the interesting sensitivity of voltage gated potassium channels to ion concentration. For example, the inward rectifying behavior of Kir2.1 (conduit of I_{K1}) is dependent on divalent cations or polyamines blocking the channel's pore. Therefore, increased intracellular Mg^{2+} and Ca^{2+} results in I_{K1} inhibition. Notably, I_{K1}, I_{Kr}, and I_{Ks} are also sensitive to extracellular K^+ via allosteric interaction[38]. Specifically, Kir2.1 shows increased outward conductance due to electrostatic interactions between K^+ ions and pore-blocking ions, so that the divalent cations or polyamines are pushed away and outward K^+ flow resumes[38]. Increased extracellular K^+ is therefore correlated with increased repolarizing currents and shortened APD. Dysregulation of serum potassium is a known substrate for arrhythmias, and hyperkalemia is in fact a very common pathogenic state. Serum potassium >5.0mM has canonically been associated with APD shortening due to this increase in I_{K1} that overpowers the reduced chemical driving force from this disease state[38]. In chapter 3, we explore how changes in other ions, such as sodium and calcium, modulate the APD response to hyperkalemia.

3. Relationship between conduction and repolarization in the epicardium

Tissue activation and repolarization are distinct phenomena, determined by unique channels and pumps, but while they are often studied in isolation, they are not independent. In order to fully assess cardiac function, attention must be given to both activation and repolarization.

Commonly, activation is measured as activation time (AT), the time between the wavefront-initiating stimulus and the maximum upstroke of the action potential of the cell or tissue region of interest. As described above, repolarization is often measured using action potential duration (APD), the amount of time the cell spends in a depolarized state. Alternatively, repolarization may be measured as repolarization time (RT), that is, the length of time between the stimulus and repolarization of the cell or

region in question. Therefore, RT is calculated as AT + APD, and changes in either AT or APD may result in changes in RT. However, it has been observed that there is often an inverse relationship between AT and APD[39–42], so that a homeostatic balance of RT is generally maintained, and exacerbations of existing RT gradients are minimized. This is important because large gradients in repolarization time are a known substrate of arrythmias[43]. Interestingly, increased repolarization gradients on their own do not increase risk of arrhythmia, but an increased gradient is a critical substrate for arrhythmia initiation[44]. Therefore, while repolarization time is not homogenous across the ventricles, the distribution of RTs across the ventricles must be maintained to allow for "safe" conduction.

On the scale of the intact heart, it has been noted that the inverse relationship between AT and APD is a strong determinant of T wave morphology[44]. Specifically, this relationship modifies T wave concordance, which is the parallel polarity of the QRS and T wave components of the ECG. In humans and guinea pig, the T wave shows concordance under baseline physiology, while in mice it shows discordance at baseline[40,45]. This is because early repolarization in the mouse heart initiates before completion of the depolarizing wavefront across the ventricles[45]. As seen in Figure 4, an inverse relationship between AT and APD (with a slope ≤ -1) is necessary for maintenance of T wave concordance in the human and larger mammal[44]. Interestingly, clinical evidence suggests that cardiac disease states such as heart failure often present with inverted T waves, suggesting a disturbance in the AT-APD relationship during such conditions[40].

The inverse relationship between AT and APD has been observed across a variety of tissue preparations (cell sheets, isolated hearts, in vivo electrophysiology mapping) and a variety of animal models (guinea pig, rabbit, dog, human). However, the precise mechanism by which this relationship exists has not been investigated. While this relationship has been modulated and measured for the sake of assessing cardiac memory, its mechanism has been assumed to be electrotonic coupling via gap junctions. Knowledge of its exact mechanism may lend insight to disease states known to result in T

wave inversion. Chapter 4 will assess how electrical coupling and determinants of conduction and repolarization modify the AT-APD relationship in the guinea pig epicardium.

As described above, cardiac arrhythmias may arise from dysregulation of ventricular conduction, repolarization, or the relationship between the two. The following chapters investigate mechanisms by which each of these phenomena are regulated, particularly in the context of reduced sodium channel function, a condition associated with multiple disease states, with the goal of better understanding possible catalysts for sudden cardiac death.

References

1. Hodgkin, A. L., Huxley, A. F. & Katz, B. Measurement of current-voltage relations in the membrane of the giant axon of Loligo. *J. Physiol.* **116**, 424–448 (1952).
2. Grant, A. O. Cardiac ion channels. *Circ. Arrhythm. Electrophysiol.* **2**, 185–194 (2009).
3. Grant, A. O. & Starmer, C. F. Mechanisms of closure of cardiac sodium channels in rabbit ventricular myocytes: single-channel analysis. *Circ. Res.* **60**, 897–913 (1987).
4. Patlak, J. B. & Ortiz, M. Slow currents through single sodium channels of the adult rat heart. *J. Gen. Physiol.* **86**, 89–104 (1985).
5. Reuter, H. The dependence of slow inward current in Purkinje fibres on the extracellular calcium-concentration. *J. Physiol.* **192**, 479–492 (1967).
6. Yue, D. T. & Marban, E. A novel cardiac potassium channel that is active and conductive at depolarized potentials. *Pflugers Arch.* **413**, 127–133 (1988).

7. Sanguinetti, M. C. & Jurkiewicz, N. K. Two components of cardiac delayed rectifier K+ current. Differential sensitivity to block by class III antiarrhythmic agents. *J. Gen. Physiol.* **96**, 195–215 (1990).
8. Gerdes, A. M. *et al.* Structural remodeling of cardiac myocytes in patients with ischemic cardiomyopathy. *Circulation* **86**, 426–430 (1992).
9. Lindner, E. Die submikroskopische Morphologie des Herzmuskels. *Zeitschrift für Zellforschung und Mikroskopische Anatomie* **45**, 702–746 (1957).
10. Sperelakis, N. & Rubio, R. An orderly lattice of axial tubules which interconnect adjacent transverse tubules in guinea-pig ventricular myocardium. *J. Mol. Cell. Cardiol.* **2**, 211–220 (1971).
11. Weber, P. A., Chang, H.-C., Spaeth, K. E., Nitsche, J. M. & Nicholson, B. J. The permeability of gap junction channels to probes of different size is dependent on connexin composition and permeant-pore affinities. *Biophys. J.* **87**, 958–973 (2004).
12. van Rijen, H. V. M. *et al.* Slow conduction and enhanced anisotropy increase the propensity for ventricular tachyarrhythmias in adult mice with induced deletion of connexin43. *Circulation* **109**, 1048–1055 (2004).
13. Beauchamp, P. *et al.* Electrical propagation in synthetic ventricular myocyte strands from germline connexin43 knockout mice. *Circ. Res.* **95**, 170–178 (2004).
14. Morley, G. E. *et al.* Characterization of conduction in the ventricles of normal and heterozygous Cx43 knockout mice using optical mapping. *J. Cardiovasc. Electrophysiol.* (1999) doi:10.1111/j.1540-8167.1999.tb00192.x.
15. Thomas, S. P. *et al.* Impulse Propagation in Synthetic Strands of Neonatal Cardiac Myocytes With Genetically Reduced Levels of Connexin43. *Circ. Res.* **92**, 1209–1216 (2003).
16. Vaidya, D. *et al. Null Mutation of Connexin43 Causes Slow Propagation of Ventricular Activation in the Late Stages of Mouse Embryonic Development*. http://www.circresaha.org (2001).

17. Eloff, B. C. *et al.* High resolution optical mapping reveals conduction slowing in connexin43 deficient mice. *Cardiovasc. Res.* **51**, 681–690 (2001).

18. Guerrero, P. A. *et al.* Slow ventricular conduction in mice heterozygous for a connexin43 null mutation. *J. Clin. Invest.* **99**, 1991–1998 (1997).

19. Dhillon, P. S. *et al.* Relationship Between Gap-Junctional Conductance and Conduction Velocity in Mammalian Myocardium. *Circ. Arrhythm. Electrophysiol.* **6**, 1208–1214 (2013).

20. George, S. A. *et al.* Extracellular sodium and potassium levels modulate cardiac conduction in mice heterozygous null for the Connexin43 gene. *Pflugers Arch.* (2015) doi:10.1007/s00424-015-1698-0.

21. Rhett, J. M. & Gourdie, R. G. The perinexus: a new feature of Cx43 gap junction organization. *Heart Rhythm* **9**, 619–623 (2012).

22. Veeraraghavan, R. *et al.* Sodium channels in the Cx43 gap junction perinexus may constitute a cardiac ephapse: an experimental and modeling study. *Pflugers Arch.* **467**, 2093–2105 (2015).

23. Veeraraghavan, R., Lin, J., Keener, J. P., Gourdie, R. & Poelzing, S. Potassium channels in the Cx43 gap junction perinexus modulate ephaptic coupling: an experimental and modeling study. *Pflugers Arch.* **468**, 1651–1661 (2016).

24. Struckman, H. L. *et al.* Unraveling Chamber-specific Differences in Intercalated Disc Ultrastructure and Molecular Organization and Their Impact on Cardiac Conduction. *bioRxiv* 2023.02.13.528369 (2023) doi:10.1101/2023.02.13.528369.

25. Sperelakis, N. An electric field mechanism for transmission of excitation between myocardial cells. *Circ. Res.* **91**, 985–987 (2002).

26. Moise, N., Struckman, H. L., Dagher, C., Veeraraghavan, R. & Weinberg, S. H. Intercalated disk nanoscale structure regulates cardiac conduction. *J. Gen. Physiol.* **153**, (2021).

27. Wu, X. *et al.* Hypernatremia and intercalated disc edema synergistically exacerbate long-QT syndrome type 3 phenotype. *Am. J. Physiol. Heart Circ. Physiol.* **321**, H1042–H1055 (2021).

28. King, D. R. *et al.* The Conduction Velocity-Potassium Relationship in the Heart is Modulated by Sodium and Calcium. *Pflügers Archiv - European Journal of Physiology*.
29. George, S. A., Calhoun, P. J., Gourdie, R. G., Smyth, J. W. & Poelzing, S. TNFα modulates cardiac conduction by altering electrical coupling between myocytes. *Front. Physiol.* (2017) doi:10.3389/fphys.2017.00334.
30. Lin, J. *et al.* Ephaptic Coupling Is a Mechanism of Conduction Reserve During Reduced Gap Junction Coupling. *Front. Physiol.* **13**, 848019 (2022).
31. Milman, A. *et al.* Age of First Arrhythmic Event in Brugada Syndrome. *Circ. Arrhythm. Electrophysiol.* **10**, e005222 (2017).
32. Probst, V. *et al.* Haploinsufficiency in combination with aging causes SCN5A-linked hereditary Lenègre disease. *J. Am. Coll. Cardiol.* **41**, 643–652 (2003).
33. Xu, H., Guo, W. & Nerbonne, J. M. Four kinetically distinct depolarization-activated K+ currents in adult mouse ventricular myocytes. *J. Gen. Physiol.* **113**, 661–678 (1999).
34. *Cardiac electrophysiology : from cell to bedside*. (Elsevier, 2018).
35. Luo, W. *et al.* Targeted ablation of the phospholamban gene is associated with markedly enhanced myocardial contractility and loss of beta-agonist stimulation. *Circ. Res.* **75**, 401–409 (1994).
36. Rouslin, W. & Broge, C. W. Isoform-independent heart rate-related variation in cardiac myofibrillar Ca(2+)-activated Mg(2+)-ATPase activity. *Am. J. Physiol.* **270**, C1271-6 (1996).
37. Yang, K.-C. & Nerbonne, J. M. Mechanisms contributing to myocardial potassium channel diversity, regulation and remodeling. *Trends Cardiovasc. Med.* **26**, 209–218 (2016).
38. Weiss, J. N., Qu, Z. & Shivkumar, K. Electrophysiology of Hypokalemia and Hyperkalemia. *Circ. Arrhythm. Electrophysiol.* **10**, (2017).

39. Osaka, T., Kodama, I., Tsuboi, N., Toyama, J. & Yamada, K. Effects of activation sequence and anisotropic cellular geometry on the repolarization phase of action potential of dog ventricular muscles. *Circulation* **76**, 226–236 (1987).

40. Cowan, J. C. *et al.* Sequence of epicardial repolarisation and configuration of the T wave. *Br. Heart J.* **60**, 424–433 (1988).

41. Chan, Y.-H. *et al.* Small-Conductance Calcium-Activated Potassium Current Is Activated During Hypokalemia and Masks Short-Term Cardiac Memory Induced by Ventricular Pacing. *Circulation* **132**, 1377–1386 (2015).

42. Costard-Jäckle, A., Goetsch, B., Antz, M. & Franz, M. R. Slow and long-lasting modulation of myocardial repolarization produced by ectopic activation in isolated rabbit hearts. Evidence for cardiac "memory." *Circulation* **80**, 1412–1420 (1989).

43. Janse, M. J. & Wit, A. L. Electrophysiological mechanisms of ventricular arrhythmias resulting from myocardial ischemia and infarction. *Physiol. Rev.* **69**, 1049–1169 (1989).

44. Opthof, T. *et al.* Dispersion in ventricular repolarization in the human, canine and porcine heart. *Prog. Biophys. Mol. Biol.* **120**, 222–235 (2016).

45. Offerhaus, J. A. *et al.* The mechanism underlying J-waves and T-waves in the electrocardiogram of mice and zebra finches. *bioRxiv* 2020.07.20.211763 (2020) doi:10.1101/2020.07.20.211763.

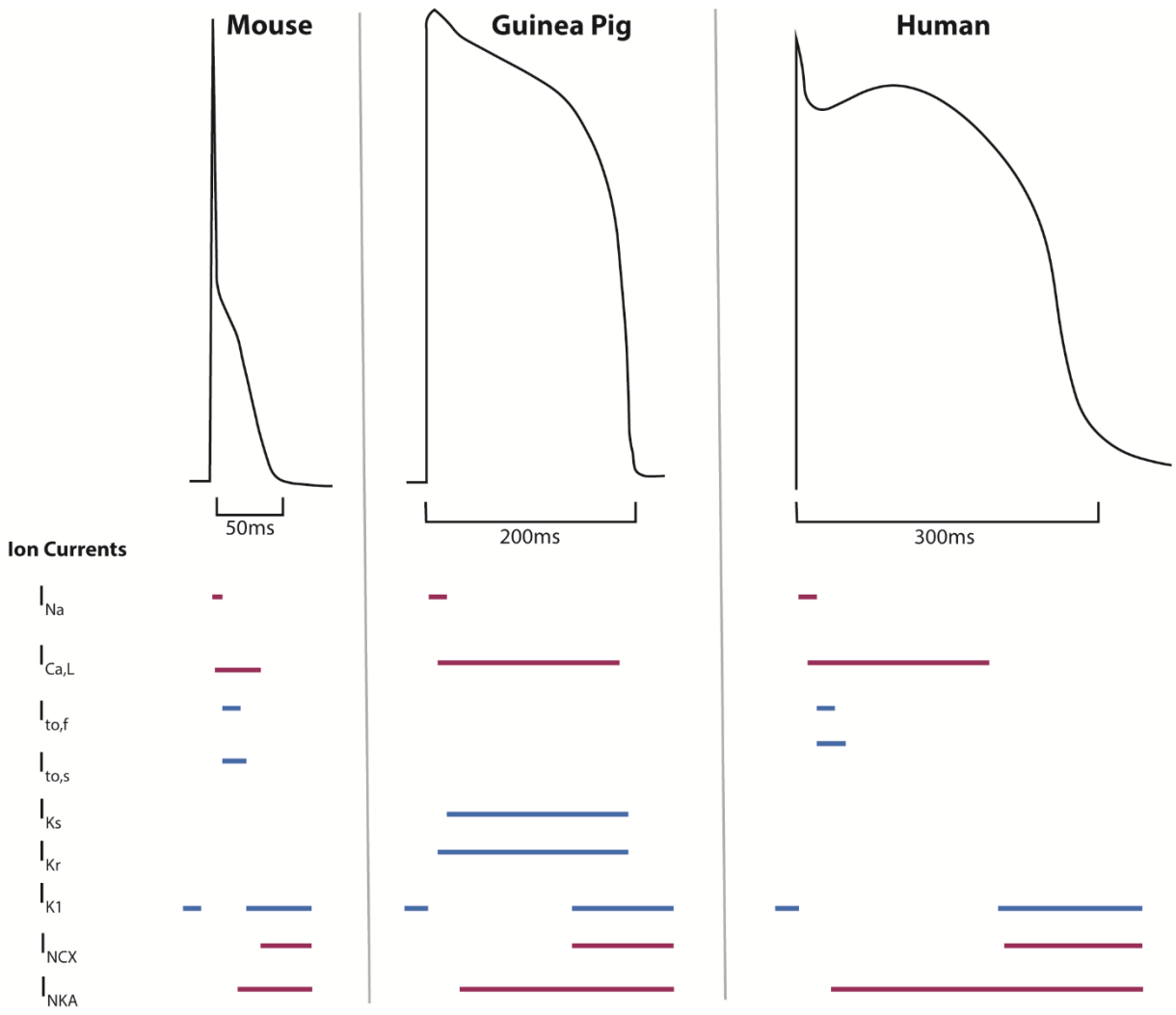

Figure 1. Ion channel expression and current kinetics are species-specific and contribute to the distinct action potential morphology of mouse, guinea pig, and human ventricular cardiomyocytes.

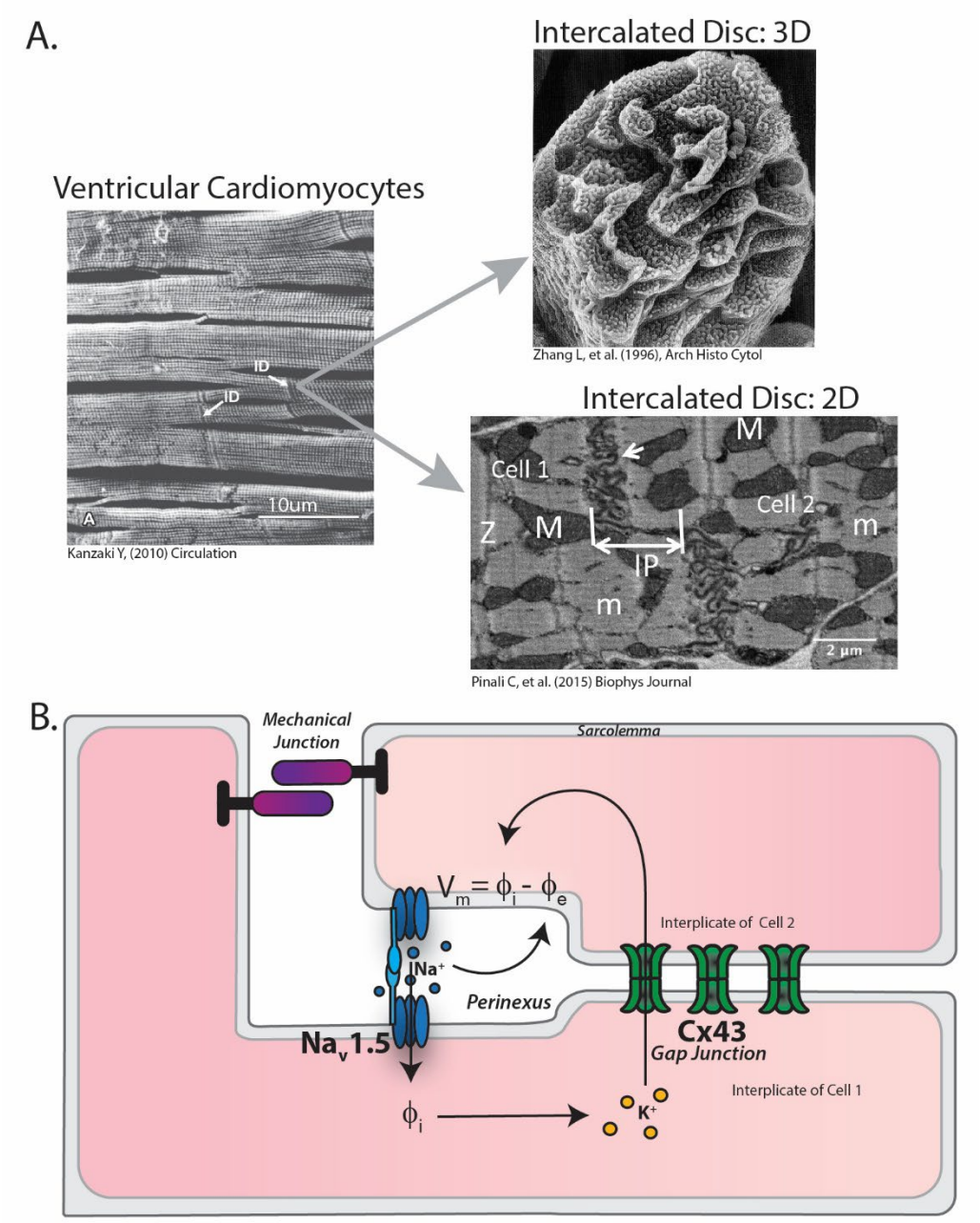

Figure 2. (A) The intercalated disc (ID) of cardiomyocytes is comprised of a stair-step structure, with the steps referred to as the plicate and risers as the interplicate. (B). A schematic of the mechanism of ephaptic coupling as proposed to occur between the interplicate membranes of two cells. As sodium ions are removed from the intercellular space, the membrane potential of the apposing cell becomes relatively depolarized and transactivates sodium channels on cell 2.

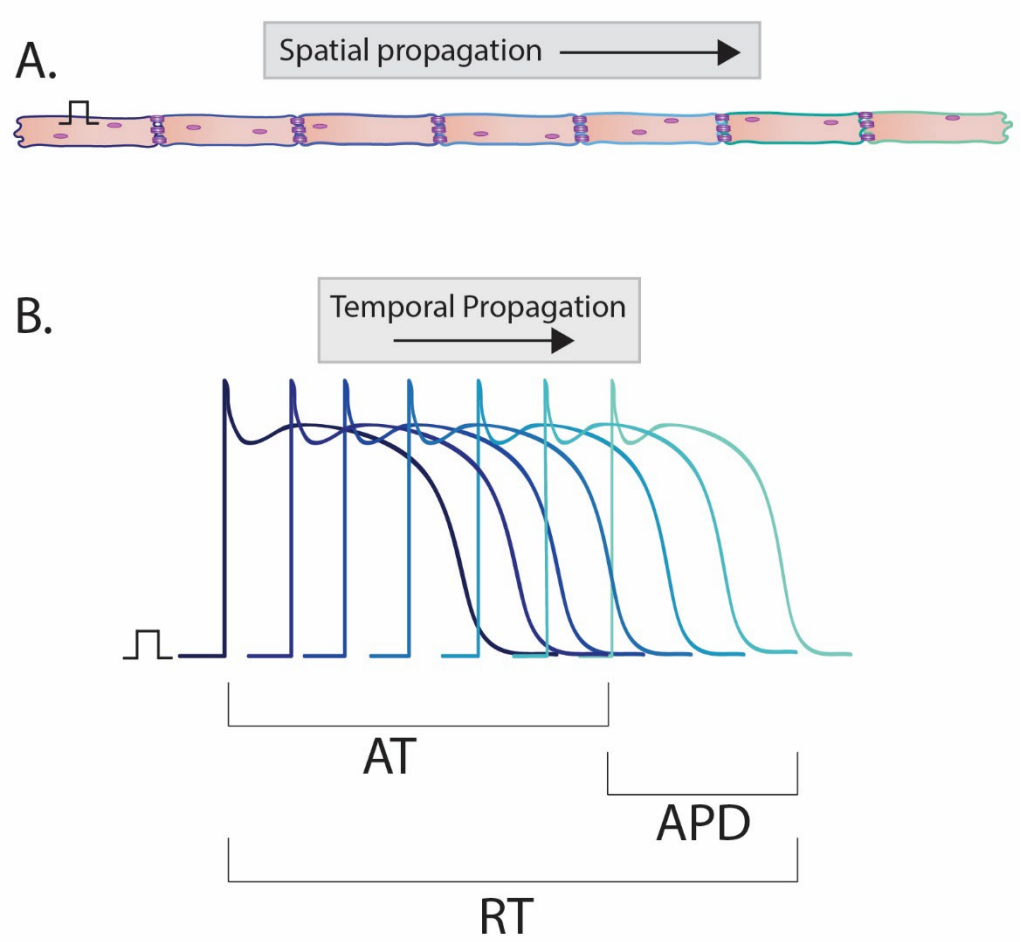

Figure 3. (A) A schematic of electrical propagation as it proceeds down a cell strand. (B) A schematic of electrical propagation across time, where AT indicates activation time of the last action potential, APD indicates the action potential duration of the last action potential, and RT indicates the repolarization time of the activated strand. Created with BioRender.com

Chapter 2

Mannitol and hyponatremia regulate cardiac ventricular conduction in the context of sodium channel loss of function

Mannitol and hyponatremia regulate ventricular conduction in the context of sodium channel loss of function

Grace A. Blair, Xiaobo Wu, Chandra Bain, Gregory S. Hoeker, Steve Poelzing

This manuscript has been submitted for review to AJP Heart and Circulatory Physiology

Abstract

Background: Scn5a heterozygous null (Scn5a+/-) mice have historically been used to investigate arrhythmogenic mechanisms of diseases such as Brugada Syndrome and Lev's disease. Interestingly, previous studies have reported both no conduction change and significant conduction slowing in Scn5a+/- animals. Prior publications from our lab suggest that reducing ephaptic coupling (EpC) in ex vivo hearts exacerbates pharmacological $Na_v1.5$ loss of function (LOF). Whether this effect is consistent in a genetic $Na_v1.5$ LOF model is yet to be determined. We hypothesized that loss of EpC would result in greater reduction in conduction velocity (CV) for the Scn5a+/- mouse relative to wild type (WT).

Methods: *In vivo* ECGs and *ex vivo* optical maps were recorded from langendorff-perfused Scn5a+/- and WT mouse hearts. CV was calculated after optically mapping hearts perfused with a normonatremic solution (150mM Na^+). Next, EpC was reduced with hyponatremia (120mM Na^+), the clinically relevant osmotic agent mannitol, or a combination of the two.

Results: Neither *in vivo* QRS duration nor *ex vivo* CV during normonatremia was significantly different between the two genotypes. In agreement with our hypothesis, we found that hyponatremia resulted in severe CV slowing and disrupted conduction for 4/5 HZ mice, but 0/6 WT mice. Additionally, treatment with mannitol slowed CV to a greater extent in HZ hearts relative to WT hearts. Unexpectedly, treatment with mannitol during hyponatremia did not further slow CV in either genotype, but instead resolved the disrupted conduction observed in HZ hearts.

Conclusion: Loss of EpC through either reduced Na^+ or mannitol alone will result in slowed or disrupted conduction in a genetic model of $Na_v1.5$ LOF. When these interventions are combined, however, conduction slowing is attenuated.

Introduction

Since the early 2000s, murine models with loss of function (LOF) of the cardiac isoform of the voltage-gated sodium channel ($Na_v1.5$) have been studied in hopes of elucidating the mechanisms of arrhythmogenesis in diseases such as Brugada Syndrome (BrS) and Lenegre Disease (Lev's disease)[1–5]. However, previous reports have not reached a consensus as to whether a mouse with 50% reduced $Na_v1.5$ function has slower ventricular conduction velocity (CV) than wild type (WT) animals under baseline conditions. Initial characterizations presented no significant difference in CV relative to the WT mouse[2,3], while subsequent studies report reduced CV in the heterozygous animal relative to WT[4,5]. This discrepancy highlights the importance of experimental conditions in making such conduction measurements, and also parallels clinical evidence of "concealed" phenotypes in Nav1.5 LOF diseases such as BrS[6].

Our lab has previously shown that changes in the osmotic or electrolyte composition of Langendorff perfusion solutions can modulate CV slowing in multiple *ex vivo* models of impaired ventricular conduction. Using flecainide-treated guinea pig hearts as a pharmacological model of $Na_v1.5$ LOF, we demonstrated that the osmotic agent mannitol could exacerbate CV slowing by inducing intercalated disc dehiscence[7]. In another study, increasing perfusate potassium concentration (indirectly inducing $Na_v1.5$ LOF through increased resting membrane potential and sodium channel inactivation) and reducing sodium concentration preferentially slowed CV in *ex vivo* connexin-43 (Cx43) heterozygous mouse hearts relative to WT[8]. Both of these previous findings support a mechanism of CV modulation via altered ephaptic coupling. The theory of ephaptic coupling posits that the activation of a sodium current on one side of a small intercellular cleft (such as the intercalated disc nanodomain known as the perinexus[9]) results in a more negative extracellular cleft potential, transactivating the distal sodium channels and propagating conduction of the action potential. Accordingly, widening junctional extracellular spaces can reduce this mode of sodium channel transactivation and decrease CV. Additionally,

reducing extracellular sodium can theoretically reduce CV via ephaptic coupling by reducing the driving force for sodium.

Interestingly, numerous clinical case reports describe that a BrS ECG phenotype can be unmasked by hyponatremia[10–14]. While many of these studies report the phenomenon as a BrS "phenocopy" due to its transient nature (resolving upon recovery of serum sodium concentration), they nevertheless highlight the efficacy of hyponatremia as a substrate for electrophysiological conduction disturbance. Therefore, $Na_v1.5$ LOF patients may be more vulnerable to changes in serum sodium concentration relative to unaffected individuals.

Considering our previous publications as well as clinical case reports of BrS patients, we hypothesize that the heart's extracellular osmotic and ionic composition plays a pivotal role in modulating conduction, particularly in the context of $Na_v1.5$ LOF. This study was conducted in order to assess whether mice heterozygous null for the *Scn5a* gene encoding $Na_v1.5$ (Scn5a+/-) are more susceptible to CV slowing than WT in response to mannitol-induced perinexal widening and decreased extracellular sodium. We found that conduction is modestly reduced in Scn5a+/- mouse hearts relative to WT under baseline conduction, but Scn5a+/- hearts demonstrate greater slowing after mannitol treatment and unidirectional conduction block during hyponatremia. Surprisingly, we found that hyponatremia attenuated conduction slowing during mannitol treatment for both genotypes.

Methods

Mouse Model

Original breeder wild type (WT) and Scn5a+/- mice on a 129/SvEv-C57BL/6 background were acquired from Taconic biosciences and bred onsite in Roanoke, VA. Mice of both sexes, age 14-30 weeks, were utilized in all protocols, though due to availability at the time of

experimentation the distribution of sexes was uneven. All protocols were approved by the Institutional Animal Care and Use Committee at Virginia Polytechnic Institute and State University and conform to the guidelines of the National Institutes of Health Guide for the Care and Usage of Laboratory Animals.

RNA purification and qRT-PCR

RNA was isolated from snap-frozen left ventricles. Tissues were lysed in Trizol (ThermoFisher #15596026) per manufacturer's protocol and separated into phases using Phase lock gel tubes (Fisher #NC1093153). The top clear aqueous layer was further purified using the NucleoSpin RNA Kit (MACHEREY-NAGEL #740955), and cDNA was generated using the SuperScript IV First-Strand Synthesis System (ThermoFisher #18091050), according to the manufacturers' instructions. cDNA was used at a concentration of 20 ng per qRT-PCR reaction with gene-specific primers (SCN5A forward: 5'-GCT GCC AGA TCT CTA TGG CAA CCC – 3', SCN5A reverse: 5'-CAA GGC ATT GGT GGC ACT GAA CC -3'; HPRT1 forward: 5'-CCC CAA AAT GGT TAA GGT TGC, HPRT1 reverse: 5'-AAC AAA GTC TGG CCT GTA TCC-3'; GAPDH forward: 5'-AAT GGT GAA GGT CGG TGT G-3', GAPDH reverse: 5'-GTG GAG TCA TAC TGG AAC ATG TAG-3') and SYBR Select Master Mix for CFX (ThermoFisher #4472937). All samples were normalized to the combined threshold values of HPRT1 & GAPDH together as housekeeping genes and data are represented relative to WT Scn5a expression.

Western Blots

Left ventricular tissue samples were snap frozen and western blotting was performed. Briefly, the samples were homogenized in RIPA lysis buffer (containing 50mM Tris pH 7.4, 150mM NaCl, 1mM EDTA, 1% Triton X-100, 1% sodium deoxycholate, 0.1% sodium dodecyl sulfate, 200μM

Na3VO34, 1mM NaF, and 5.6mM N-Ethylmaleimide) supplemented with Roche Protease Inhibitor Cocktail (Millipore Sigma #4693159001). Protein concentration was determined by a BioRad DC protein assay (#500-0112) and concentrations were normalized prior to analysis. Electrophoresis was performed to separate proteins which were then transferred to a PVDF membrane, blocked with 5% bovine serum albumin for 1 hour at room temperature and incubated overnight with a primary antibody against either the principal ventricular gap junction protein Cx43 phosphorylated at Ser368 (pCx43, Cell Signaling Technology #3511S) or against the voltage-gated sodium channel protein $Na_v1.5$ (Cell Signaling Technology #14421s), at 4°C. The membranes were then washed and incubated with secondary antibody (Abcam #ab6721) at room temperature for 1 hour. After washing, bound antibody was detected using West Pico Plus chemiluminescent substrate (ThermoFisher #34579) and imaged using the Licor Odyssey Fc system. Membranes were stripped with ReBlot Plus (Millipore Sigma #2504) according to manufacturer's instructions, blocked in Intercept Blocking Buffer (Licor #927-60001) at room temperature for 1 hour and incubated with primary antibodies against total Cx43 (Millipore Sigma #C6219) and GAPDH (VWR #101983-284). Membranes were then washed and incubated with secondary antibodies for 1 hour (Licor #925-32211 & 925-68070) and washed again. Membranes were again imaged using the Licor Odyssey Fc system to determine protein expression. Total Cx43 and $Na_v1.5$ protein expression were normalized to GAPDH and pCx43 was normalized to total Cx43.

In vivo ECG

Noninvasive, unanesthetized ECG recordings were acquired using an ECGenie system (Mouse Specifics, inc. Framingham, MA). Mice of each genotype (n= 6 WT, 6 Scn5a+/-) were placed on the recording platform for a habituation period of 15 minutes before recording commenced. Recording continued until 10 seconds of stable ECG signal was acquired. Signals were

acquired using EzCG software (Mouse Specifics, Famingam MA), and signal processing was performed using LabChart ECG Analysis (ADInstruments Inc, Colorado Springs CO).

Langendorff-perfused heart preparations

Mouse

Mice (Scn5a+/- n= 10, WT n= 12) were anesthetized by 4% isoflurane in O_2; anesthesia was confirmed by the absence of response to toe pinch. Cervical dislocation was then performed and immediately followed by thoracotomy and excision of the heart. The *ex vivo* heart was retrogradely perfused via the aorta using a rolling pump at 1.5 ml/min. The perfusate consisted of oxygenated solution containing (in mM) 1.8 CaCl2·2H2O, 144.5 NaCl, 1.0 MgCl2· 6H2O, 5.5 NaOH, 1.2 NaH2PO4, 4.0 KCl, 5.5 dextrose, 10 HEPES, titrated to pH 7.4. Total sodium content of this solution was 150mM Na^+, which will be referred to as “baseline”. After cannulation, hearts were immersed in perfusion solution within a custom-designed optical mapping bath maintained at 37°C[15].

Guinea Pig

Adult male Hartley albino guinea pigs (Hilltop, Scottdale, PA, male, age 14-16months, n= 6) were anesthetized using 4% isofluorant in O_2. After loss of response to toe pinch, thoracotomy was performed, and the heart was rapidly excised and cannulated (<4 minutes). The *ex vivo* heart was retrogradely prefused via the aorta with a crystalloid solution consisting of, in mM, 140 NaCl, 5.0 NaOH, 4.56 KCl, 1.25 $CaCl_2$•$2H_2O$, 5.5 Dextrose, 0.7 $MgCl_2$•$6H_2O$, and 10 HEPES. Total sodium content of this solution was 145mM Na^+, which will be referred to as “baseline” for the guinea pig experiments. The perfusate was equilibrated to a pH of 7.4 using NaOH or HCl, as necessary, and was oxygenated and maintained at 37.0 °C. Perfusion occurred at 20mL/min. After cannulation, atria were removed to prevent competitive stimulation

with the pacing electrode, and hearts were immersed in perfusion solution within a custom-designed optical mapping bath, also maintained at 37°C[15].

Optical Mapping

For both species, conduction velocity (CV) was quantified by optical mapping using the voltage sensitive dye, Di-4 ANEPPS (7.5 μM, Biotium #61010). A custom Matlab program was employed to quantify transverse and longitudinal CV (CVT and CVL respectively), as previously described[16].

Mouse

After a 10-minute stabilization period following cannulation, the preparation was stained with Di-4 ANEPPS by retrograde aortic perfusion for approximately 12 minutes. The electromechanical uncoupler blebbistatin (10uM, Sigma, B0560) was added to all solutions following dye loading. A 20-minute dye wash-out period was provided using baseline solution to remove excess dye. For each image acquisition, the tissue was excited by 510nm light from an LED (LEX2-LZ4, SciMedia) and the emitted light was transmitted through a 610nm long-pass filter (Andover Corp.). Filtered emissions were captured by a Micam Ultima L-type CMOS camera over 100x100 pixels and a magnification of 1.60X, with a field of view of of 6.25mm x 6.25mm. Hearts were stimulated using a unipolar Ag-Ag/Cl electrode on the anterior epicardium, with the ground lead placed in the rear of the bath. Pacing was performed at a basic cycle length of 150ms with a 1ms wide cathodal pulse at 1.5x the minimum current required to elicit tissue excitation. In one cohort, baseline solution was perfused for 20 minutes during dye washout, followed by the same solution with the addition of mannitol (Sigma-Aldrich M4125, D-Mannitol, 26.1 g/L) for 30 minutes. In the second cohort, baseline solution was perfused for 20 minutes during dye washout, followed by 30 minutes of perfusion with a hyponatremic version of control

solution (120mM Na^+), followed by 30 minutes of perfusion with the addition of mannitol (26.1g/L) to the hyponatremic solution. Optical maps were recorded at a 1kHz sample rate for a duration of ~2 seconds during both intrinsic activity and steady-state pacing at 150ms after each perfusion solution. All representative isochrone maps presented below illustrate activation time in 2ms time steps.

Guinea Pig

After a 10-minute stabilization period following cannulation, the preparation was stained with Di-4 ANEPPS by retrograde aortic perfusion for approximately 5 minutes. The electromechanical uncoupler blebbistatin (10uM, Sigma, B0560) was added to all solutions following dye loading. A 10-minute dye wash-out period was provided using baseline solution to remove excess dye. For each image acquisition, the tissue was excited by 510nm light from an LED (LEX2-LZ4, SciMedia) and the emitted light was transmitted through a 610nm filter. Filtered emissions were captured by a Micam Ultima L-type CMOS camera over 100x100 pixels and a magnification of 0.63X, with a field of view of of 15.9mm x 15.9mm. Hearts were stimulated using a unipolar Ag-Ag/Cl electrode on the anterior epicardium, with the ground lead placed in the rear of the bath. Pacing was performed at a basic cycle length of 300ms with a 5ms wide cathodal pulse at 1.5x the minimum current required to elicit tissue excitation. After dye washout, all hearts were perfused with baseline solution for 10 minutes, followed by 15 minutes of perfusion with a hyponatremic version of “baseline” (120mM Na^+) and the sodium channel inhibitor flecainide (0.5 μM). Lastly, mannitol (26.1g/L) was added to the hyponatremia and flecainide solution, and this was perfused for a further 15 minutes. Optical maps were recorded at a 1kHz sample rate for a duration of ~2 seconds during both intrinsic activity and steady-state pacing at 150ms after each perfusion solution. All representative isochrone maps presented below illustrate activation time in 3ms time steps.

Transmission Electron Microscopy

Anterior epicardial tissue from the base of the left ventricle was collected from hearts after conclusion of the optical mapping experiments (N= 3 WT, 3 Scn5a+/-). Tissue was cut into 1 mm^3 cubes which were fixed in 2.5% glutaraldehyde at 4°C for 24 hours, and then washed thrice and stored in phosphate-buffered saline (PBS) at 4°C. As previously described, samples were prepared for transmission electron microscopy (TEM) and imaged using a JEM JEOL 1400 Electron Microscope at 150,000x magnification. To quantify perinexal width (W_P), at least 15 images were collected and analyzed per heart using a previously-described custom Matlab program[17]. The average perinexal width measured between 30-105nm from the edge of the gap junction plaque is reported as W_P.

Statistical Analysis

All statistical analysis was performed using Graphpad Prism 8 (San Diego, CA). Specific n values and details of specific statistical tests used for each experiment are included in figure legends. All summary data is reported as mean +/- standard deviation. All tests were considered statistically significant if $p<0.05$.

Results

Baseline Characteristics

As expected, mRNA expression of the *Scn5a* gene was reduced by approximately 60% in the Scn5a+/- mouse heart relative to WT, as measured with qRT PCR (Figure 1A). Additionally, Scn5a+/- hearts express a 50% reduction in $Na_v1.5$ relative to WT as measured by western blot. Additionally, neither expression of the principle ventricular gap junction protein connexin 43 (Cx43) nor phosphorylated connexin 43 (pCx43) were significantly different

between WT and Scn5a+/- mouse hearts, seen in Figure 1B and 1C. It has previously been observed that the beta 1 subunit of voltage-gated sodium channels may play a role in maintaining the structural integrity of the intercalated disc, particularly with the perinexal nanodomain[18]. We therefore utilized transmission electron microscopy to evaluate perinexal width, and found no significant difference between the two genotypes (Figure 1D).

In vivo Conduction Measurements

An *in vivo*, non-anesthetized ECG study revealed no measurable difference in QRS width between the WT and Scn5a+/- mice, suggesting little to no ventricular CV slowing in the hearts of intact Scn5a+/- animals (Figure 2A,B). The QRSJ interval, however, was significantly longer in the heterozygous group, potentially implicating differences in repolarization distribution across the murine heart[19] (Figure 2C). No difference in RR interval was measured between the genotypes, suggesting no differences in sinoatrial function at baseline. Resolution of this technique was not fine enough to identify P waves in this model or subsequently measure PR intervals to further assess atrioventricular and specialized conduction system dysfunction.

Normonatremia: Ex Vivo Ventricular Conduction Slowing

Hearts were Langendorff perfused and optically mapped to calculate an *ex vivo* measure of ventricular CV. CVT was not significantly different between WT and Scn5a+/- hearts during perfusion of the baseline, normonatremic solution (WT: 35.3±7.1cm/s, Scn5a+/-: 29.4±8.4 cm/s). However, CVL was significantly slower in Scn5a+/- relative to WT hearts. These results are depicted as representative data in Figure 3A and summary data in Figure 3B.

Previous work from our lab identified mannitol as an osmotic agent capable of inducing edema within the intercalated disc and resulting in slowed CVT[16]. Summary data in Figure 3C

demonstrate that mannitol significantly slows CVT of both WT and Scn5a+/- hearts, though to a significantly greater extent in Scn5a+/- hearts (ΔWT: -2.6± 1.7cm/s, ΔScn5a+/-: -6.8± 1.9 cm/s relative to 150mM Na^+ alone). CVL decreased relative to baseline in both WT and Scn5a+/- hearts after mannitol treatment (ΔWT: -2.8±3.4 cm/s, ΔScn5a+/-: -11.9±9.3 cm/s) , but the difference between genotypes was not significant. Therefore, the data suggest that CV in Scn5a+/- hearts, at least in the transverse direction of propagation, is more sensitive to mannitol challenge.

Hyponatremia: Ex Vivo Ventricular CV Slowing and Block

Hyponatremia has been clinically identified as a potential trigger for a BrS ECG pattern[10–14]. We therefore perfused WT and Scn5a+/- hearts with a hyponatremic solution containing 120mM Na^+. Representative data in Figure 4A reveal significant conduction slowing in both genotypes with hyponatremia WT (ΔCVT: -6.6±2.7cm/s, ΔCVL:-8.5±9.2 cm/s) and in Scn5a+/- hearts (ΔCVT: -10.8±4.9, ΔCVL: -15.8±19.0cm/s) relative to 150mM Na^+. Interestingly, hyponatremia resulted in disrupted conduction in the left ventricle of 4/5 Scn5a+/- hearts during epicardial pacing, as observed by the isochrone line crowing and severe conduction delay depicted in Figure 4B. Conversely, this hyponatremia-induced disrupted conduction presented in none of the WT hearts (0/6). The data suggest that hyponatremia slows CV and increases the likelihood for conduction failure and unidirectional block in the presence of $Na_v1.5$ LOF.

Hyponatremia and Mannitol: Attenuated Conduction Slowing and Rescue from Conduction Block

Representative optical maps of activation time (Figure 4A) and summary data (Figure 4C) demonstrate that WT hearts treated with hyponatremia and mannitol did not significantly slow relative to hearts perfused with a hyponatremic solution alone. These results are in

contrast to CV slowing observed in response to mannitol treatment in hearts perfused with 150mM Na^+.

Unexpectedly, conduction block caused by hyponatremia alone resolved for all affected Scn5a+/- hearts after treatment with a combination of hyponatremia and mannitol. This is again in contrast to results of mannitol treatment during normonatremia, which resulted in significant CV slowing both longitudinally and transversely. In conclusion, hyponatremia attenuates CV slowing due to mannitol for both Scn5a+/- and WT hearts.

Comparative CV Response to Hyponatremia and Mannitol in Guinea Pig

Our lab previously demonstrated that isolated guinea pig hearts treated with both flecainide and mannitol (maintained at a physiological sodium concentration) show an additive effect on CV slowing, similar to the findings above in mouse hearts perfused with normonatremia and then mannitol. However, it is unknown if the unexpected result that hyponatremia attenuates CV slowing due to mannitol challenge is specific to mice or can be replicated pharmacologically in a larger animal species. Representative images of the optical maps for hearts perfused with normonatremia, hyponatremia and flecainide, and a hyponatremia-flecainide-mannitol solution are shown in Figure 5A. Summary data (Figure 5B) during hyponatremia demonstrates that the addition of mannitol to flecainide-treated guinea pig hearts at 120mM Na^+ does not further reduce CV. This parallels results in the Scn5a+/- mouse model above, suggesting that mannitol-induced CV slowing is dependent on extracellular sodium concentration.

Discussion

This study was conducted in order to determine whether a congenital mouse model of $Na_v1.5$ LOF would be more susceptible to ventricular conduction slowing in response to reduced ephaptic coupling relative to WT littermates. Specifically, we measured ventricular conduction in *in vivo* and *ex vivo* WT and Scn5a+/- mouse hearts, and challenged the *ex vivo* heart preparations with perinexal widening via mannitol during normo- and hyponatremia. We found that conduction is relatively similar between WT and Scn5a+/- hearts, albeit longitudinal CV is modestly faster in WT hearts. Importantly, the Scn5a+/- hearts are more susceptible to CV slowing via mannitol than WT at normonatremia. Scn5a+/- hearts also experience unidirectional disrupted conduction in the form of severe unidirectional delay during hyponatremia, while WT experience reduced CV but not severe delay. Interestingly, while mannitol slowed CV during normonatremia in both WT and Scn5a+/- hearts, mannitol did not further slow CV during hyponatremia. This effect was also independent of $Na_v1.5$ expression levels.

Previously, other laboratories have noted downregulation of Cx43 is a comorbidity in Scn5a+/- mice that exacerbates conduction deficits during $Na_v1.5$ LOF.[1,4,20]. Our group, however, failed to find such a reduction in Cx43 or pCx43 expression via western blot. This discrepancy may be attributed to the age of the respective cohorts, as age-associated Cx43 down-regulation has been demonstrated in WT mouse cardiac tissue[21]. Previous studies reporting reduced Cx43 expression employed Scn5a+/- mice >30 weeks of age, and Derangeon et. al demonstrate that downregulation of Cx43 doesn't begin until after the age of 45 weeks[22]. Mice in this study, however, were all between 10 and 30 weeks of age. Therefore, it remains unknown whether aging itself confounds Cx43 down-regulation and conduction deficits concomitant with $Na_v1.5$ LOF.

Interestingly, the observation of worsening electrophysiological phenotype with increased age described in prior Scn5a+/- mouse studies does not correspond to the clinical

data for BrS patients. To the contrary, symptomatic BrS most commonly presents in the fourth decade of life[23]. Beyond this time, the prognosis for BrS patients appears to improve with age[24–26]. Therefore, even if progressive down-regulation or remodeling of Cx43 secondary to $Na_v1.5$ LOF is exacerbated with age, our data from this pre-clinical murine model suggests that other mechanisms for conduction slowing or disruption may underlie arrhythmogenesis in young adult $Na_v1.5$ LOF patients.

The osmotic agent mannitol has previously been validated as a means of widening the perinexal nanodomain and reducing ventricular CV via ephaptic coupling[27,28]. We therefore proposed that a mannitol challenge may further exacerbate conduction slowing in the Langendorff-perfused Scn5a+/- mouse heart. Optical mapping after administration of mannitol during normonatremia resulted in greater CV slowing in the Scn5a+/- heart relative to WT, suggesting that the heterozygous animal is more sensitive to this form of osmotic stress. As mannitol widens W_P[16,28,29], but does not significantly reduce peak I_{Na}[30] itself, the data support the hypothesis that reduced sodium channel expression is functionally unmasked by perinexal widening via mannitol during hypernatremia. Mechanistically, perinexal widening reduces ephaptic transactivation of $Na_v1.5$ by attenuating extracellular potential changes, and this appears to have an additive effect with the reduced sodium current intrinsic to our mouse model.

Reducing extracellular sodium is another mechanism previously demonstrated to reduce ventricular CV in the Langendorff-perfused heart[8,31]. Interestingly, hyponatremia has also been associated with unmasking a BrS ECG pattern in human patients[10–14]. We therefore tested the hypothesis that hyponatremia exacerbates the conduction phenotype of $Na_v1.5$ LOF. In our study, perfusion of Scn5a+/- hearts with a 120mM Na^+ solution not only exacerbated conduction slowing, but hypernatremia caused severely delayed conduction into the left ventricle in 4/5 heterozygous hearts. Conversely, delayed conduction was observed in 0/6 WT hearts. It is also

important to note that this conduction abnormality was observed under conditions of epicardial pacing, so the intrinsic conduction pathways were not physiologically engaged. This is a possible explanation for why we did not observe delayed conduction in the right ventricle, even though the right ventricular outflow tract is canonically associated with the site of arrhythmogenesis in BrS patients. Importantly, it is not known whether the delayed conduction is due to inexcitability caused by extracellular epicardial stimulation, since it always occurred adjacent to the site of pacing, or if the response is functional conduction block.

Surprisingly, conduction did not respond similarly when hearts were challenged with mannitol in the context of hyponatremia. While mannitol with hypernatremia slowed CV for both genotypes (though to a greater extent for Scn5a+/-), hyponatremia appears to attenuate this effect. Specifically, hyponatremia attenuated mannitol-induced conduction slowing independent of $Na_V1.5$ functional expression.

While precisely identifying the mechanism by which hyponatremia blunts conduction slowing induced by mannitol challenge is beyond the scope of this study, we can offer a few hypotheses. First, we previously published evidence that suggests mannitol-induced perinexal widening slows CV[27,28,30]. However, reducing extracellular sodium decreases the equilibrium potential of sodium, which in turn may alter the biphasic relationship between CV and W_P. Alternatively, reducing extracellular sodium can indirectly increase intracellular calcium by decreasing the forward rate of the sodium calcium exchanger (NCX)[32]. Increased intracellular calcium has repeatedly been shown to alter posttranslational modifications of a number of ion channels, which may in turn modify CV[33]. Additionally, a decrease in the forward rate of NCX may result in the reduction of extracellular calcium in diffusion limited nanodomains such as the perinexus. Given the dependence of extracellular adhesion on extracellular calcium concentrations, hyponatremia may indirectly modify W_P, ultimately reducing CV to a range that is less sensitive to perinexal widening[31,34]. Lastly, recent work suggests that perinexal widening

may result in redistribution of associated ion channels. Specifically, edema-induced perinexal widening was associated with more diffuse $Na_v1.5$ expression throughout the ID, relative to the dense expression near gap junctions seen in control tissue[35]. Theoretically, a smaller population of $Na_v1.5$ may provide relief for the source-sink mismatch of sodium ion availability that results from hyponatremia. Regardless of the specific hypothesis, the surprising finding that mannitol appears to rescue conduction delay in the *Scn5a+/-* mouse heart requires additional investigation.

Limitations

A number of limitations are inherent to the use of *ex vivo* Langendorff perfused hearts. These include removal of autonomic inputs that may modulate determinants of conduction, as well as the non-working preparation. Additionally, the optical mapping experiments utilized blebbistatin as an electromechanical uncoupler. Like all electromechanical uncouplers, blebbistatin has been associated with off target effects, such as APD prolongation via altered intracellular calcium handling[36–38].

Mannitol has also been associated with off target effects, most noteably hERG inhibition[39,40]. However, we have previously demonstrated that mannitol does not significantly affect peak sodium current[30] which is more relevant to the conductive nature of our results. We cannot completely discount the possibility that hERG inhibition may preserve and/or improve conduction under conditions of severely reduced peak sodium current. Some evidence for this hypothesis exists based on a previous study that demonstrated modulating hERG altered conduction preferentially during rapid pacing[41].

The observed responses in this study could be due to changes in cellular structure beyond the perinexus, such as changes in cell size. However, computational models evaluating

the effects of cell size on conduction predict that increases in size, as would be expected during a hypoosmotic treatment (hyponatremia) should result in increased CV, which is opposite to what we observe experimentally[42]. Addition of mannitol should osmotically reduce cell size, which models predict would decrease CV. Again, this is opposite to our experimental observations. Instead, both our mouse and guinea pig models show that mannitol exacerbates $Na_v1.5$ LOF during normonatremia, which is consistent with previous reports[27]. Additionally, prior work in Langendorff-perfused guinea pig hearts demonstrates that ventricular conduction slowing during hyponatremia is due to reduced extracellular sodium per se, and not hypoosmolality, NCX activity, stretch-activatied channels, or reduced chloride concentration[43]. Novelly, our data suggest that hyponatremia attenuates CV slowing due to mannitol challenge regardless of $Na_v1.5$ function.

Conclusion

To our knowledge, this is the first preclinical evidence that hyponatremia and mannitol independently induce conduction deficits in a $Na_v1.5$ LOF model. These data may suggest that exposure to either hyponatremia or mannitol could be detrimental to patients with $Na_v1.5$ LOF. However, without a mechanistic understanding of how hyponatremia attenuates conduction slowing secondary to mannitol, caution should be exercised prior to attempting clinical translation. Nevertheless, these data add to a growing body of literature that suggests modulating ephaptic coupling may be a viable diagnostic or therapeutic intervention for diseases of reduced sodium channel function.

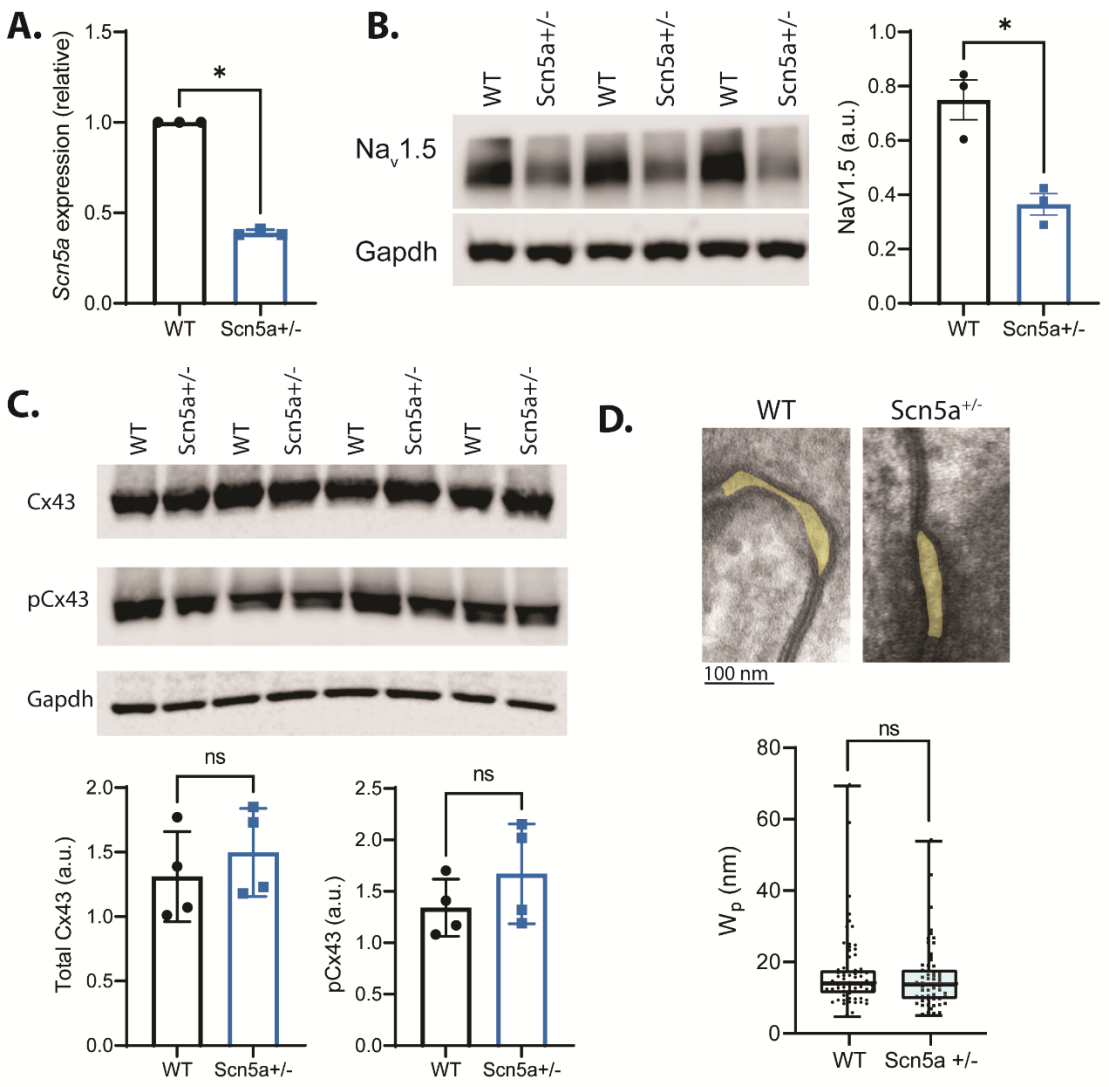

Figure 1. Characterizing the Scn5a+/- mouse heart. (A, B) Relative to WT, the Scn5a+/- mouse expresses ~60% reduced mRNA and ~52% reduced Nav1.5 protein. Nav1.5 protein expression is normalized to GAPDH. N= 3 WT, Scn5a+/- hearts, significance determined by student's t-test, * denotes $p<0.05$ compared to WT. (C) No significant difference was measured in total Cx43 expression (normalized to GAPDH) or Cx43 phosphorylation at Ser368 (normalized to total Cx43) between the genotypes. N= 3 WT, Scn5a+/- hearts. p=n.s. via one-way ANOVA. (D) Perinexal width, highlighted in yellow, was not significantly different between WT and Scn5a+/- hearts under baseline conditions. N= 3 WT, Scn5a+/- hearts, n= 15 images per heart. Significance determined by nested t test, * denotes $p<0.05$ compared to WT.

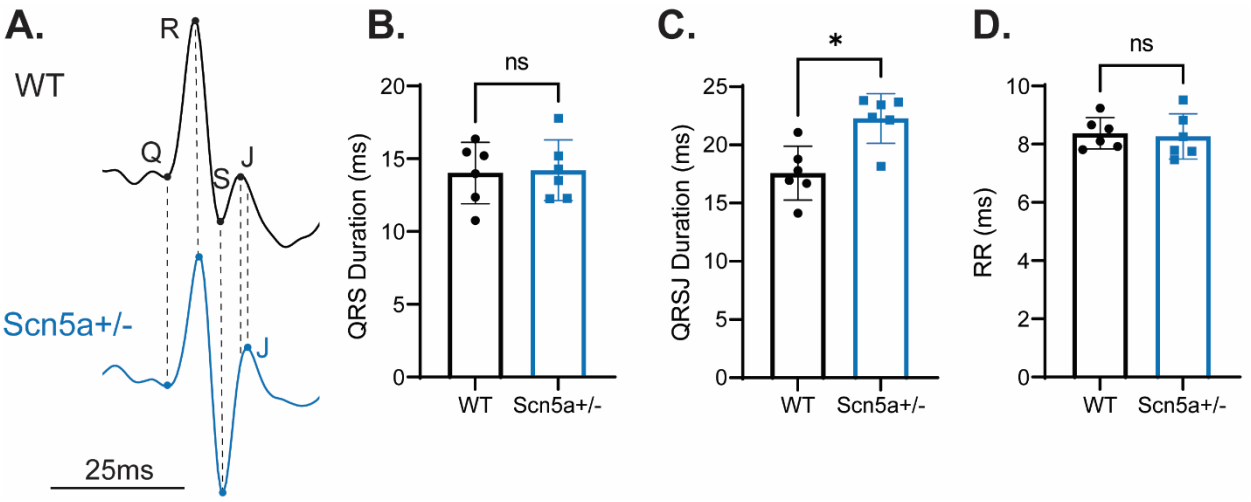

Figure 2. In vivo ventricular conduction is not significantly different between Scnta+/- and WT. (A) Typical example of an ECG trace acquired with the ECGenie system for the WT (black) and Scn5a+/- (blue) heart. (B) QRS duration is not significantly different between the two genotypes, though QRSJ is significantly longer in the Scn5a+/- mouse (C). (D) RR duration is not different between the WT and Scn5a+/- mouse. N= 6 WT, 6 Scn5a+/-, significance was determined using students t test, * denotes $p<0.05$ compared to WT.

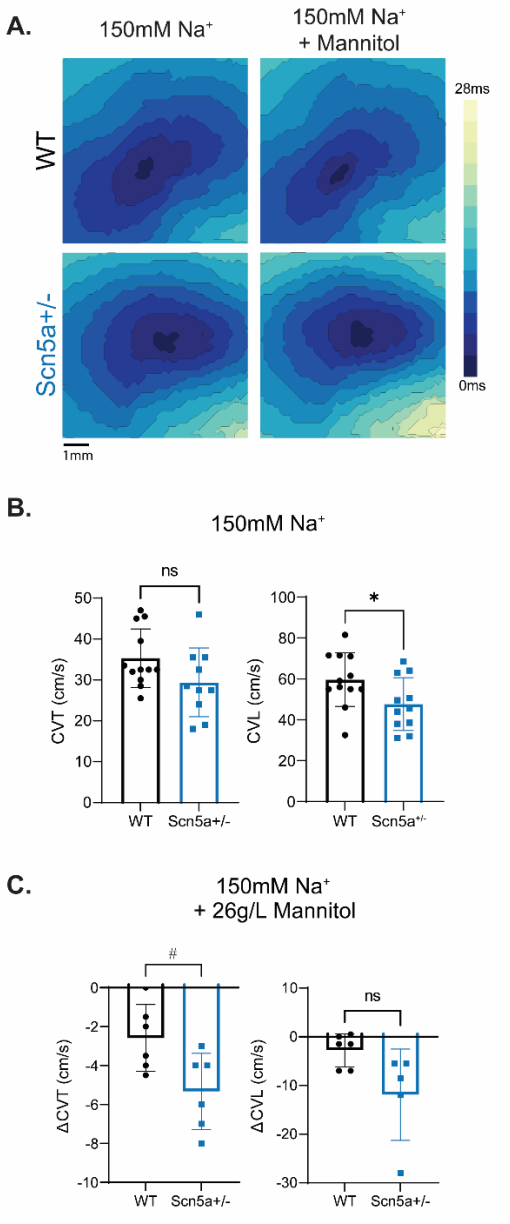

Figure 3. CV of Scn5a+/- hearts is modestly slower than WT at baseline, but more sensitive to CV slowing due to mannitol challenge. (A,B) CVL but not CVT is significantly slower for Scn5a+/- relative to WT. Isochrone lines represent 2ms N= 12 WT, 10 Scn5a+/- (C) Perfusion with mannitol results in significantly greater CV slowing in Scn5a+/- hearts relative to WT. N = 6 WT, 5 Scn5a+/-. Significance was determined using students t test, * denotes $p<0.05$ compared to WT, # denotes $p<0.05$ compared to ΔCVT of WT after mannitol treatment.

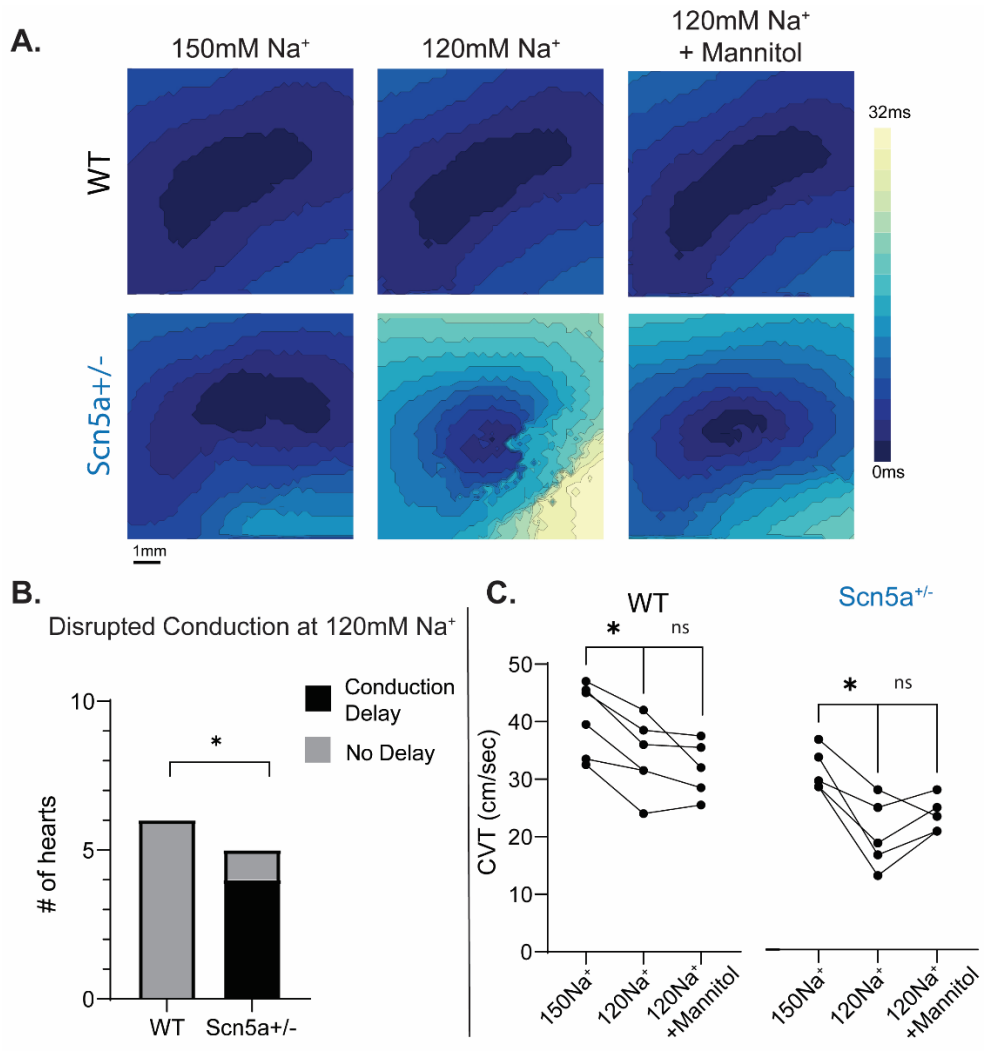

Figure 4. Hyponatremia attenuates mannitol-induced CV slowing and relieves conduction block in Scn5a+/- hearts. (A,B) WT and Scn5a+/- hearts have significantly slowed CVT in response to hyponatremia. N= 6 WT, 5 Scn5a+/-, significance determined by one-way ANOVA with Tukey's multiple comparisons test, * denotes $p<0.05$ compared to $150Na^+$ condition. (C) WT does not exhibit severe conduction delay during hyponatremia, but 4/5 Scn5a+/- exhibit severe conduction delay under these conditions. N= 6 WT, 5 Scn5a+/-. Significance determined by Fisher's Exact test, * denotes $p<0.05$ compared to WT.

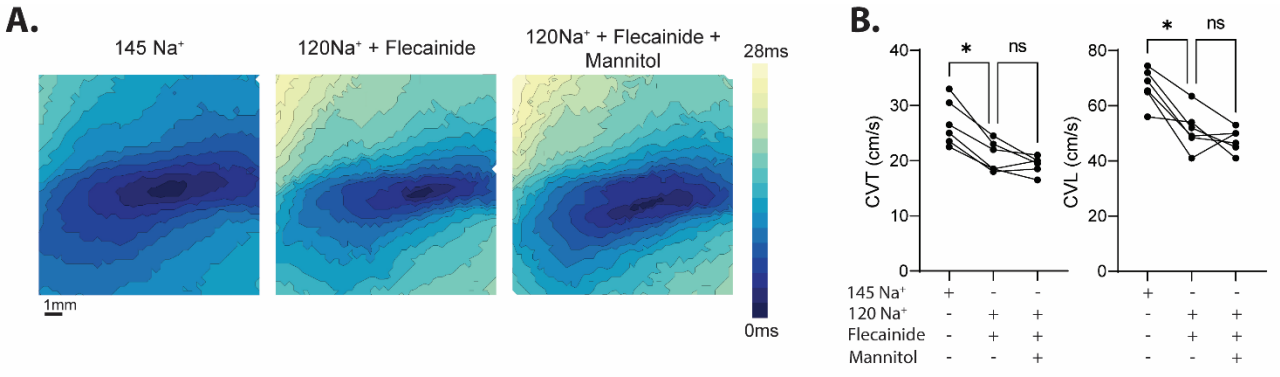

Figure 5. Hyponatremic attenuation of mannitol-induced slowing is not species specific. (A,B) Significant reductions in CVT and CVL are observed after perfusion with 120mM Na^+ and flecainide in *ex vivo* guinea pig hearts. Addition of mannitol does not show additive CV slowing effect in the context of sodium channel inactivation. N= 6, significance determined by one-way ANOVA with Tukey's multiple comparisons test, * denotes $p<0.05$ compared to 145mM Na^+ condition.

References

1. Royer, A. *et al.* Mouse model of SCN5A-linked hereditary Lenègre's disease: age-related conduction slowing and myocardial fibrosis. *Circulation* **111**, 1738–1746 (2005).
2. Martin, C. A., Zhang, Y., Grace, A. A. & Huang, C. L. H. In Vivo studies of Scn5a+/-mice modeling brugada syndrome demonstrate both conduction and repolarization abnormalities. *J. Electrocardiol.* **43**, 433–439 (2010).
3. Jeevaratnam, K. *et al.* Differences in sino-atrial and atrio-ventricular function with age and sex attributable to the Scn5a+/- mutation in a murine cardiac model. *Acta Physiol.* **200**, 23–33 (2010).
4. Van Veen, T. A. B. *et al.* Impaired impulse propagation in Scn5a-knockout mice: Combined contribution of excitability, connexin expression, and tissue architecture in relation to aging. *Circulation* **112**, 1927–1935 (2005).
5. Jeevaratnam, K. *et al.* Delayed conduction and its implications in murine Scn5a+/- hearts: Independent and interacting effects of genotype, age, and sex. *Pflugers Arch.* **461**, 29–44 (2011).
6. Bayés De Luna, A. *et al.* Current electrocardiographic criteria for diagnosis of Brugada pattern: a consensus report ☆. *J. Electrocardiol.* **45**, 433–442 (2012).
7. Veeraraghavan, R., Lin, J., Keener, J. P., Gourdie, R. & Poelzing, S. Potassium channels in the Cx43 gap junction perinexus modulate ephaptic coupling: an experimental and modeling study. *Pflugers Arch.* **468**, 1651–1661 (2016).
8. George, S. A. *et al.* Extracellular sodium and potassium levels modulate cardiac conduction in mice heterozygous null for the Connexin43 gene. *Pflugers Arch.* (2015) doi:10.1007/s00424-015-1698-0.
9. Rhett, J. M. & Gourdie, R. G. The perinexus: a new feature of Cx43 gap junction organization. *Heart Rhythm* **9**, 619–623 (2012).

10. Amusina, O., Mehta, S. & Nelson, M. E. Brugada phenocopy secondary to hyperkalemia and hyponatremia in primary adrenal insufficiency. *J Am Coll Emerg Physicians Open* **3**, e12800 (2022).
11. Ayad, S. *et al.* Fever and Hyponatremia Unmasking Brugada Pattern Electrocardiogram in a Patient With SARS-CoV-2 Infection. *Cureus* **13**, e18578 (2021).
12. Ramsaroop, K. *et al.* Suspected hyponatremia-induced Brugada phenocopy. *International Medical Case Reports Journal* **12**, 61–65 (2019).
13. Rattanawong, P. & Senthong, V. Hyponatremia induced Brugada syndrome mimicking ST segment elevation myocardial infarction. *Journal of Arrhythmia* **37**, 1377 (2021).
14. Agrawal, Y., Aggarwal, S., Kalavakunta, J. K. & Gupta, V. All that looks like “Brugada” is not “Brugada”: Case series of Brugada phenocopy caused by hyponatremia. *Journal of the Saudi Heart Association* **28**, 274–277 (2016).
15. Entz, M., King, D. R. & Poelzing, S. Design and validation of a tissue bath 3-D printed with PLA for optically mapping suspended whole heart preparations. *American Journal of Physiology - Heart and Circulatory Physiology* **313**, H1190–H1198 (2017).
16. Veeraraghavan, R., Salama, M. E. & Poelzing, S. Interstitial volume modulates the conduction velocity-gap junction relationship. *American Journal of Physiology - Heart and Circulatory Physiology* **302**, (2012).
17. Raisch, T., Khan, M. & Poelzing, S. Quantifying Intermembrane Distances with Serial Image Dilations. *J. Vis. Exp.* (2018) doi:10.3791/58311.
18. Veeraraghavan, R. *et al.* The adhesion function of the sodium channel beta subunit (β1) contributes to cardiac action potential propagation. *Elife* **7**, (2018).
19. Boukens, B. J., Rivaud, M. R., Rentschler, S. & Coronel, R. Misinterpretation of the mouse ECG: “Musing the waves of Mus musculus.” *Journal of Physiology* vol. 592 4613–4626 Preprint at https://doi.org/10.1113/jphysiol.2014.279380 (2014).

20. Patin, J. *et al.* Gap-134, a Connexin43 activator, prevents age-related development of ventricular fibrosis in Scn5a+/− mice. *Pharmacol. Res.* **159**, 104922 (2020).
21. Boengler, K. *et al.* Loss of ischemic preconditioning's cardioprotection in aged mouse hearts is associated with reduced gap junctional and mitochondrial levels of connexin 43. *Am. J. Physiol. Heart Circ. Physiol.* **292**, H1764-9 (2007).
22. Derangeon, M. *et al.* Transforming growth factor β receptor inhibition prevents ventricular fibrosis in a mouse model of progressive cardiac conduction disease. *Cardiovasc. Res.* **113**, 464–474 (2017).
23. Milman, A. *et al.* Age of First Arrhythmic Event in Brugada Syndrome. *Circ. Arrhythm. Electrophysiol.* **10**, e005222 (2017).
24. Kamakura, T. *et al.* Evaluation of the necessity for cardioverter-defibrillator implantation in elderly patients with Brugada syndrome. *Circ. Arrhythm. Electrophysiol.* **8**, 785–791 (2015).
25. Conte, G. *et al.* Clinical characteristics, management, and prognosis of elderly patients with Brugada syndrome. *J. Cardiovasc. Electrophysiol.* **25**, 514–519 (2014).
26. Kitamura, T. *et al.* Clinical Characteristics and Long-Term Prognosis of Senior Patients With Brugada Syndrome. *JACC Clin Electrophysiol* **3**, 57–67 (2017).
27. Veeraraghavan, R. *et al.* Sodium channels in the Cx43 gap junction perinexus may constitute a cardiac ephapse: an experimental and modeling study. *Pflugers Arch.* **467**, 2093–2105 (2015).
28. George, S. A. *et al.* Modulating cardiac conduction during metabolic ischemia with perfusate sodium and calcium in guinea pig hearts. *American Journal of Physiology-Heart and Circulatory Physiology* **316**, H849–H861 (2019).
29. Wu, X. *et al.* Hypernatremia and intercalated disc edema synergistically exacerbate long-QT syndrome type 3 phenotype. *Am. J. Physiol. Heart Circ. Physiol.* **321**, H1042–H1055 (2021).

30. Nowak, M. B. *et al.* Intercellular sodium regulates repolarization in cardiac tissue with sodium channel gain-of-function. *Biophys. J.* (2020) doi:10.1016/j.bpj.2020.04.014.
31. George, S. A. *et al.* Extracellular sodium dependence of the conduction velocity-calcium relationship: Evidence of ephaptic self-attenuation. *American Journal of Physiology - Heart and Circulatory Physiology* **310**, H1129–H1139 (2016).
32. Zhong, X., You, N., Wang, Q., Li, L. & Huang, C. Reverse mode of sodium/calcium exchanger subtype 1 contributes to detrusor overactivity in rats with partial bladder outflow obstruction. *Am. J. Transl. Res.* **10**, 806–815 (2018).
33. Shah, V. N., Chagot, B. & Chazin, W. J. Calcium-Dependent Regulation of Ion Channels. *Calcium Bind. Proteins* **1**, 203–212 (2006).
34. George, S. A., Calhoun, P. J., Gourdie, R. G., Smyth, J. W. & Poelzing, S. TNFα modulates cardiac conduction by altering electrical coupling between myocytes. *Front. Physiol.* (2017) doi:10.3389/fphys.2017.00334.
35. Mezache, L. *et al.* Vascular endothelial growth factor promotes atrial arrhythmias by inducing acute intercalated disk remodeling. *Sci. Rep.* **10**, 1–14 (2020).
36. Brack, K. E., Narang, R., Winter, J. & Ng, G. A. The mechanical uncoupler blebbistatin is associated with significant electrophysiological effects in the isolated rabbit heart. *Exp. Physiol.* **98**, 1009–1027 (2013).
37. Kappadan, V. *et al.* High-Resolution Optical Measurement of Cardiac Restitution, Contraction, and Fibrillation Dynamics in Beating vs. Blebbistatin-Uncoupled Isolated Rabbit Hearts. *Front. Physiol.* **11**, 464 (2020).
38. Fedorov, V. V. *et al.* Application of blebbistatin as an excitation-contraction uncoupler for electrophysiologic study of rat and rabbit hearts. *Heart Rhythm* **4**, 619–626 (2007).
39. Taglialatela, M. *et al.* Regulation of the human ether-a-gogo related gene (HERG) K^+ channels by reactive oxygen species. *Proc. Natl. Acad. Sci. U. S. A.* **94**, 11698–11703 (1997).

40. Yabuuchi, F., Beckmann, R., Wettwer, E., Hegele-Hartung, C. & Heubach, J. F. Reduction of hERG potassium currents by hyperosmolar solutions. *Eur. J. Pharmacol.* **566**, 222–225 (2007).
41. Larsen, A. P., Olesen, S.-P., Grunnet, M. & Poelzing, S. Pharmacological activation of IKr impairs conduction in guinea pig hearts. *J. Cardiovasc. Electrophysiol.* **21**, 923–929 (2010).
42. Nowak, M. B., Veeraraghavan, R., Poelzing, S. & Weinberg, S. H. Cellular Size, Gap Junctions, and Sodium Channel Properties Govern Developmental Changes in Cardiac Conduction. *Front. Physiol.* **12**, 731025 (2021).
43. Nobuhito Yanagi, Toru Maruyama, Makoto Arita, Yoshikazu Kaji, Yoshiyuki Niho. Alterations in electrical and mechanical activity in Langendorff-perfused guinea pig hearts exposed to decreased external sodium concentration with or without hypotonic insult. *Pathophysiology* **7**, 251–261 (2001).

Chapter 3

Modulation of the Action Potential Duration – Potassium Relationship by Sodium and Calcium

Modulation of the Action Potential Duration – Potassium Relationship by Sodium and Calcium

Grace A. Blair, D. Ryan King, Michael Entz II, Gregory S. Hoeker, Steven Poelzing

Introduction

The primary metric of repolarization on a cellular scale is action potential duration (APD), the amount of time between activation and repolarization of a cell or tissue. It is well established that arrhythmias can result from dysregulation of APD, regardless of whether the resulting APD is exceedingly long or short[1–5]. Drastic aberrations may lead to fatal consequences, though even minor dysregulation can result in chronic health problems such as reduced cardiac output[6]. In ventricular myocardium, APD is largely determined by a complex combination of potassium (K^+) currents, and therefore is susceptible to changes in serum K^+ concentration[7,8]. In fact, an inverse relationship between APD and extracellular K^+ has been established by prior literature, which is particularly pronounced in conditions of hyperkalemia (>5.5 mmol/L)[9,10]. Mechanistically, it has been demonstrated that during hyperkalemia, extracellular K^+ allosterically increases potassium channel conductance to the extent that it can overcome the decreased driving force for K^+ and result in excess repolarizing current, ultimately reducing APD[2].

Extracellular K^+ also has a well-established relationship with conduction velocity, which is biphasic in nature. We recently demonstrated that this relationship could be modulated by changes in extracellular sodium (Na^+) and calcium (Ca^{2+}), potentially by modulating the degree of ephaptic coupling within the tissue[11]. The following series of experiments was therefore pursued in order to determine whether Na^+ and Ca^{2+} might similarly modulate the known relationship between K^+ and APD. In analyzing the first set of experiments, we determined that modulating Na^+ had indirectly by caused APD prolongation via asystole of the perfused hearts. The second set of experiments was therefore performed in order to account for this change in

ECG rhythm during the experiment. When accounting for rhythm, we found that the APD of paced hearts with hyperkalemia-induced asystole was dependent on extracellular Na^+ and Ca^{2+} concentrations. Conversely, APD of hearts that retained intrinsic rhythm during hyperkalemia was independent of extracellular Na^+ and Ca^{2+}.

Methods

All studies were designed to adhere to the guidelines set forth by the Institutional Animal Care and Use Committee at Virginia Polytechnic Institute and State University and NIH *Guide for the Care and Usage of Laboratory Animals*.

Langendorff Perfusion

Hartley albino guinea pigs (Hilltop, Scottdale, PA, n = 31, 800-1300 g, 14-16 months old, male) were anesthetized using 4% isofluorane in O_2. After cessation of peripheral stimuli response, thoracotomy was performed. The heart was rapidly excised and cannulated for retrograde perfusion (<4 minutes), and then submerged in a 3D printed polyactic acid bath[12]. The lab standard crystalloid perfusate contained, in mM: 140 NaCl, 5.0 NaOH, 4.56 KCl, 1.25 $CaCl_2$, 5.5 Dextrose, 0.7 $MgCl_2$, and 10 HEPES, equilibrated to pH 7.4 using NaOH or HCl, as necessary. The perfusate and bath solution were oxygenated and maintained at 37.0 °C. The lab standard solution was perfused at a constant flow of 20mL/min to maintain coronary pressure of 40-60 mmHg. In order to avoid competitive stimulation with epicardial pacing, the atria were removed. During acquisition of optical maps, ventricles were paced with a unipolar AgCl wire placed on the anterior left ventricular epicardium. Pacing was delivered at a basic cycle length of 300ms with 5ms pulse duration, and stimulation strength was set at 1.5x the excitation threshold.

Electrocardiography

A volume conducted bath electrocardiogram (ECG) was recorded using AgCl electrodes for the duration of the experiment. Electrodes were placed on either side of the ventricles, with the ground lead placed at the rear of the bath. Data were sampled at 1kHz. Asystole was defined as the absence of a discernable ECG morphology (P waves, T waves, or QRS complex) during the perfusion protocol.

Optical Mapping

Following a 15 minute stabilization period in the lab standard solution, hearts were perfused with the voltage sensitive dye di-4-ANEPPS (7.5 μM), followed by a dye washout period of 10 minutes. To minimize motion artifacts, 2,3-butanedione monoxime (BDM, 7.5 μM), an electromechanical uncoupler, was included in all solutions. Light mechanical pressure was placed on the posterior surface of the ventricles as the anterior surface was positioned behind a glass imaging window in order to further stabilize the preparation during imaging. Di-4-ANEPPS was excited by a LED light source (LEX2-LZ4, BrainVision) equipped with a fiber light guide. The excitation light was emitted through a 520/35-nm band-pass filter (Brightline) and then directed onto a dichroic mirror (565nm, Chroma Technology) to be reflected onto the heart. Light emitted from the preparation was transmitted through a tandem lens system (magnification 0.63X, field of view 15.9mm x 15.9mm) and a 610nm long-pass filter (Andover Corp.) before detection by a MiCam Ultima L-type CMOS camera (SciMedia: 100x100 pixels). Optical action potentials were recorded for ~2 seconds at a 1-kHz sample rate during intrinsic activity and steady-state pacing at a 300ms basic cycle length for baseline conditions and after all subsequent interventions.

Action potential duration (APD) of the optical action potentials was calculated using a custom Matlab program as previously described[13,14]. Briefly, AT was measured from the time of maximal rate of upstroke of the first stimulated action potential in the field of view to that of the action potential of interest. APD was measured from AT to 80% repolarization.

Experimental Protocol

Two cohorts of guinea pigs were used in this study. For data depicted in figures 1 and 2, the protocol was as follows: Hearts were treated with various combinations of Na^+, Ca^{2+}, and K^+. Specifically, hearts were cannulated with one of four Na^+/ Ca^{2+} combinations: 145mM Na^+/1.25 mM Ca^{2+}; 145mM Na^+/2.00 mM Ca^{2+}; 155mM Na^+/1.25 mM Ca^{2+}; or 155mM Na^+/2.00 mM Ca^{2+}. The heart was allowed to stabilize for 15 minutes in this solution before dye loading and washout, described in "optical mapping", above. Next, hearts were perfused with each of the four K^+ concentrations (4.6, 6.4, 8.0, 10.0mM) while the Na^+/ Ca^{2+} combination was kept constant. The K^+ concentrations were randomized, and each was perfused for 10 minutes before pacing commenced (10 second duration) and optical maps were acquired.

For data depicted in figures 3-6, a second protocol was performed: All hearts were cannulated and stabilized with the baseline perfusate described above. Dye loading and washout proceeded as described above. Next, the four Na^+/Ca^{2+} combinations were perfused for 10 minutes each, all in combination with severe hyperkalemia (10mM K^+). Importantly, pacing during this protocol was sustained for 60 seconds, and four optical maps were acquired for every treatment, capturing paced beat 1, 4, 33, and 200.

Statistical Analysis

All statistical analyses were performed in Prism 8 (GraphPad Software Inc., San Diego, CA). For all data, $p<0.05$ was considered statistically significant. Data from a total of 73 hearts are reported in this study, with specific n-values for each intervention included in the figure legends. Summary data are presented as mean ± standard error, with the specific statistical test indicated in each figure legend. For both protocols, perfusate order was randomized and the experimentalist was blinded to the perfusate composition. Similarly, data analysis was blinded until completion of the study.

Results

APD dependence on Extracellular K+

As depicted in the representative APD traces and summary data in Figure 1A and B, varying Na^+ from 145mM to 155mM or Ca^{2+} from 1.25mM to 2.0mM did not result in significant changes to epicardial APD during normokalemia (4.6mM K^+) in *ex vivo* guinea pig ventricles.

After varying K^+ from normokalemia (4.6mM K^+) to moderate hyperkalemia (8.0mM K^+), we observed the expected inverse relationship between APD and extracellular K^+ for all four combinations of Na^+ and Ca^{2+}, though not to a statistically significant extent in 155 Na^+/2.0Ca^{2+} (Figure 1C). Surprisingly, when hearts were treated with severe hyperkalemia (10mM K^+), we observed that the inverse K-APD relationship was only maintained in hearts perfused with 155mM Na^+, regardless of Ca^{2+} concentration (Figure 1D). Hearts perfused with lower Na^+ (145mM) during severe hyperkalemia frequently underwent APD prolongation, regardless of Ca^{2+} concentration (Figure 1D).

Effect of ECG Rhythm during Hyperkalemia on APD

In our previous investigation of extracellular K^+ and conduction velocity, we found that hearts perfused with 145mM Na^+ during severe hyperkalemia were significantly more likely to experience asystole than those perfused with higher sodium (155mM Na^+). We therefore regrouped the APD data described above based on whether the intrinsic rhythm immediately preceding pacing and imaging was present or not (asystole). As depicted in Figure 2, we found that APD prolongation during hyperkalemia was strongly associated with the occurrence of asystole. It is also visually apparent from this figure that nearly all of the hearts perfused with 145mM Na^+ were both asystolic and had APD prolongation during hyperkalemia (relative to normokalemia).

To further investigate the impact of asystole on APD changes between normo- and hyperkalemia, we optically mapped an additional cohort of hearts that each experienced all four of the possible Na^+/Ca^{2+} combinations (in randomized order) in conjunction with 10mM K^+. Interestingly, the ratio of asystole development to maintenance of intrinsic rhythm was nearly equally distributed in the 155mM Na^+ groups (regardless of Ca^{2+}), allowing for isolation of the effects of rhythm on APD. There was no difference in APD at normokalemia (4.6mM K+) between the hearts that would ultimately develop asystole compared to those that would maintain intrinsic rhythm at 10mM K+ in the high sodium-treated group (Figure 3A). This suggests there is no predictive value for APD at normokalemia on the rhythm observed during severe hyperkalemia. In agreement with the results of cohort/protocol 1, hearts that developed asystole during hyperkalemia had significantly prolonged APD, while hearts that maintained intrinsic rhythm during hyperkalemia had no significant change in APD (Figure 3B,C).

APD adaptation during steady-state pacing

We also performed a sustained pacing protocol in cohort 2, so that optical maps were acquired during each treatment on the 1st, 4th, 33rd, and 200th paced beat. The purpose of this was twofold: (1) to evaluate whether sustained pacing would ameliorate the APD response to loss of intrinsic rhythm, and (2) to assess whether APD adaptation in response to sustained pacing was dependent on Na^+ or Ca^{2+} concentrations.

Figure 4 depicts the results of hearts that were asystolic immediately prior to pacing. When only considering asystolic hearts, there was no significant difference in APD during the first paced beat between all four Na^+/Ca^{2+} combinations (Figure 4A). However, by beat 200, asystolic hearts in high Ca^{2+} (2.0mM) conditions presented with reduced APD relative to lower Ca^{2+} (1.25mM), regardless of Na^+. This difference was not significant in the 155 Na^+ group, though this is likely

due to low n and insufficient statistical power. Notably, the APD change between beat 1 and 200 was significantly greater (more negative) in both high Ca^{2+} groups (Figure 4C).

Finally, we evaluated the rate of APD change in response to sustained pacing for all Na^{+}/Ca^{2+} combinations. For hearts asystolic immediately prior to pacing (Figure 5), sustained pacing significantly decreased APD relative to the first paced beat. This significant reduction was achieved by beat 4 in the 145mM Na^{+}/2.0mM Ca^{2+} group, by beat 33 in both 155mM Na^{+} groups, and not until beat 200 in the 145mM Na^{+}/1.25mM Ca^{2+} group. Alternatively, hearts that maintained intrinsic rhythm during severe hyperkalemia experienced no significant change in APD after sustained pacing (Figure 6). Note that only 155mM Na^{+} groups could be evaluated in this condition as no 145mM Na^{+} hearts maintained intrinsic rhythm during severe hyperkalemia.

Discussion

The inverse relationship between APD and extracellular K+ has been well documented, and multiple mechanisms for this behavior have been identified[2,9,10]. First, given the high permeability of the membrane to potassium at rest, an increase in extracellular K^{+} (and thus more positive E_k) results in a more positive resting membrane potential (RMP)[15,16]. As RMP increases, the voltage change required to reach the threshold of Na^{+} channel activation is decreased, and the slope of the action potential upstroke increases[2,17,18]. As cells more rapidly reach their maximum depolarized voltage, the APD decreases slightly. Secondly, increased extracellular K^{+} allosterically activates the rapid component of the delayed-rectifier K^{+} channel and increases hyperpolarizing current[2,15]. This ultimately yields faster phase 3 repolarization and shorter APD.

We were therefore surprised to observe APD prolongation in hearts perfused with 145mM Na^{+}/1.25 mM Ca^{2+} or 145mM Na^{+}/2.00mM Ca^{2+} during severe hyperkalemia (10mM K^{+}). Noting

that in our prior study 145mM Na^+ was associated with increased incidence of asystole[11], further inspection of this dataset revealed that indeed hearts that experienced asystole immediately prior to pacing frequently demonstrated APD prolongation once pacing had commenced. While asystole was more likely to occur in hearts perfused with 145mM Na^+, any heart, regardless of Na^+ or Ca^{2+} concentration, which did experience asystole was more likely to experience APD prolongation. Therefore, ECG rhythm, rather than Na^+ or Ca^{2+}, was the driver of the APD prolongation we observed during hyperkalemia. This phenomenon makes sense when we consider it in conjunction with investigations of cytosolic Ca^{2+} changes during bradycardia. Other labs have previously shown that bradycardia causes decreased cytosolic Ca^{2+}concentrations, which in turn increase the driving force for calcium and yield an increased Ca^{2+} duration and amplitude, and ultimately an increased APD[19]. The opposite is has also been observed – shortened APD is observed during tachycardia due to increased cytosolic Ca^{2+} which allosterically decreases the L-type calcium current[20]. We suspect that the asystole observed in the present experiments exacerbates the calcium transient increases seen during bradycardia, as the prolonged quiescent interval provides even more time for removal of Ca^{2+} from the cytosol and further increase in the L-type calcium current via allosteric disinhibition.

While this protocol revealed ways in which extracellular Na^+ indirectly modulates the APD-K relationship via rhythm control, we also wanted to assess the more direct contributions of extracellular Na^+ and Ca+ on APD during hyperkalemia. We therefore developed a second protocol to account for the rhythm changes observed during severe hyperkalemia to get a clearer idea of the contributions of Na^+ and Ca^{2+} to APD during hyperkalemia. In protocol 2, we were able to control for rhythm, as every heart was perfused with each of the four Na^+/ Ca^{2+} combinations and hearts that became asystolic were grouped and analyzed separately. Additionally, all hearts were paced for 60 seconds to achieve steady state pacing, and optical maps were analyzed for APD on beats 1, 4, 33, and 200. We were therefore able to assess how extracellular Na^+ and Ca^{2+}

modified APD adaptation in response to steady state pacing. Interestingly, we found that, in the asystolic group, APD became significantly shorter after 200 beats of pacing in the context of 2.0mM Ca^{2+} relative to 1.25mM Ca^{2+}, regardless of Na^{+} concentration. Additionally, asystolic hearts perfused with 145mM Na^{+}/2.0 Ca^{2+} were the fastest to adapt to a significantly shorter APD upon initiation of pacing, while hearts perfused with 145 Na^{+}/1.25 Ca^{2+} were the slowest. This may suggest that the lower Na^{+} conditions are more sensitive to changes in extracellular Ca^{2+}, as the rate of APD adaptation for the high Na^{+} groups did not appear to be dependent on Ca^{2+} concentration.

Translational application of this data is somewhat limited, as the greatest effects we observed due to extracellular Na^{+} and Ca^{2+} took place after multiple minutes of asystole and in the context of 10mM K^{+}, which is a severe degree of hyperkalemia infrequently seen in the clinic[23]. However, interstitial hyperkalemia is not uncommon in the context of trauma or ischemic disease and can result in severe hyperkalemia in localized regions of a given tissue[2]. With this in mind, the APD adaptation data may be insightful. Ionic conditions that allow APD to be more responsive to changes in pacing rate may be safer serum values to maintain during trauma or disease states associated with hyperkalemia. If these unique ionic conditions aid the tissue in adapting APD to rate changes in the context of local hyperkalemia, they may in turn prevent the development of large APD gradients across the heart, which are a known arrhythmogenic substrate[24,25]. In this way, the combination of physiologic sodium (145mM Na^{+}) and high calcium (2.0 Ca^{2+}) may be protective in the context of interstitial hyperkalemia.

Conclusion

In the preceding data, we've shown that, in the guinea pig heart, increased extracellular Na^{+} (155mM) is less likely to develop asystole in the context of severe hyperkalemia (10mM K+). Hearts that do develop asystole present with elongated APD on the early beats of epicardial

pacing, regardless of extracellular Na^+ or Ca^{2+}. Elongated pacing resolves the APD prolongation observed in asystolic hearts, but steady state APD is shorter in solutions with high extracellular Ca^{2+} (2.0mM). Finally, APD adaptation to pacing rate is dependent on Ca^{2+} in the context of physiologically normal Na^+ (145mM). These data suggest that higher serum Ca^{2+} may be beneficial in the context of resuscitation during severe hyperkalemia, or may be protective in the context of severe interstitial hyperkalemia due to myocardial injury.

References

1. Weiss, J. N. *et al.* Perspective: a dynamics-based classification of ventricular arrhythmias. *J. Mol. Cell. Cardiol.* **82**, 136–152 (2015).
2. Weiss, J. N., Qu, Z. & Shivkumar, K. Electrophysiology of Hypokalemia and Hyperkalemia. *Circ. Arrhythm. Electrophysiol.* **10**, (2017).
3. ten Tusscher, K. H. W. J. & Panfilov, A. V. Alternans and spiral breakup in a human ventricular tissue model. *American Journal of Physiology-Heart and Circulatory Physiology* **291**, H1088–H1100 (2006).
4. Sato, D. *et al.* Synchronization of chaotic early afterdepolarizations in the genesis of cardiac arrhythmias. *Proceedings of the National Academy of Sciences* **106**, 2983–2988 (2009).
5. Devenyi, R. A. *et al.* Differential roles of two delayed rectifier potassium currents in regulation of ventricular action potential duration and arrhythmia susceptibility. *J. Physiol.* **595**, 2301–2317 (2017).
6. Jeong, D. U. & Lim, K. M. The effect of myocardial action potential duration on cardiac pumping efficacy: a computational study. *Biomed. Eng. Online* **17**, 79 (2018).
7. Bartos, D. C., Grandi, E. & Ripplinger, C. M. Ion Channels in the Heart. *Compr. Physiol.* **5**, 1423–1464 (2015).

8. Grunnet, M. Repolarization of the cardiac action potential. Does an increase in repolarization capacity constitute a new anti-arrhythmic principle? *Acta Physiol.* **198 Suppl 676**, 1–48 (2010).
9. Yang, T., Snyders, D. J. & Roden, D. M. Rapid inactivation determines the rectification and [K+]o dependence of the rapid component of the delayed rectifier K+ current in cardiac cells. *Circ. Res.* **80**, 782–789 (1997).
10. Sanguinetti, M. C. & Jurkiewicz, N. K. Role of external Ca2+ and K+ in gating of cardiac delayed rectifier K+ currents. *Pflugers Arch.* **420**, 180–186 (1992).
11. King, D. R. *et al.* The conduction velocity-potassium relationship in the heart is modulated by sodium and calcium. *Pflugers Arch.* **473**, 557–571 (2021).
12. Entz, M., King, D. R. & Poelzing, S. Design and validation of a tissue bath 3-D printed with PLA for optically mapping suspended whole heart preparations. *American Journal of Physiology - Heart and Circulatory Physiology* **313**, H1190–H1198 (2017).
13. George, S. A. *et al.* Extracellular sodium and potassium levels modulate cardiac conduction in mice heterozygous null for the Connexin43 gene. *Pflugers Arch.* (2015) doi:10.1007/s00424-015-1698-0.
14. Entz, M., 2nd *et al.* Heart Rate and Extracellular Sodium and Potassium Modulation of Gap Junction Mediated Conduction in Guinea Pigs. *Front. Physiol.* **7**, 16 (2016).
15. Parham, W. A., Mehdirad, A. A., Biermann, K. M. & Fredman, C. S. Hyperkalemia revisited. *Tex. Heart Inst. J.* **33**, 40–47 (2006).
16. Hunter, R. W. & Bailey, M. A. Hyperkalemia: pathophysiology, risk factors and consequences. *Nephrol. Dial. Transplant* **34**, iii2–iii11 (2019).
17. Shaw, R. M. & Rudy, Y. Electrophysiologic Effects of Acute Myocardial Ischemia. *Circ. Res.* **80**, 124–138 (1997).

18. Kagiyama, Y., Hill, J. L. & Gettes, L. S. Interaction of acidosis and increased extracellular potassium on action potential characteristics and conduction in guinea pig ventricular muscle. *Circ. Res.* **51**, 614–623 (1982).
19. Suto, F. *et al.* Ventricular rate determines early bradycardic electrical remodeling. *Heart Rhythm* **2**, 293–300 (2005).
20. Dibb, K. M., Eisner, D. A. & Trafford, A. W. Regulation of systolic [Ca2+]i and cellular Ca2+ flux balance in rat ventricular myocytes by SR Ca2+, L-type Ca2+ current and diastolic [Ca2+]i. *J. Physiol.* **585**, 579–592 (2007).
21. Mahoney, B. A. *et al.* Emergency interventions for hyperkalaemia. *Cochrane Database Syst. Rev.* **2005**, CD003235 (2005).
22. Mustroph, J., Maier, L. S. & Wagner, S. CaMKII regulation of cardiac K channels. *Front. Pharmacol.* **5**, 20 (2014).
23. Celebi Yamanoglu, N. G. & Yamanoglu, A. The effect of calcium gluconate in the treatment of hyperkalemia. *Turk J Emerg Med* **22**, 75–82 (2022).
24. Kuo, C. S., Munakata, K., Reddy, C. P. & Surawicz, B. Characteristics and possible mechanism of ventricular arrhythmia dependent on the dispersion of action potential durations. *Circulation* **67**, 1356–1367 (1983).
25. Janse, M. J. & Wit, A. L. Electrophysiological mechanisms of ventricular arrhythmias resulting from myocardial ischemia and infarction. *Physiol. Rev.* **69**, 1049–1169 (1989).

Figures

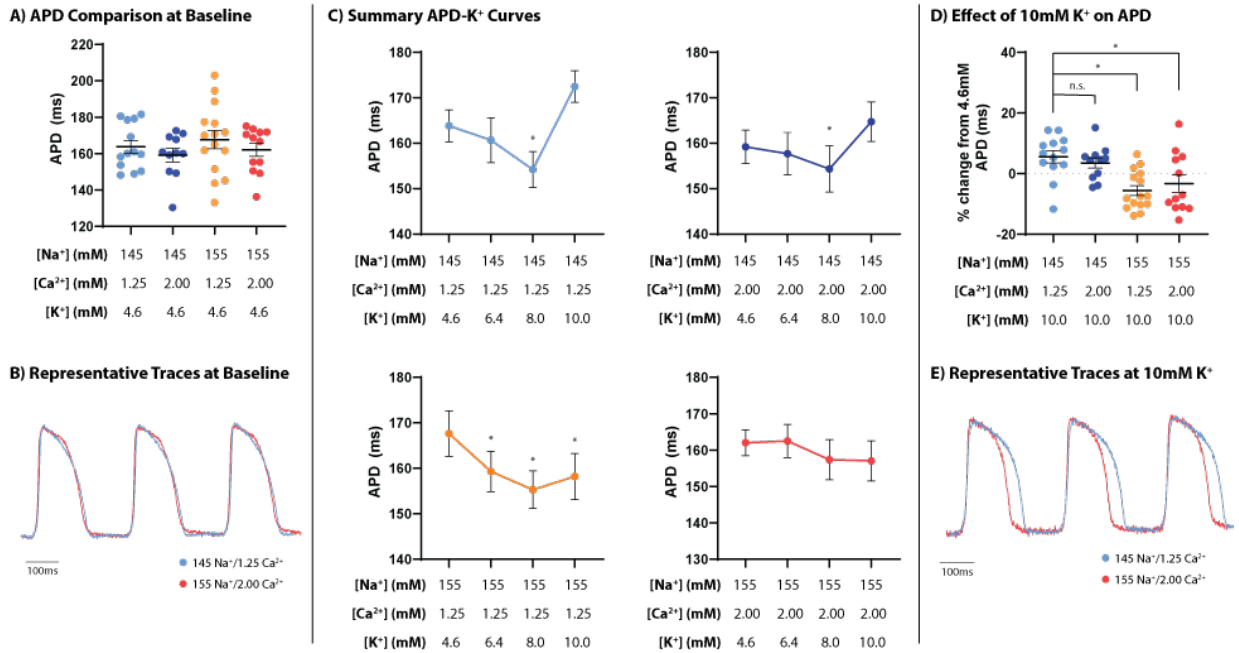

Figure 1. The APD-K+ relationship is dependent on perfusate Na^+ concentration. A) Representative action potential traces and summary data comparing APD at baseline (4.6mM K^+) across all Na^+ and Ca^{2+} perfusate combinations. B) Representative APD traces at 4.6mM K^+. C) Summary curves detailing APD as a function of K+ for all Na+ and Ca2+ perfusate combinations. D) Representative action potential traces and summary. E) Representative APD traces at 10.0mM K+ In this figure, * denotes $p<0.05$ as determined by a repeated measures ANOVA applying Dunnett's correction for multiple comparisons to the left most column in each panel.

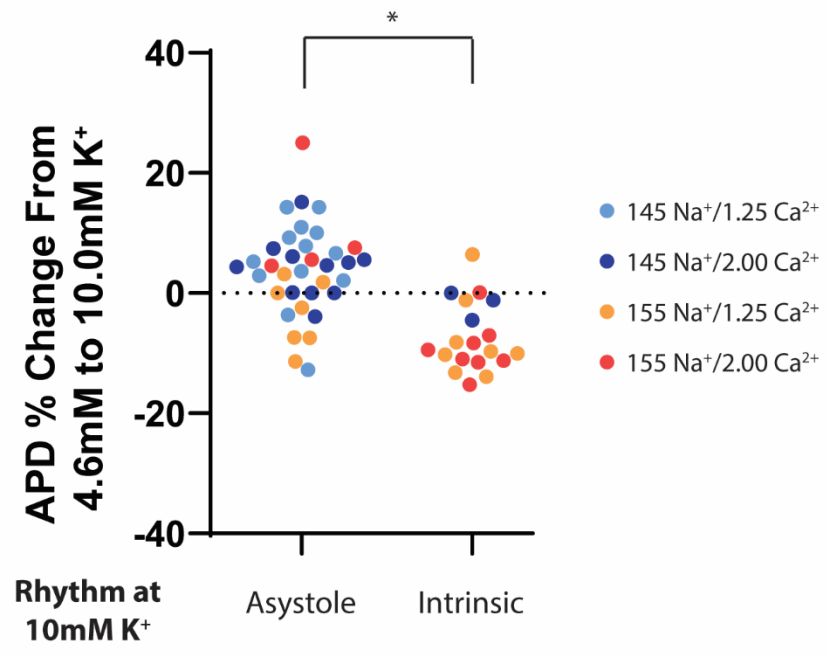

Figure 2. Development of asystole during hyperkalemia yields increased APD upon initiation of pacing. Perfusion of 145mM Na^+ nearly always results in asystole during hyperkalemia, but 155 mM Na^+ preserves intrinsic rhythm in about half of all hearts. * denotes $p<0.05$ as determined by unpaired Student's t-test.

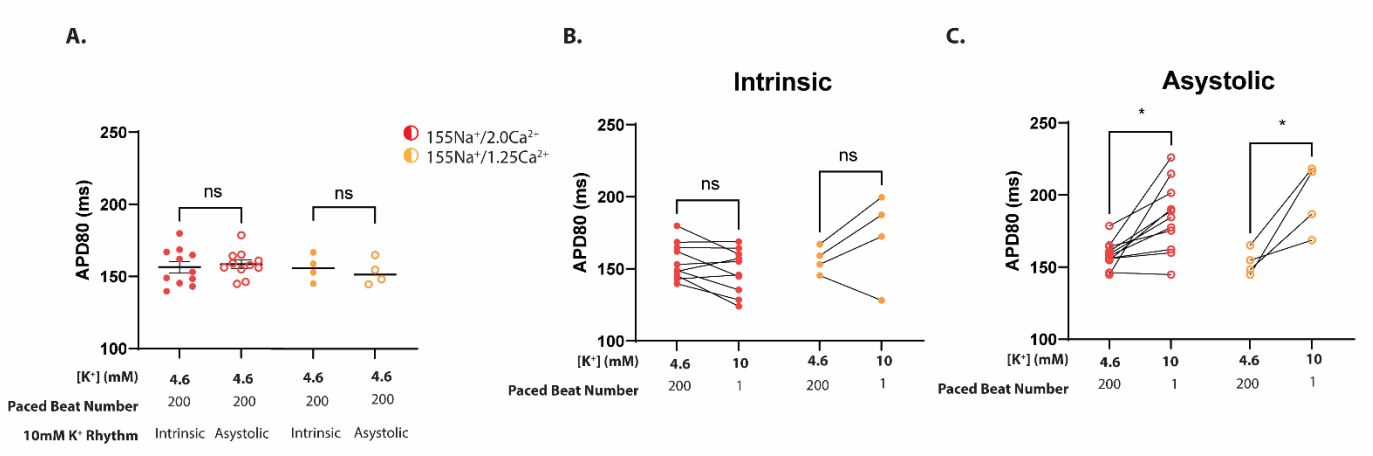

Figure 3. Asystole during hyperkalemia results in APD prolongation on beat 1, independent of Ca^{2+}. A) Comparison of baseline APD in hearts prior to their perfusion with 10mM K^+, data separated by development of asystole or maintained intrinsic rhythm during perfusion. B) Elevating K^+ does not result in significant changes to APD in intrinsic hearts C) Elevating K+ results in significant APD prolongation in asystolic hearts. In this figure, * denotes $p<0.05$ as determined by a paired Student's t-test.

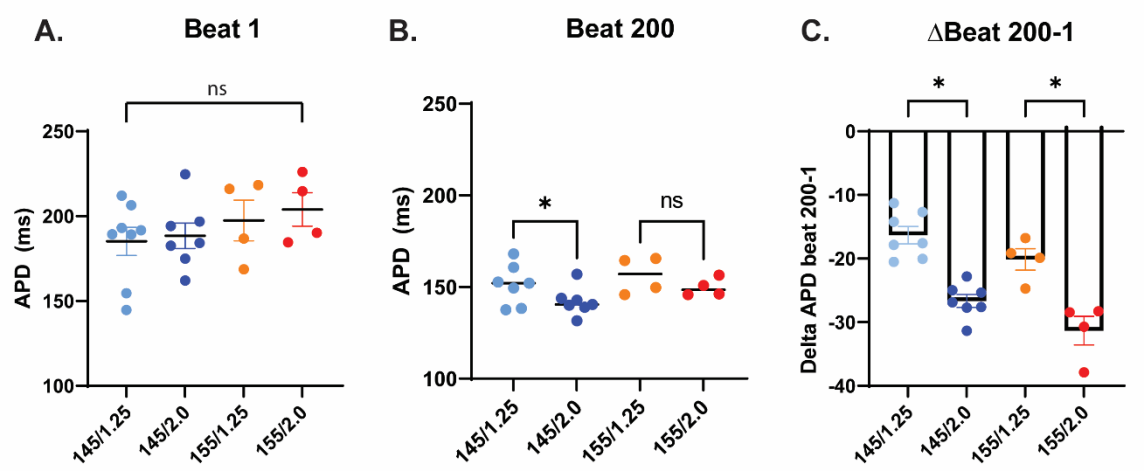

Figure 4. Steady state pacing after hyperkalemia-induced asystole results in preferential APD shortening in high Ca^{2+} perfusates. A) Comparison of APD in all Na^{+}/Ca^{2+} combinations during beat 1 of pacing after hyperkalemia-induced asystole. B) Comparison of APD in all Na^{+}/Ca^{2+} combinations during beat 200 of pacing after hyperkalemia-induced asystole. C) Change in APD between beats 1 and 200 after asystole. * denotes $p<0.05$ as determined by a repeated measures ANOVA applying Dunnett's correction for multiple comparisons.

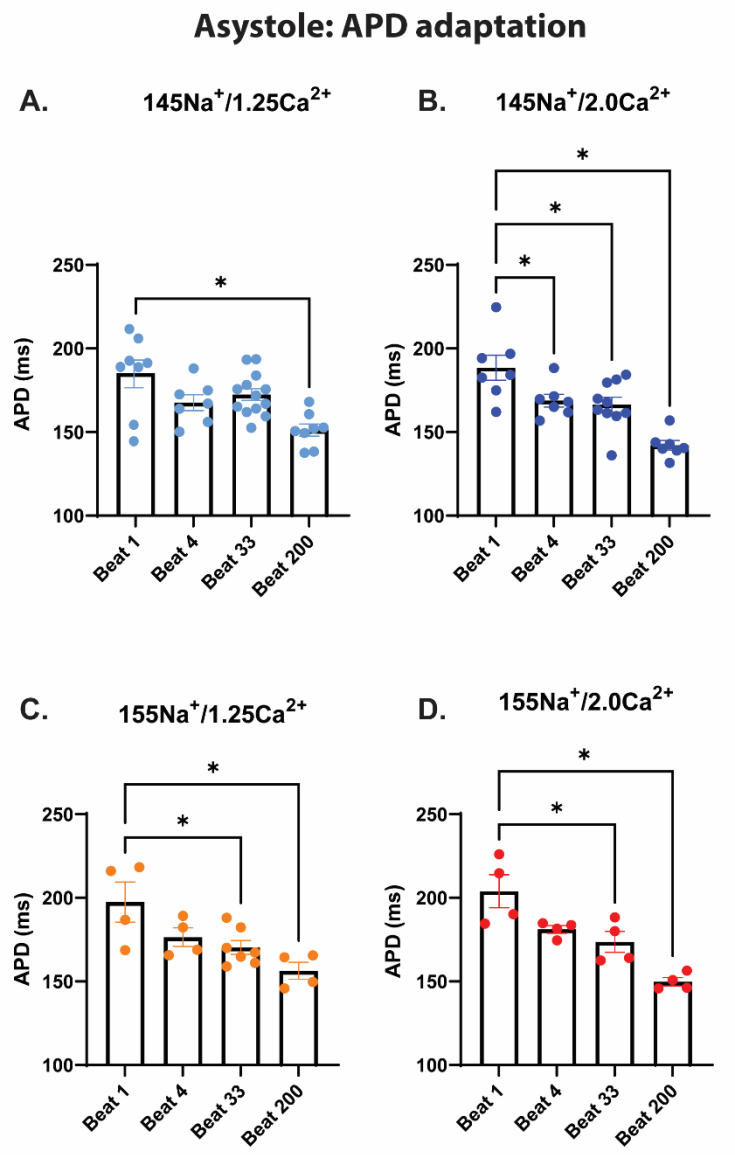

Figure 5. APD adaptation to steady state pacing after hyperkalemia-induced asystole is dependent on Na^+ and Ca^{2+} concentration. A) Comparison of APD during beat 1,4,33, and 200 of pacing after asystole in 145mM Na+/ 1.25mM Ca^{2+} solution. B) Comparison of APD during beat 1,4,33, and 200 of pacing after asystole in 145mM Na+/ 2.0mM Ca^{2+} solution. C) Comparison of APD during beat 1,4,33, and 200 of pacing after asystole in 155mM Na+/ 1.25mM Ca^{2+} solution. D) Comparison of APD during beat 1,4,33, and 200 of pacing after asystole in 155mM Na+/ 2.0mM Ca^{2+} solution. * denotes $p<0.05$ as determined by a repeated measures ANOVA applying Dunnett's correction for multiple comparisons.

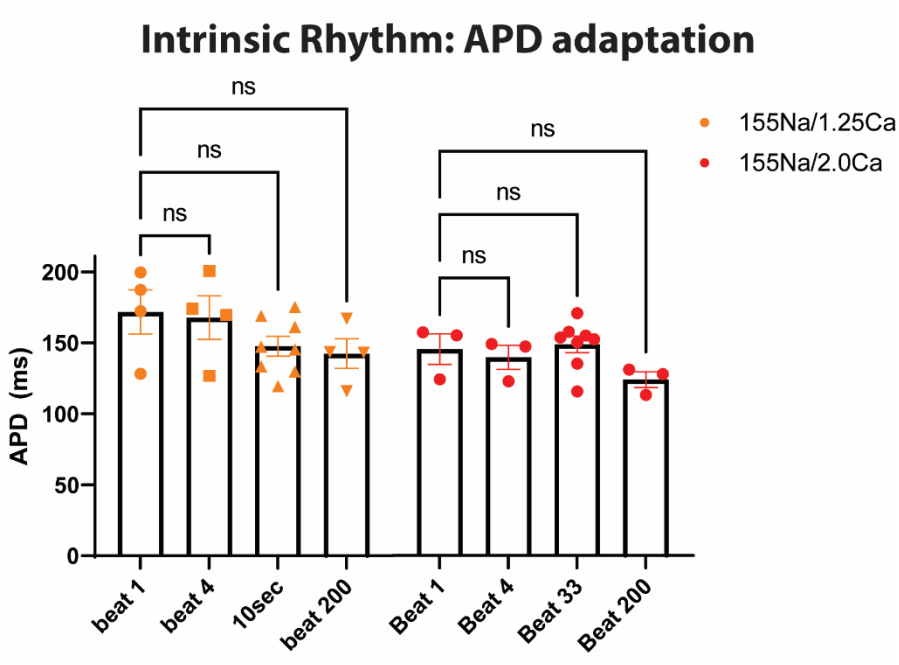

Figure 6. APD does not adapt to steady state pacing after maintenance of intrinsic rhythm during hyperkalemia. * denotes $p<0.05$ as determined by a repeated measures ANOVA applying Dunnett's correction for multiple comparisons.

Chapter 4

Sequence-dependent repolarization is modulated by endogenous APD gradients rather than electrical coupling in ventricular myocardium

Sequence-dependent repolarization is modulated by endogenous APD gradients rather than electrical coupling in ventricular myocardium

Grace A. Blair, Madeline Depman, William Adams, Elina Baltins, Gregory S. Hoeker, Seth Weinberg, Steve Poelzing

This manuscript has been submitted for review to the Journal of the American Heart Association

Abstract

Background: Previous studies have suggested the relationship between electrical activation time (AT) and action potential duration (APD) in the heart is dependent on electrotonic coupling, but this has not been directly tested. The purpose of this study was to determine whether acute changes in electrical coupling, or other determinants of conduction or repolarization, modulate the AT-APD relationship.

Methods: Langendorff-perfused guinea pig hearts were epicardially paced and optically mapped after treatment with the gap junction uncoupler carbenoxolone, ephaptic uncoupler mannitol, ephaptic enhancer dextran 2MDa, sodium channel inhibitor flecainide, and inhibitor of the rapid component of the delayed rectifier potassium channel E4031. The slope and coefficient of determination (R^2) of the AT-APD relationship was obtained through linear regression analysis.

Results: The AT-APD slope was not changed by any intervention after 15 minutes of perfusion. In contrast, while R^2 did not change with carbenoxolone, it decreased with mannitol, increased with dextran 2MDa, increased with flecainide, and decreased with E4031. Surprisingly, changes in conduction velocity, APD, or standard deviation of APD induced by each of these interventions did not consistently correlate with changes in R^2. Mathematical simulations predict that the endogenous APD gradient, rather than electrical coupling, is a stronger determinant of the AT-APD relationship.

Conclusion: Taken together, past and present studies suggest that cellular remodeling is likely responsible for previously reported AT-APD changes in response to chronic interventions, and

acute changes in the AT-APD slope and R^2 may be more dependent on endogenous APD gradients than cell-cell electrical coupling, determinants of conduction, or repolarization.

Introduction

Cardiac repolarization is partially dependent on the sequential nature of cellular activation, as demonstrated by experimental data from a variety of tissue preparations[1–6]. Specifically, an inverse relationship between activation time (AT) and action potential duration (APD) is frequently observed, in which cells proximal to the origin of activation have longer APDs and those distal have progressively shorter APDs. Functionally, this behavior is important for synchronizing repolarization across the tissue, minimizing temporal gradients of repolarization that may contribute to arrhythmia susceptibility[7,8]. Maintenance of this relationship is therefore a critical homeostatic behavior, and identification of the fundamental mechanism behind this behavior is of key importance for better understanding arrhythmogenic disease states.

The inverse relationship between AT and APD is generally assumed to be due to electrotonic coupling[1,3,9]. By this mechanism, as an electrical wavefront propagates along the tissue, cells with earlier activation times repolarize sooner and create a voltage potential gradient with downstream cells. Depolarizing current then flows upstream towards the origin of activation via gap junctional coupling. Repolarization time and APD are thereby prolonged in cells proximal to the site of activation and shortened in cells distal to the stimulus. While some mathematical models lend support to the theory that electrotonic interaction can modulate repolarization[10], experimental studies have not been designed to directly assess the role of electrical coupling on modulating the AT-APD gradient. More frequently, previous studies were developed for quantifying the AT-APD relationship for the purpose of assessing cardiac memory[1–4].

The field of cardiac memory investigates the activation sequence-dependent nature of repolarization and APD, but employs chronic interventions, lasting from hours in *ex vivo*

preparations to weeks in *in vivo* models. To quantify the effect of activation sequence on repolarization, previous studies measured the slope and coefficient of determination (R^2) of the linear regression between AT and APD. In such analyses, slope is interpreted as the electrotonic influence on APD as a function of AT, while R^2 is interpreted as the uniformity of the AT-APD relationship across the tissue. Prior studies suggest these parameters can be modulated using chronic pacing regimes or pharmacological interventions. For example, Chan et al. reported that inhibition of the small-conductance calcium-activated potassium current (I_{Kas}) reverses the AT-APD slope polarity and increases R^2 in isolated rabbit ventricles[2]. This suggests that the I_{Kas} current is partially responsible for maintaining the inverse AT-APD relationship and modulates the uniformity of this relationship across the ventricle. Other groups demonstrated that altering pacing rates or pacing sites can modulate sequence-dependent changes in the action potential over the course of chronic intervention[1,4]. However, the time course of such protocols suggests that these results are due to cellular adaptation and/or protein remodeling rather than acute alterations in electrical coupling. Indeed, after four weeks of *in vivo* epicardial pacing, Jeyaraj et al. measured sequence-dependent changes in cellular currents, such as reduced transient outward potassium, slow delayed rectifier potassium, and L-type calcium currents in early-activated cells relative to late-activated cells [4]. The purpose of the present study was to determine whether acute modulation of key determinants of conduction or repolarization alters the epicardial AT-APD relationship.

Methods

All studies were designed to adhere to the guidelines set forth by the Institutional Animal Care and Use Committee at Virginia Polytechnic Institute and State University and NIH *Guide for the Care and Usage of Laboratory Animals*.

Langendorff Perfusion

Hartley albino guinea pigs (Hilltop, Scottdale, PA, n = 31, 800-1300 g, 14-16 months old, male) were anesthetized using 4% isofluorane in O_2. After cessation of peripheral stimuli response, thoracotomy was performed. The heart was rapidly excised and cannulated for retrograde perfusion (<4 minutes), and then submerged in a 3D printed polyactic acid bath[11]. The lab standard crystalloid perfusate contained, in mM: 140 NaCl, 5.0 NaOH, 4.56 KCl, 1.25 $CaCl_2$, 5.5 Dextrose, 0.7 $MgCl_2$, and 10 HEPES, equilibrated to pH 7.4 using NaOH or HCl, as necessary. The perfusate and bath solution were oxygenated and maintained at 37.0 °C. The lab standard solution was perfused at a constant flow of 20mL/min to maintain coronary pressure of 40-60 mmHg. In order to avoid competitive stimulation with epicardial pacing, the atria were removed. During acquisition of optical maps, ventricles were paced with a unipolar AgCl wire placed on the anterior left ventricular epicardium. Pacing was delivered at a basic cycle length of 300ms with 5ms pulse duration, and stimulation strength was set at 1.5x the excitation threshold.

Using the lab standard perfusate as a baseline, hearts were treated with one of the following interventions for 15 minutes[12]. Gap junctions were inhibited by perfusion with the gap junction uncoupler carbenoxolone (CBX, 30 μM), which has previously been shown to decrease ventricular conduction velocity (CV)[13]. The osmotic agent mannitol (26.1 g/L) has been previously shown to widen the intercalated disc (ID) nanodomain known as the perinexus and decrease CV[14]. Dextran 2MDa (40 g/L), another osmotic agent, has been previously shown to narrow the perinexus and increase CV[15]. Flecainide (0.5 μM) was used to inhibit the cardiac isoform of the voltage gated sodium channel ($Na_v1.5$) and decrease CV[14], without affecting gap junctional coupling via connexin 43[16]. Finally, E4031 (1 μM), an inhibitor of the rapid component of the delayed rectifier potassium channel (hERG) was used to increase average APD without modifying CV, an effect that has been demonstrated at pacing rates greater than 250ms[17,18].

Electrocardiography

A volume conducted bath electrocardiogram (ECG) was recorded using AgCl electrodes for the duration of the experiment. Electrodes were placed on either side of the ventricles, with the ground lead placed at the rear of the bath. Data were sampled at 1kHz.

Optical Mapping

Following a 15 minute stabilization period in lab standard perfusate, hearts were perfused with the voltage sensitive dye di-4-ANEPPS (7.5 μM), followed by a dye washout period of 10 minutes. To minimize motion artifacts, blebbistatin (10 μM), an electromechanical uncoupler, was added to all solutions following dye washout. Light mechanical pressure was placed on the posterior surface of the ventricles as the anterior surface was positioned behind a glass imaging window in order to further stabilize the preparation during imaging. Di-4-ANEPPS was excited by a LED light source (LEX2-LZ4, BrainVision) equipped with a fiber light guide. The excitation light was emitted through a 520/35-nm band-pass filter (Brightline) and then directed onto a dichroic mirror (565nm, Chroma Technology) to be reflected onto the heart. Light emitted from the preparation was transmitted through a tandem lens system (magnification 0.63X, field of view 15.9mm x 15.9mm) and a 610nm long-pass filter (Andover Corp.) before detection by a MiCam Ultima L-type CMOS camera (SciMedia: 100x100 pixels). Optical action potentials were recorded for ~2 seconds at a 1-kHz sample rate during intrinsic activity and steady-state pacing at a 300ms basic cycle length for baseline conditions and after all subsequent interventions.

Activation time (AT) and action potential duration (APD) of the optical action potentials were calculated using a custom Matlab program as previously described[19,20]. Briefly, AT was measured from the time of maximal rate of upstroke of the first stimulated action potential in the field of view to that of the action potential of interest. Conduction vectors were then calculated using an algorithm by Bayley et. al[21]. As the majority of the resulting conduction vectors were in

the transverse direction, this metric yields higher confidence than longitudinal CV and therefore all summary CV data refers to conduction measured in the transverse direction of propagation (CVT), as previously described[22]. All APD values were measured from AT to 90% repolarization.

Statistical Analysis

All statistical analyses were performed in Prism 9 (GraphPad Software Inc., San Diego, CA). For all data, $p<0.05$ was considered statistically significant. Data from a total of 31 hearts are reported in this study, with specific n-values for each intervention included in the figure legends. Simple linear regression was performed using Matlab (R2021a) for each acquired optical map for the calculation of AT-APD slope and R^2. The paired Student's t-test was used for statistical comparisons of CV, APD, standard deviation of APD, slope, and R^2 before and after intervention.

Computational Modeling

We simulated a 201-cell cable (one-dimensional tissue, 2cm long) comprised of individual myocytes coupled via gap junctions and ephaptic coupling, as in prior work by us and others[23–28]. We accounted for non-uniform sodium channel subcellular localization by spatially discretizing each cell into an axial membrane patch along the length of the cell and two ID membrane patches at the ends of the cell. It was assumed that 90% of sodium channels were localized in the ID patches[29–31]. A cleft radial resistance, inversely proportional to the intercellular cleft width (W_p), governed extracellular potentials at the ID and cleft. ID sodium currents and diffusion with the bulk extracellular space governed the extracellular cleft sodium ion concentration ($[\mathrm{Na}^+]_e^{cleft}$) dynamics, which also depended on the cleft volume (and therefore on W_p). We utilized an established human ventricular myocyte ionic model[32] to represent individual ion channel dynamics.

We modeled three conditions of imposed repolarization gradients by scaling the conductance of the rapid component of the delayed rectifier potassium current (I_{Kr}) as a function of cell number: no gradient (0ms/2cm), moderate gradient (30ms/2cm), and steep gradient (50ms/2cm). For no gradient, the I_{Kr} current scaling factor is 1, i.e., baseline conditions, for all cells. For the moderate gradient, the I_{Kr} current scaling factor linearly increased from 0.875 (cell 1) to 1.125 (cell 201). For the steep gradient, the I_{Kr} current scaling factor linearly increased from 0.625 (cell 1) to 1.375 (cell 201). Note that a scaling factor less than 1 denotes an I_{Kr} current conductance less than baseline. Full model equations, parameters, and simulation codes can be found in our prior work[23,28].

Baseline conditions of tissue simulations correspond with W_p of 20 nm, gap junction conductance (g_{gap}) of 153 nS, and 100% I_{Na} current conductance, where we note that the original model I_{Na} current conductance value was increased by a factor of 7 to approximately match experimental CV measurements. Numerical experiments considered perturbations of (i) reduced gap junctional coupling (decreasing g_{gap} to 77 nS), (ii) reduced ephaptic coupling (increasing W_p to 40 nm), and (iii) reduced I_{Na} conductance (decreasing I_{Na} conductance to 50%), relative to baseline conditions. Electrical activity was simulated by either initiating a propagating wave or simultaneously activating the entire cable at once, in both cases at a cycle length of 500 ms. A propagating wave was initiated in the cable center by pacing cells 99-103, and the cable was simultaneously activated by pacing all cells (1-201). For each simulation, APD was calculated by taking the difference between the action potential repolarization time (defined as the time membrane voltage (V_m) crossed below -60 mV) and activation time (above -60 mV) for each cell. Results below depict only cells 25-175 in order to remove edge-boundary conditions from analysis and interpretation of the strand model.

Results

Optical Mapping

Time Control

Time control consisted of 15 minutes of baseline perfusion solution; representative AT and APD maps from the anterior epicardium of guinea pig ventricular myocardium can be seen in Figure 1A. Representative AT-APD plots are depicted in Figure 1B, wherein each point displays the AT and APD of a single pixel of the corresponding optical maps. Summary data (Figure 1C) demonstrates that 15 minutes of baseline perfusion did not significantly change conduction velocity (CV). Average APD increased modestly but significantly by 4.9 ± 2.6ms, though there was no significant change in the standard deviation of APD across the anterior-ventricular imaging surface. Neither the slope nor R^2 of AT-APD were significantly different after 15 minutes of baseline perfusion (Figure 1C).

Carbenoxolone

Electrotonic coupling via gap junctions has previously been hypothesized to be the primary determinant of the AT-APD relationship. Therefore, our first intervention was to disrupt this coupling modality using the gap junction inhibitor carbenoxolone (CBX). Representative optical maps of AT and APD in Figure 2A demonstrate that CBX resulted in both slowed conduction, as expected, and decreased average APD. Representative AT-APD plots before and after CBX treatment are depicted in Figure 2B. Specifically, gap junctional inhibition significantly decreased CV by 6.4±0.9 cm/s, and decreased average APD slightly but significantly by 3.9±2.1ms (Figure 2C), which was also a significant reduction relative to the change in APD observed in the time control group (-4.9 ± 2.6ms). The standard deviation of APD significantly increased by 1.4±0.4ms. Surprisingly, neither slope nor R^2 changed significantly after CBX treatment (Figure 2C).

Mannitol

Experimental evidence suggests that ephaptic coupling, a mechanism of intercellular electrical communication, arises from the generation of relatively large extracellular fields in regions of the ID that are closely apposed and densely express ion channels. One such region is the gap junction-adjacent perinexus[33]. Mannitol, a clinically relevant osmotic agent, has previously been shown to reduce CV by inducing interstitial edema and widening the perinexal nanodomain, thereby reducing ephaptic coupling[34]. Thus, mannitol was perfused to determine whether ephaptic coupling modulates the AT-APD relationship. The resulting representative activation and APD maps are presented in Figure 3A, with the resulting AT-APD plots in Figure 3B. Treatment with mannitol in this study significantly reduced CV by 5.9±3.3 cm/s, and significantly increased APD relative to baseline by 16.4±7.6ms (Figure 3C). APD also significantly increased relative to the APD change measured after time control (10.7±3.3ms). The standard deviation of APD significantly increased by 4.4±2.6ms after mannitol treatment as well (Figure 3C). As seen in in Figure 3B and 3C, the slope of the AT-APD relationship was not significantly different after mannitol treatment, but R^2 was significantly reduced by 0.2±0.1.

Dextran 2MDa

As a complement to the mannitol study, isolated hearts were next treated with dextran 2MDa. Our lab has previously demonstrated that 15 minutes of perfusion with dextran 2MDa results in narrowed perinexi between cardiomyocytes and enhances ephaptic coupling[15]. As seen in the representative AT and APD maps in Figure 4A, 15 minutes of perfusion with dextran 2MDa did not significantly change CV or the standard deviation of APD in this study. However, dextran 2MDa did significantly increase APD by 15.5 ± 10.6ms relative to baseline (Figure 4C). This

increase in APD was significantly greater than the APD change measured after time control (10.6±4.9ms). Representative AT-APD plots are shown in Figure 4B, and demonstrate that slope did not significantly change after dextran 2MDa treatment. Interestingly, R^2 significantly increased by 0.1±0.06 (Figure 4C), which is opposite of the R^2 change observed after treatment with mannitol.

Flecainide

Sodium current is a critical component of both canonical mechanisms of conduction via gap junctions as well as via ephaptic coupling. Therefore, we next treated isolated hearts for 15 minutes with the sodium channel inhibitor flecainide as another means of reducing electrical coupling and slowing conduction without affecting gap junctional coupling. The resulting AT and APD maps of the anterior epicardium are depicted in Figure 5A. After flecainide treatment, CV significantly decreased relative to baseline by 3.5±1.4cm/s, as expected (Figure 5C). Further, flecainide did not significantly change average APD, and the change in average APD before and after flecainide treatment was not significantly different from the change in average APD over time in the control group. Additionally, the standard deviation of APD and the slope of the linear regression of the AT-APD relationship were not significantly different relative to baseline after flecainide treatment (Figure 5C). Unexpectedly, R^2 significantly increased relative to baseline by 0.2±0.1 after treatment with flecainide (Figure 5B,C).

E4031

Finally, tissue was treated with the hERG inhibitor E4031 in order to explore the effects of increasing APD without altering CV. Treatment with E4031 did not significantly change CV relative

to baseline, as expected (Figure 6A,C). The average APD after E4031 treatment increased significantly from baseline by 23.5± 3.6ms (Figure 6C), which was also a significant increase relative to the change recorded in time control (18.5±1.9ms). The standard deviation of APD increased (Figure 6C), though this was not statistically different from baseline. Representative AT-APD plots in Figure 6B demonstrate no change in the slope of the line of regression after treatment. However, R^2 decreased significantly by 0.1±0.1 (Figure 6C).

Mathematical Model

At present, it is experimentally difficult to separate endogenous APD from the effects of propagation on APD in an isolated heart preparation. Therefore, we used a computational model to explore the role of endogenous APD gradients on the AT-APD relationship. APD was measured after stimulation from either the center of the strand with propagation to the ends of the strand, or simultaneous stimulation of all the cells in the strand. Henceforth, the APD gradient observed during simultaneous stimulation will be referred to as the "endogenous" APD gradient, while the APD resulting from wavefront propagation will be "propagation APD". The diagrams provided in Figure 7A and 7C are for illustrative purposes only and do not depict actual data resulting from the mathematical simulations, because, as will be discussed below, the changes to APD by any intervention were often smaller than 4ms. The strand modelled in Figure 7 has an endogenous APD gradient of 30ms over 2cm, which approximates the experimentally measured APD gradient across the anterior ventricles of the guinea pig heart[35]. Note that the results shown exclude the first and last 25 cells in order to remove boundary effects from interpretation of the model.

The results of reducing gap junctional coupling, widening the perinexal cleft, or reducing sodium current on AT and APD after center stimulation of the strand are shown in Figure 7. In all conditions, APD increases in cells proximal to the stimulation site, but this change attenuates at

cells more distal to the stimulus (Figure 7B). For baseline, reduced gap junctional coupling, and reduced ephaptic coupling, propagation APD becomes shorter than endogenous APD at the distal end of each strand. In contrast, reducing I_{Na} minimizes the shortening of propagation APD relative to endogenous APD at the distal end of the strand. Reduced I_{Na} also results in an upward shift in the APD curve for the entire strand.

Figure 7D is the subtraction of the simultaneously stimulated APD (endogenous) from the APD measured during stimulation from the center of the strand (propagation), which represents the sequence-dependent change in APD. As noted previously[3], the greatest prolongation of APD is observed proximal to the stimulus, regardless of the intervention. Reducing gap junctional coupling (Figure 7D, yellow line) modestly increases sequence-dependent APD as evidenced by a small upward shift in ΔAPD. Increasing cleft width (blue line) or inhibiting I_{Na} (pink line) similarly and modestly increases sequence-dependent APD. However, the interventions do not substantively change the shape of the curves.

Interestingly, there is a differential response in ΔAPD depending on whether the electrical wavefront propagates toward longer or shorter APDs as depicted with solid and dashed lines, respectively, in Figure 7D. ΔAPD is consistently more negative when the electrical wavefront is propagating toward longer APDs, regardless of coupling intervention.

A second simulation was developed in order to evaluate the effect of endogenous APD gradient magnitude on sequence-dependent changes in APD. As depicted in Figure 8, this model includes three simulations of endogenous APD gradients varying from 0 to 50ms over the 2cm strand length without changing electrical coupling. Once again, when stimulating from the center of the strand, APD increases proximal to the site of stimulation regardless of the endogenous APD gradient magnitude. Figure 8B demonstrates that while APD in the center-proximal cells elongate to a similar degree, the degree of change for distal cells is dependent on both the magnitude of the endogenous APD gradient and the direction of electrical wavefront propagation.

As the wavefront propagates towards cells with longer APDs, ∆APD becomes more negative. In other words, APD shortens more when wavefronts propagate up an APD gradient. When the wavefront propagates towards cells with a shorter APD, ∆APD becomes less negative, i.e. APD does not shorten as much when wavefronts propagate down an APD gradient. This aligns with the theory that wavefront activation itself homogenizes APD across the tissue[10]. Importantly, the largest change in APD in these simulations with endogenous gradients of up to 50ms/2cm is less than 4ms, which is a relatively small change in APD.

Discussion

This study sought to investigate the relationship between ventricular epicardial activation time (AT) and action potential duration (APD). It has previously been reported that there is an inverse relationship between epicardial AT and APD, wherein the longest APD is observed near the stimulus and progressively shorter APDs are found in cells more distal to the stimulus[1–3,5,6]. This relationship has been quantified using a linear regression of the epicardial measurements of AT and APD, and the resulting slope and coefficient of determination (R^2) have been reported as a means of evaluating the relationship's dependence on various interventions. In such analyses, slope is interpreted as the electrotonic dependence of APD on changes in AT, while R^2 is interpreted as the uniformity of the AT-APD relationship across the epicardium.

In the present series of experiments, our data consistently demonstrate an inverse relationship between AT and APD measured from the ventricular epicardium of guinea pig hearts over 15 minutes of several treatment conditions, which aligns with previous studies in a variety of animal models or human hearts[1–3,5,6]. However, our data suggest that acutely modulating AT by targeting various determinants of conduction and repolarization does not consistently or predictably modify this relationship.

Electrotonic Coupling:

To our knowledge, this is the first report where the AT-APD relationship is quantified in response to acute gap junctional uncoupling. If electrotonic coupling is indeed responsible for the APD response to AT, acute changes in gap junctional coupling should modify slope and/or R^2. We hypothesized the slope would become less negative and R^2 would decrease with gap junctional uncoupling, but we did not observe either outcome in our experiments. The data therefore do not support gap junctional coupling as a major acute determinant of the measurable AT-APD relationship in guinea pig ventricular myocardium.

Ephaptic Coupling:

Ephaptic coupling (EpC) is a form of electrical communication that is dependent on ionic transfer through extracellular nanodomains. EpC occurs when the activation of a sodium current on one side of a small intercellular cleft (such as the intercalated disc (ID) nanodomain known as the perinexus[33]) decreases the extracellular cleft potential[30]. This depolarizes the abutting cell by trans-activating sodium channels and thus facilitates conduction. Accordingly, widening junctional spaces like the perinexus can theoretically minimize these membrane potential changes and decrease conduction velocity (CV). The next series of experiments utilized the osmotic agent mannitol, previously shown to widen the perinexal cleft, reduce EpC, and slow conduction without changing gap junctional coupling[14]. We anticipated that the AT-APD slope would decrease, while R^2 would remain constant. This was hypothesized because AT, but not APD, was predicted to increase with the osmotic stress of mannitol treatment. While we did not observe any change in slope after mannitol treatment, we did measure a significant decrease in R^2. These changes were unexpected, as was the finding that mannitol increased APD in whole-heart preparations. The present increase in APD is in contrast to previous reports that mannitol does not significantly alter APD in whole-heart preparations, though it has been reported to reduce the hERG current in isolated cells[24,36–38]. This phenomenon may help explain the similarity of the AT-APD results

between the mannitol and E4031- treated hearts. The most notable difference between this and previous whole-heart studies is that the present study used blebbistatin as the electromechanical uncoupler rather than 2,3-Butanedione monoxime (BDM). The combined effects of mannitol and electromechanical uncouplers on APD require further investigation. More salient to this discussion is the observation that the standard deviation of APD also increased as R^2 decreased after hearts were treated with mannitol. Therefore, one possible explanation for why mannitol decreased R^2 could be attributed to the enhancement of APD heterogeneity, as evidenced by an increased APD standard deviation in this particular experimental approach. Additionally, while mannitol has a demonstrated osmotic effect of widening the perinexus[34], mannitol inhalation has also been shown to induce an inflammatory response *in vivo*[39–41]. Although we perfused mannitol in an *ex vivo* preparation, we cannot exclude the potential role mannitol may have on inflammation.

One way to further test whether EpC modulates the AT-APD relationship would be to increase EpC by narrowing clefts and test for the hypothesized R^2 increase. To that effect, dextran 2MDa was used as a means of osmotically enhancing EpC without modulating gap junctional coupling. While we did not measure a significant change in slope, we did measure a significant increase in R^2. Unlike mannitol however, a corresponding decrease in APD standard deviation was not observed. The opposing changes in R^2 with mannitol and dextran 2MDa might suggest that EpC mechanistically modulates the AT-APD relationship, but such a conclusion is premature, as explained below with discussion of the flecainide experiments.

Sodium Channel Mediated Conduction:

The role of sodium channels in conduction is well-established. Additionally, EpC is highly dependent on the localization of voltage gated sodium channels to the gap junction-adjacent perinexus in the ID[33]. In the present study, sodium channels were inhibited with flecainide, a drug which does not alter gap junctional coupling via connexin 43[16]. Our data demonstrate that sodium channel inhibition slowed conduction and did not change AT-APD slope, similar to mannitol.

However, unlike mannitol, sodium channel inhibition did not change APD heterogeneity, as measured by the standard deviation of APD. Furthermore, flecainide increased R^2, which is opposite to the effects of mannitol. In short, the flecainide experiments might suggest that EpC is not a direct modulator of the AT-APD relationship. It has been demonstrated that flecainide can also agonize sarcoplasmic reticulum ryanodine receptors[42], and it is therefore possible that the increase in R^2 is unrelated to the effects of conduction and instead dependent on off target effects of the compound.

Inward Rectifier Potassium Currents:

The hERG inhibitor E4031 has been reported to modify APD, however some have suggested modulating hERG may[17] or may not[43] change conduction under very specific conditions that were not explored here. In this study, E4031 did not change CV. Importantly, our observation that hERG inhibition with E4031 prolongs APD without increasing the standard deviation of APD is consistent with other reports in the same guinea pig animal model[44]. We therefore hypothesized that hERG inhibition would shift the AT-APD curve upwards without affecting either slope or R^2. As expected, treatment with E4031 did not significantly change the AT-APD slope. However, this intervention significantly decreased R^2. This observed reduction in R^2 therefore does not appear to be dependent on acute changes in CV.

Summary and Computational Predictions:

In summary, no intervention significantly changed the AT-APD slope, which remained negative for all interventions, demonstrating that this parameter is relatively stable during acute electrical uncoupling in this experimental paradigm. Additionally, R^2 did not appear to consistently be dependent on changes in CV, endogenous APD, or the standard deviation of APD throughout the five experimental conditions tested here. Three of our interventions resulted in decreased CV (namely CBX, mannitol, and flecainide), and yet the resulting R^2 from these interventions were

unchanged, decreased, and increased, respectively. Similar to changes in CV, three of our interventions increased average APD relative to our time control (E4031, mannitol, dextran 2MDa), and yet these interventions resulted in a decrease, decrease, and increase of R^2, respectively. Finally, interventions that increased the standard deviation of APD (CBX and mannitol) either did not change (CBX) or decreased (mannitol) R^2. We conclude that there is no well-defined association between CV, APD, or the standard deviation of APD and their relationship to the slope or R^2 of the AT-APD relationship.

In contrast to experimental results, our *in silico* data suggest that intrinsic APD gradients, a parameter that cannot be accounted for using *ex vivo* optical mapping, are a more meaningful determinant of the AT-APD relationship. Simulations suggest that reducing electrical coupling via either gap junctional or ephaptic mechanisms shifts the AT-APD relationship curve by changing conduction but does not alter the fundamental shape of the relationship. The AT-APD relationship instead appears to be more dependent on whether the activation wavefront propagates toward longer or shorter APDs. As electrical wavefronts propagate toward cells with longer APDs, distal cells become increasingly shorter than those at the end of a wavefront propagating toward cells with shorter APDs. As the tissue-wide endogenous APD gradient is increased from 0 to 50ms/2cm, the sequence-dependent changes in APD increase in magnitude. The model therefore suggests that APD gradients are the principal determinant of the AT-APD relationship. Importantly, even though the simulations suggest endogenous APD gradients have the greatest impact on the AT-APD relationship, even with large gradients of 50 ms/2cm, the contribution of AT to APD is less than 4ms. This degree of change is relatively small and may be of minimal acute consequence to cardiac electrophysiology.

Limitations

Ex vivo preparations like the Langendorff perfused guinea pig heart used here come with a number of limitations including isolation from neural input and lack of hemodynamic feedback as a result of the non-working nature of the preparation. Additionally, optical mapping of isolated hearts requires pharmacological motion arrest, and all hearts used in the present study were electromechanically uncoupled using blebbistatin. This compound may be associated with off target effects, such as increased APD presumably due to alterations in intracellular calcium handling[45–47]. We do note that the choice of electromechanical uncoupler may be an explanation for why we see minor differences in the APD response to mannitol in the present experiments relative to prior publications from our group that utilized the electromechanical uncoupler BDM[15,34]. Regardless, because blebbistatin is used in all of the current experiments, we do not expect the employed electromechanical uncoupler to dramatically impact the interpretation of the results. Further work is required to identify the mechanism(s) by which mannitol and blebbistatin prolongs APD, while mannitol and BDM do not.

All experiments in this study were conducted using male animals. It may be valuable to repeat these studies in a female cohort, especially recognizing the reported sex-dependent differences in potassium channel expression[48,49]. This issue is partly explored with the experiments using E4031, where I_{Kr} inhibition prolonged APD and decreased the R^2 of the AT-APD relationship without changing slope. However, coupled with the predicted minor dependence of AT-APD on endogenous APD in the *in silico* model, the difference in endogenous APD gradients between sexes would have to be far more substantial than the most extreme case used here (a 50ms gradient over 2cm).

Finally, it is important to note the simulations used in the present studies are not directly comparable to our experimental data. Not only is the geometry of the model greatly simplified as a strand of cells, but the ID itself is a structurally complicated domain that is not fully encapsulated by this particular model. Future investigations using more intricate formulations of the ID may lend further insight to changes in the AT-APD relationship as a result of modulating this nanodomain[28].

Conclusion

Considering both previous and present findings, we conclude that significant changes in slope and R^2 of the AT-APD relationship observed in prior studies are likely attributed to cellular remodeling on a time course greater than 15 minutes rather than acute electrical coupling, but this requires further investigation. Additionally, the present findings, both *ex vivo* and *in silico,* suggest that the AT-APD slope and R^2 may be more dependent on endogenous APD gradients than acute changes to determinants of conduction or repolarization.

References

1. Costard-Jäckle, A., Goetsch, B., Antz, M. & Franz, M. R. Slow and long-lasting modulation of myocardial repolarization produced by ectopic activation in isolated rabbit hearts. Evidence for cardiac “memory.” *Circulation* **80**, 1412–1420 (1989).
2. Chan, Y.-H. *et al.* Small-Conductance Calcium-Activated Potassium Current Is Activated During Hypokalemia and Masks Short-Term Cardiac Memory Induced by Ventricular Pacing. *Circulation* **132**, 1377–1386 (2015).
3. Osaka, T., Kodama, I., Tsuboi, N., Toyama, J. & Yamada, K. Effects of activation sequence and anisotropic cellular geometry on the repolarization phase of action potential of dog ventricular muscles. *Circulation* **76**, 226–236 (1987).

4. Jeyaraj, D. *et al.* Ionic bases for electrical remodeling of the canine cardiac ventricle. *Am. J. Physiol. Heart Circ. Physiol.* **305**, H410-9 (2013).
5. Cowan, J. C. *et al.* Sequence of epicardial repolarisation and configuration of the T wave. *Br. Heart J.* **60**, 424–433 (1988).
6. Franz, M. R., Bargheer, K., Rafflenbeul, W., Haverich, A. & Lichtlen, P. R. Monophasic action potential mapping in human subjects with normal electrocardiograms: direct evidence for the genesis of the T wave. *Circulation* **75**, 379–386 (1987).
7. Kuo, C. S., Munakata, K., Reddy, C. P. & Surawicz, B. Characteristics and possible mechanism of ventricular arrhythmia dependent on the dispersion of action potential durations. *Circulation* **67**, 1356–1367 (1983).
8. Janse, M. J. & Wit, A. L. Electrophysiological mechanisms of ventricular arrhythmias resulting from myocardial ischemia and infarction. *Physiol. Rev.* **69**, 1049–1169 (1989).
9. Toyoshima, H. & Burgess, M. J. Electrotonic interaction during canine ventricular repolarization. *Circ. Res.* **43**, 348–356 (1978).
10. Lesh, M. D., Pring, M. & Spear, J. F. Cellular uncoupling can unmask dispersion of action potential duration in ventricular myocardium. A computer modeling study. *Circ. Res.* **65**, 1426–1440 (1989).
11. Entz, M., King, D. R. & Poelzing, S. Design and validation of a tissue bath 3-D printed with PLA for optically mapping suspended whole heart preparations. *American Journal of Physiology - Heart and Circulatory Physiology* **313**, H1190–H1198 (2017).
12. King, D. R. *et al.* The conduction velocity-potassium relationship in the heart is modulated by sodium and calcium. *Pflugers Arch.* **473**, 557–571 (2021).
13. de Groot, J. R. *et al.* Conduction slowing by the gap junctional uncoupler carbenoxolone. *Cardiovasc. Res.* **60**, 288–297 (2003).

14. Veeraraghavan, R. *et al.* Sodium channels in the Cx43 gap junction perinexus may constitute a cardiac ephapse: an experimental and modeling study. *Pflugers Arch.* **467**, 2093–2105 (2015).
15. Raisch, T. & Poelzing, S. Abstract 12147: Osmotically Narrowing the Perinexus Improves Cardiac Conduction. *Circulation* **138**, A12147–A12147 (2018).
16. Duchêne, A. *et al.* Impact of Astroglial Connexins on Modafinil Pharmacological Properties. *Sleep* **39**, 1283–1292 (2016).
17. Larsen, A. P., Olesen, S.-P., Grunnet, M. & Poelzing, S. Pharmacological activation of IKr impairs conduction in guinea pig hearts. *J. Cardiovasc. Electrophysiol.* **21**, 923–929 (2010).
18. Sanguinetti, M. C., Jurkiewicz, N. K., Scott, A. & Siegl, P. K. Isoproterenol antagonizes prolongation of refractory period by the class III antiarrhythmic agent E-4031 in guinea pig myocytes. Mechanism of action. *Circ. Res.* **68**, 77–84 (1991).
19. George, S. A. *et al.* Extracellular sodium and potassium levels modulate cardiac conduction in mice heterozygous null for the Connexin43 gene. *Pflugers Arch.* (2015) doi:10.1007/s00424-015-1698-0.
20. Entz, M., 2nd *et al.* Heart Rate and Extracellular Sodium and Potassium Modulation of Gap Junction Mediated Conduction in Guinea Pigs. *Front. Physiol.* **7**, 16 (2016).
21. Bayly, P. V. *et al.* Estimation of conduction velocity vector fields from epicardial mapping data. *IEEE Trans. Biomed. Eng.* **45**, 563–571 (1998).
22. Veeraraghavan, R. & Poelzing, S. Mechanisms underlying increased right ventricular conduction sensitivity to flecainide challenge. *Cardiovasc. Res.* **77**, 749–756 (2008).
23. Greer-Short, A., George, S. A., Poelzing, S. & Weinberg, S. H. Revealing the Concealed Nature of Long-QT Type 3 Syndrome. *Circ. Arrhythm. Electrophysiol.* **10**, e004400 (2017).
24. Nowak, M. B. *et al.* Intercellular sodium regulates repolarization in cardiac tissue with sodium channel gain-of-function. *Biophys. J.* (2020) doi:10.1016/j.bpj.2020.04.014.

25. Wu, X. *et al.* Hypernatremia and intercalated disc edema synergistically exacerbate long-QT syndrome type 3 phenotype. *Am. J. Physiol. Heart Circ. Physiol.* **321**, H1042–H1055 (2021).
26. Weinberg, S. H. Ephaptic coupling rescues conduction failure in weakly coupled cardiac tissue with voltage-gated gap junctions. *Chaos* **27**, (2017).
27. Kucera, J. P. & Rudy, Y. Mechanistic insights into very slow conduction in branching cardiac tissue: a model study. *Circ. Res.* **89**, 799–806 (2001).
28. Moise, N., Struckman, H. L., Dagher, C., Veeraraghavan, R. & Weinberg, S. H. Intercalated disk nanoscale structure regulates cardiac conduction. *J. Gen. Physiol.* **153**, (2021).
29. Lin, X. *et al.* Subcellular heterogeneity of sodium current properties in adult cardiac ventricular myocytes. *Heart Rhythm* **8**, 1923–1930 (2011).
30. Kucera, J. P., Rohr, S. & Rudy, Y. Localization of sodium channels in intercalated disks modulates cardiac conduction. *Circ. Res.* **91**, 1176–1182 (2002).
31. Maier, S. K. G. *et al.* Distinct subcellular localization of different sodium channel alpha and beta subunits in single ventricular myocytes from mouse heart. *Circulation* **109**, 1421–1427 (2004).
32. O'Hara, T., Virág, L., Varró, A. & Rudy, Y. Simulation of the undiseased human cardiac ventricular action potential: model formulation and experimental validation. *PLoS Comput. Biol.* **7**, e1002061 (2011).
33. Rhett, J. M. & Gourdie, R. G. The perinexus: a new feature of Cx43 gap junction organization. *Heart Rhythm* **9**, 619–623 (2012).
34. Veeraraghavan, R., Salama, M. E. & Poelzing, S. Interstitial volume modulates the conduction velocity-gap junction relationship. *American Journal of Physiology - Heart and Circulatory Physiology* **302**, (2012).
35. Laurita, K. R., Girouard, S. D. & Rosenbaum, D. S. Modulation of ventricular repolarization by a premature stimulus. Role of epicardial dispersion of repolarization kinetics demonstrated by optical mapping of the intact guinea pig heart. *Circ. Res.* **79**, 493–503 (1996).

36. Li, G.-R., Zhang, M., Satin, L. S. & Baumgarten, C. M. Biphasic effects of cell volume on excitation-contraction coupling in rabbit ventricular myocytes. *Am. J. Physiol. Heart Circ. Physiol.* **282**, H1270-7 (2002).

37. Taglialatela, M. *et al.* Regulation of the human ether-a-gogo related gene (HERG) K^+ channels by reactive oxygen species. *Proc. Natl. Acad. Sci. U. S. A.* **94**, 11698–11703 (1997).

38. Yabuuchi, F., Beckmann, R., Wettwer, E., Hegele-Hartung, C. & Heubach, J. F. Reduction of hERG potassium currents by hyperosmolar solutions. *Eur. J. Pharmacol.* **566**, 222–225 (2007).

39. Brannan, J. D., Gulliksson, M., Anderson, S. D., Chew, N. & Kumlin, M. Evidence of mast cell activation and leukotriene release after mannitol inhalation. *Eur. Respir. J.* **22**, 491–496 (2003).

40. Brannan, J. D. *et al.* Inhibition of mast cell PGD2 release protects against mannitol-induced airway narrowing. *Eur. Respir. J.* **27**, 944–950 (2006).

41. Sverrild, A. *et al.* Airway responsiveness to mannitol in asthma is associated with chymase-positive mast cells and eosinophilic airway inflammation. *Clin. Exp. Allergy* **46**, 288–297 (2016).

42. Salvage, S. C., Gallant, E. M., Fraser, J. A., Huang, C. L.-H. & Dulhunty, A. F. Flecainide Paradoxically Activates Cardiac Ryanodine Receptor Channels under Low Activity Conditions: A Potential Pro-Arrhythmic Action. *Cells* **10**, (2021).

43. Ogawa, S., Mitamura, H. & Katoh, H. Effect of E-4031, a new class III antiarrhythmic drug, on reentrant ventricular arrhythmias: comparison with conventional class I drugs. *Cardiovasc. Drugs Ther.* **7 Suppl 3**, 621–626 (1993).

44. Xu, X. *et al.* Vicious LQT induced by a combination of factors different from hERG inhibition. *Front. Pharmacol.* **13**, 930831 (2022).

45. Fedorov, V. V. *et al.* Application of blebbistatin as an excitation-contraction uncoupler for electrophysiologic study of rat and rabbit hearts. *Heart Rhythm* **4**, 619–626 (2007).
46. Kappadan, V. *et al.* High-Resolution Optical Measurement of Cardiac Restitution, Contraction, and Fibrillation Dynamics in Beating vs. Blebbistatin-Uncoupled Isolated Rabbit Hearts. *Front. Physiol.* **11**, 464 (2020).
47. Brack, K. E., Narang, R., Winter, J. & Ng, G. A. The mechanical uncoupler blebbistatin is associated with significant electrophysiological effects in the isolated rabbit heart. *Exp. Physiol.* **98**, 1009–1027 (2013).
48. Gaborit, N. *et al.* Gender-related differences in ion-channel and transporter subunit expression in non-diseased human hearts. *J. Mol. Cell. Cardiol.* **49**, 639–646 (2010).
49. Trépanier-Boulay, V., St-Michel, C., Tremblay, A. & Fiset, C. Gender-based differences in cardiac repolarization in mouse ventricle. *Circ. Res.* **89**, 437–444 (2001).

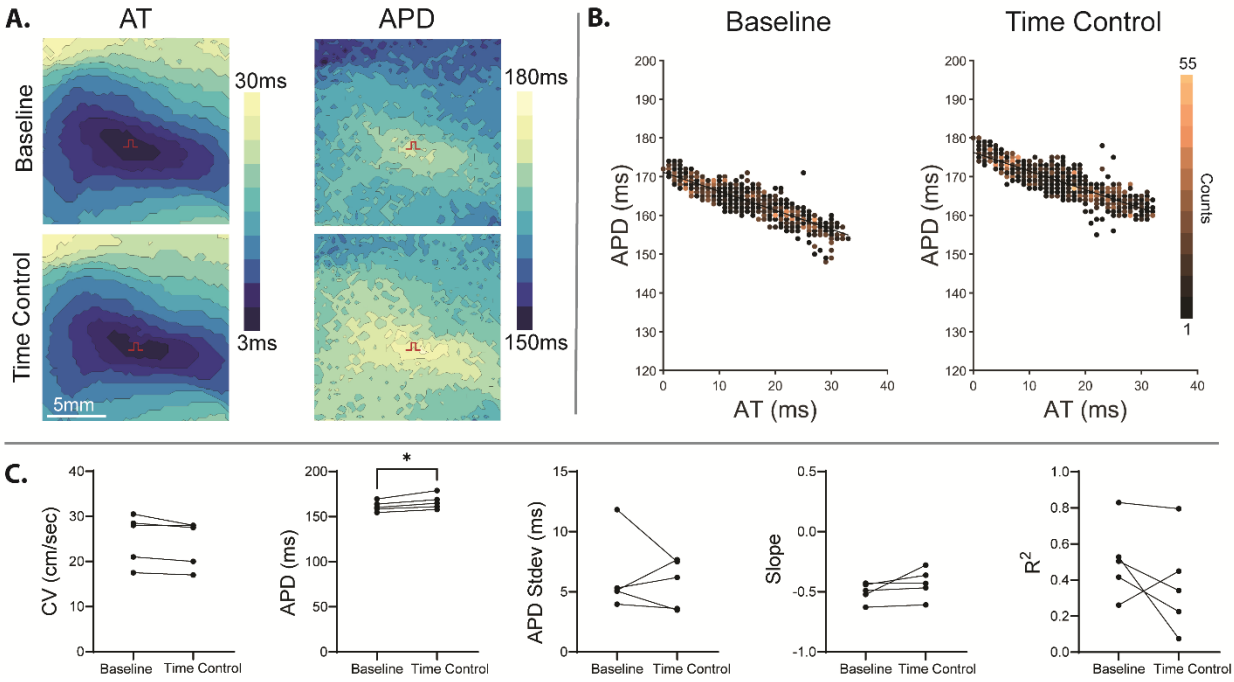

Figure 1. The AT-APD relationship does not significantly change after 15 minute time control. A. Representative optical maps of AT and APD with 3ms isochrones. Site of stimulus is indicated in red. **B.** A scatter plot of the AT-APD relationship derived from optical mapping and the corresponding line of best fit. The number of pixels with a given AT-APD coordinate is indicated by color, ranging from black (1) to light orange (55). **C.** Summary data of time control indicates no change in CV, standard deviation of APD, slope or R^2 of AT-APD. There was a small but significant increase in average APD. n=5, * $p<0.05$ relative to baseline, paired Student's t-test.

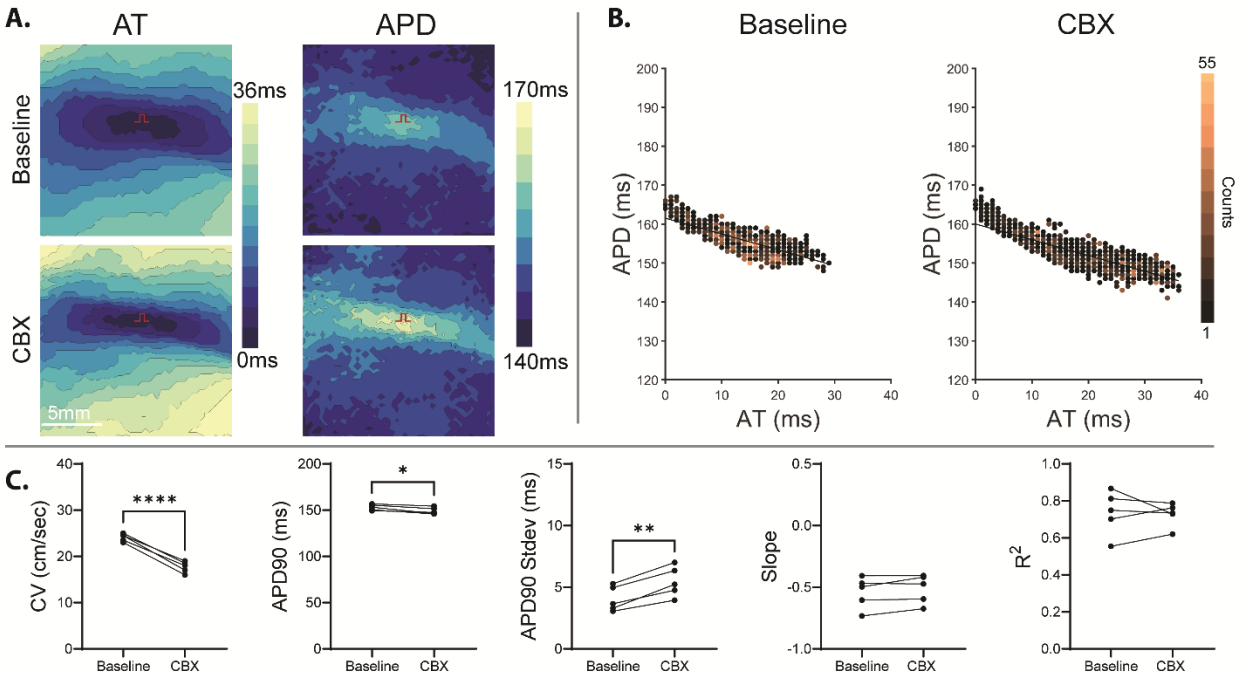

Figure 2. The gap junction inhibitor carbenoxolone does not modulate the AT-APD relationship. **A.** Representative optical maps of AT and APD with 3ms isochrones. Site of stimulus is indicated in red. **B.** A scatter plot of the AT-APD relationship derived from optical mapping and the corresponding line of best fit. The number of pixels with a given AT-APD coordinate is indicated by color, ranging from black (1) to light orange (55). **C.** Summary data of CBX treatment indicates a significant decrease in CV and APD, but no change in the standard deviation of APD or the slope or R^2 of AT-APD. n=5, * $p<0.05$ relative to baseline, paired Student's t-test.

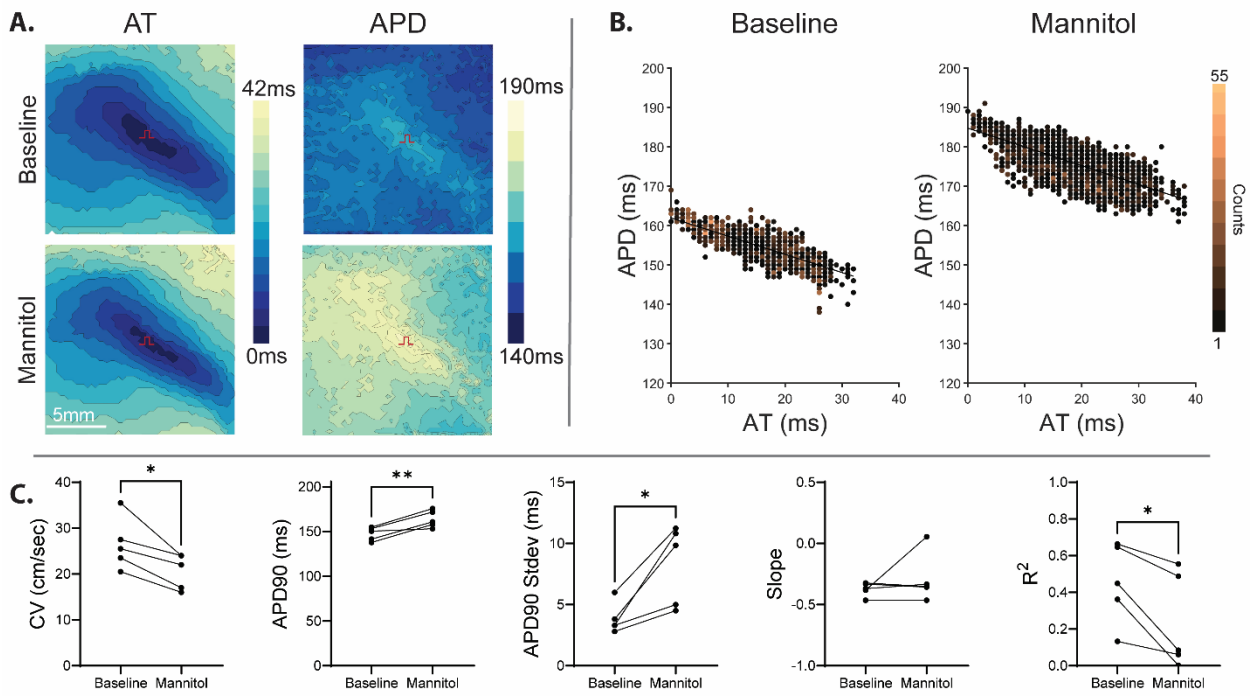

Figure 3. The osmotic agent mannitol decreases the R^2 of the AT-APD relationship. **A.** Representative optical maps of AT and APD with 3ms isochrones. Site of stimulus is indicated in red. **B.** A scatter plot of the AT-APD relationship derived from optical mapping and the corresponding line of best fit. The number of pixels with a given AT-APD coordinate is indicated by color, ranging from black (1) to light orange (55). **C.** Summary data of mannitol treatment demonstrates a significant decrease in CV, APD and standard deviation in APD, and a significant increase in the R^2 of AT-APD. No change was measured in slope. n=5, * $p<0.05$ relative to baseline, paired Student's t-test.

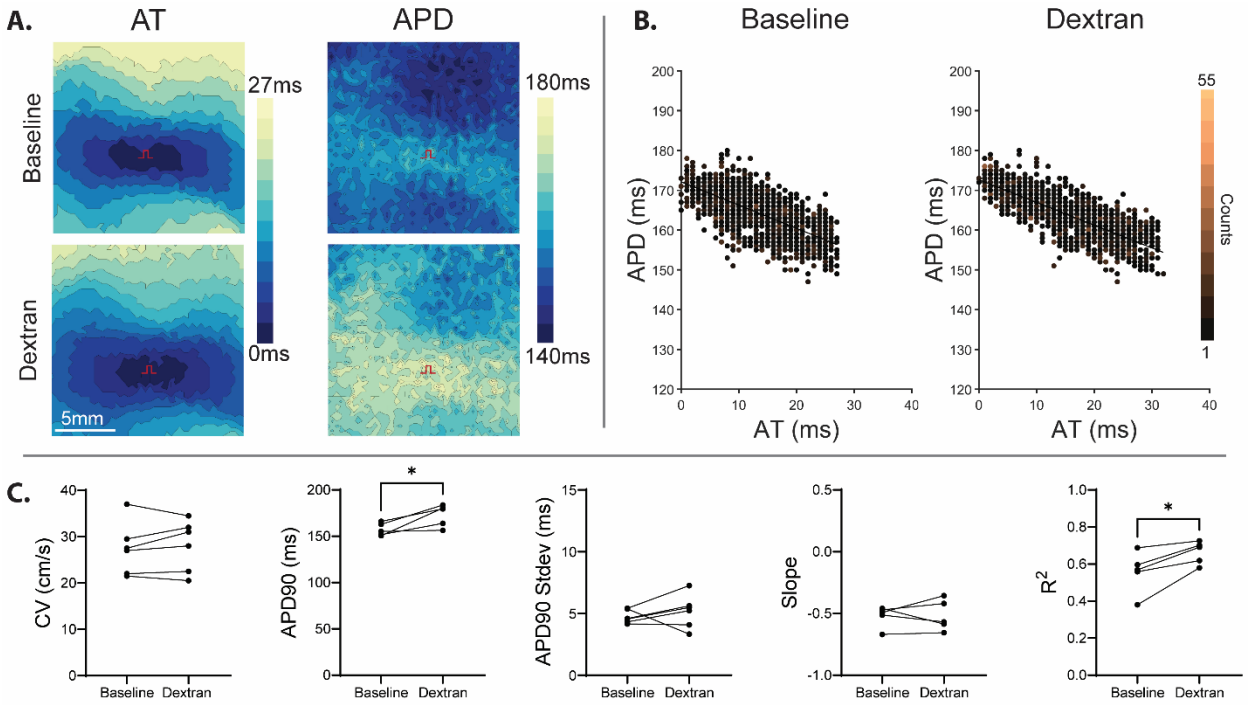

Figure 4. The osmotic agent dextran increases the R^2 of the AT-APD relationship. A. Representative optical maps of AT and APD with 3ms isochrones. Site of stimulus is indicated in red. **B.** A scatter plot of the AT-APD relationship derived from optical mapping and the corresponding line of best fit. The number of pixels with a given AT-APD coordinate is indicated by color, ranging from black (1) to light orange (55). **C.** Summary data of dextran treatment demonstrates a significant increase in the R^2 of AT-APD, but no change in CV, standard deviation of APD, or slope. n=6, * $p<0.05$ relative to baseline, paired Student's t-test.

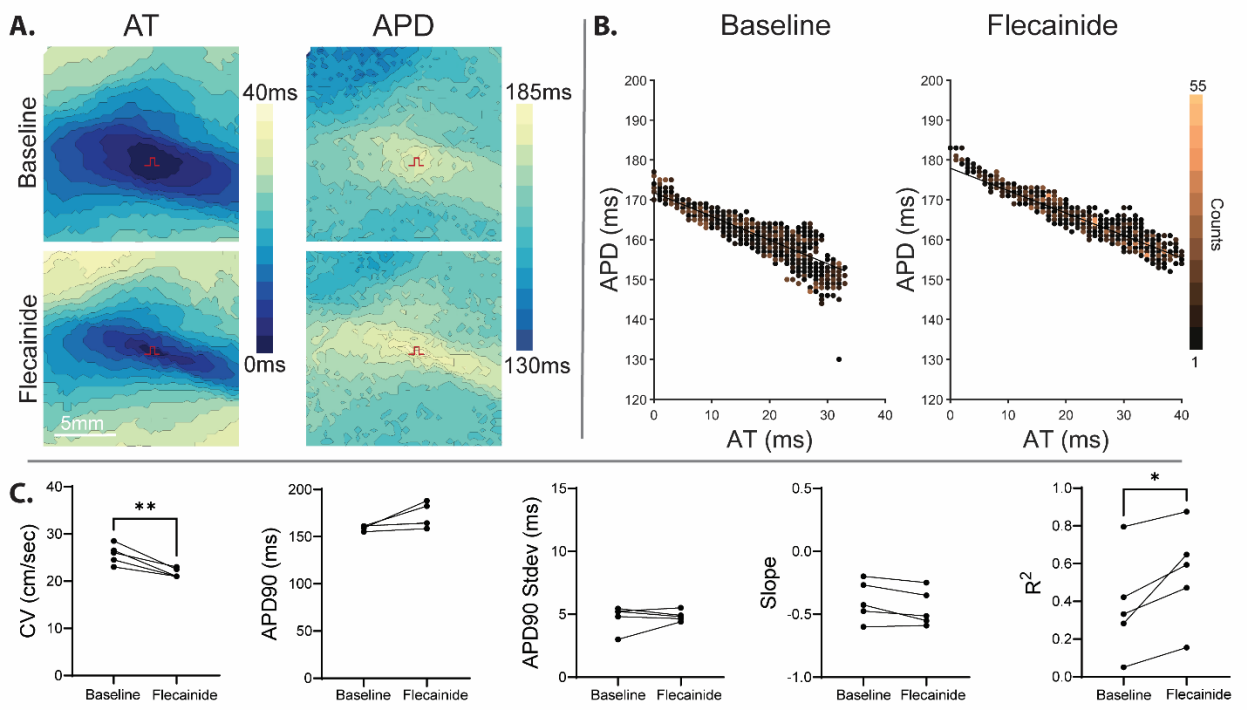

Figure 5. The sodium channel inhibitor flecainide increases R^2 of the AT-APD relationship.

A. Representative optical maps of AT and APD with 3ms isochrones. Site of stimulus is indicated in red. **B.** A scatter plot of the AT-APD relationship derived from optical mapping and the corresponding line of best fit. The number of pixels with a given AT-APD coordinate is indicated by color, ranging from black (1) to light orange (55). **C.** Summary data of flecainide treatment demonstrates a significant decrease in CV, no change in APD, standard deviation of APD, or the slope of AT-APD, and an increase in the R^2 of AT-APD. n=5, * $p<0.05$ relative to baseline, paired Student's t-test.

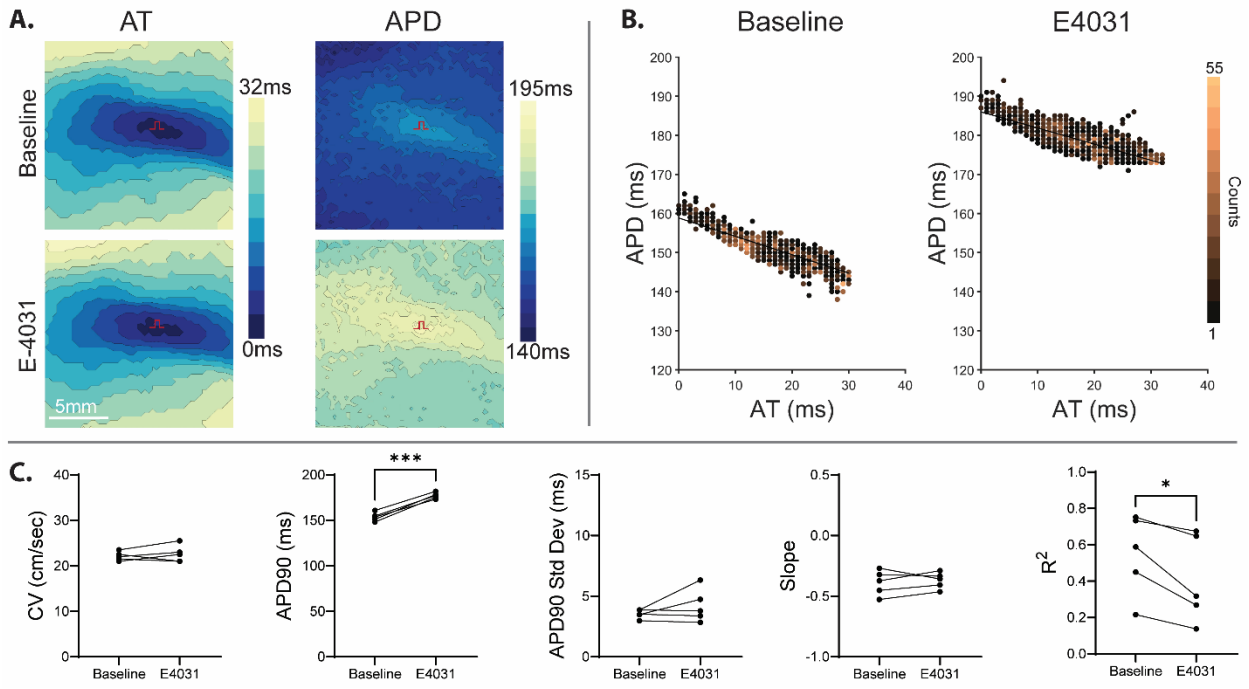

Figure 6. The hERG inhibitor E4031 decreases the R^2 of the AT-APD relationship. **A.** Representative optical maps of AT and APD with 3ms isochrones. Site of stimulus is indicated in red. **B.** A scatter plot of the AT-APD relationship derived from optical mapping and the corresponding line of best fit. The number of pixels with a given AT-APD coordinate is indicated by color, ranging from black (1) to light orange (55). **C.** Summary data of E4031 treatment demonstrates a significant increase in APD and decrease in the R^2 of AT-APD, but no change in CV, standard deviation of APD, or slope. n=5, * $p<0.05$ relative to baseline, paired Student's t-test.

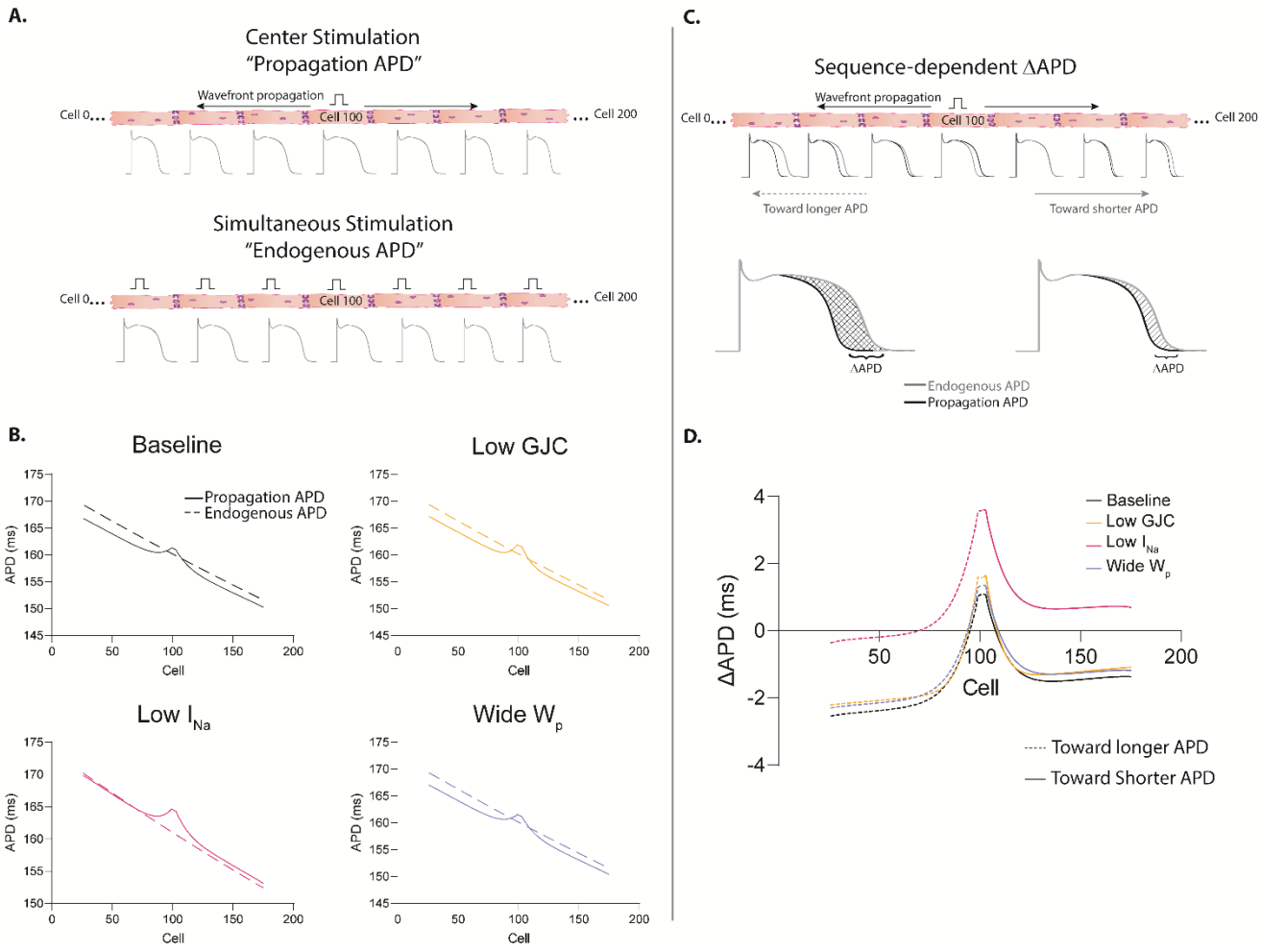

Figure 7. Computational predictions of modulating gap junctional coupling, perinexal width, and sodium current on the relationship between AT and APD in a cell strand with an endogenous APD gradient of 30ms. A. Diagram depicting simultaneous stimulation of every cell in the strand, resulting in the "endogenous APD", while stimulation from the center cells of the strand results in the "propagated APD". **B.** Center stimulation prolongs APD in cells proximal to the stimulus regardless of intervention to electrical coupling. Distal cells show depressed APD for all interventions except reduced I_{Na}, which shifts APD for all cells upward. **C.** Diagram depicting the activation sequence-dependent changes on APD and their relationship with endogenous APD gradients in the strand. **D.** The sequence-dependent change in APD is calculated by subtracting the endogenous APD from the center

stimulated APD. The model predicts that delta APD is more negative when the electrical wavefront propagates up the endogenous APD gradient (toward cells with longer APD) than down the APD gradient, regardless of coupling intervention. Created with BioRender.com

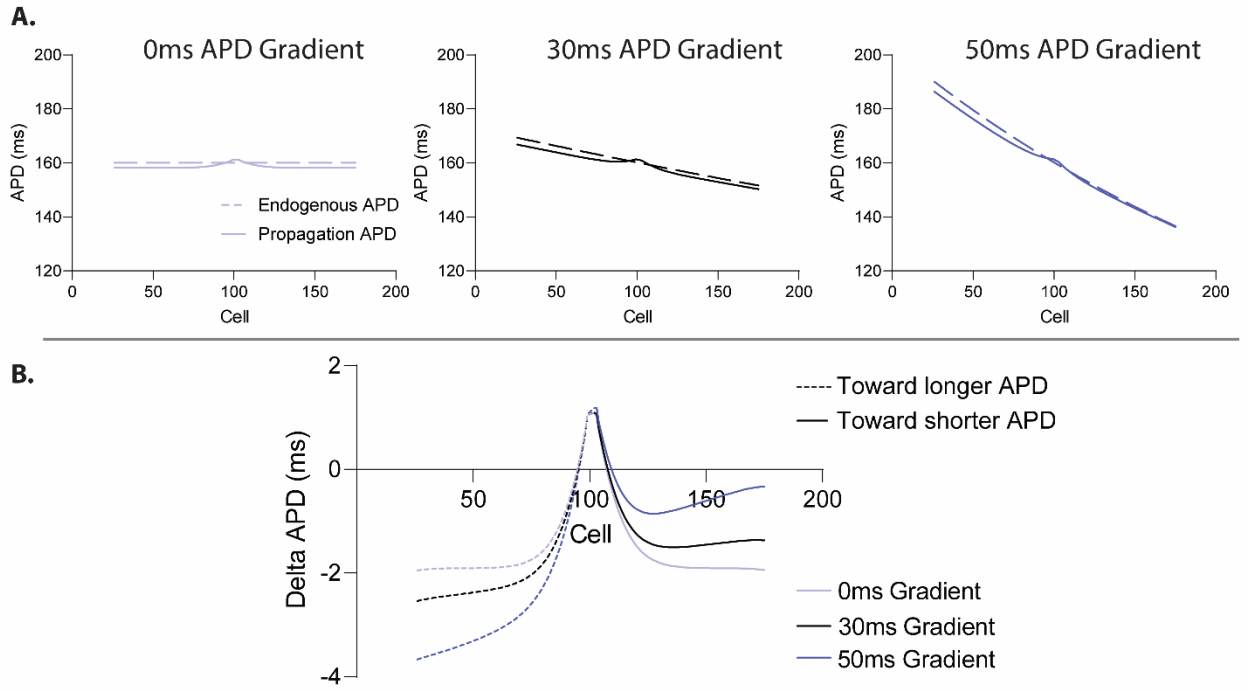

Figure 8. Computational predictions of modulating the endogenous APD gradient on the relationship between AT and APD. A. Center stimulation prolongs APD in cells proximal to the stimulus regardless of endogenous APD gradient. **B.** The sequence-dependent change in APD is calculated by subtracting the endogenous APD from the center stimulated APD. The model predicts that delta APD is more negative when the electrical wavefront propagates up the endogenous APD gradient (toward cells with longer APD), and this degree of change is dependent on the magnitude of the endogenous APD gradient.

Chapter 5

Summary and Future Directions

Summary and Future Directions

Cardiac electrophysiology has made great strides since the writing of Sydney Ringer, who identified that precise ratios of sodium, potassium, and calcium are critical to the maintenance of coordinated electrical activity across the cardiac ventricle. Our laboratory has repeatedly shown that manipulating the extracellular composition of these three ions can unmask or modulate cardiac disease states, as explored in chapters 2 and 3, and can yield valuable insight to the mechanisms of cardiac conduction and repolarization, as investigated in chapter 4.

Mannitol and Hyponatremia in the Scn5a+/- Mouse

Previous work from our lab has demonstrated ways in which modulating ephaptic coupling (EpC) can either ameliorate or exacerbate a variety of disease states. For example, varying determinants of EpC can unmask conduction slowing due to reduced Cx43[1], exacerbate QT prolongation in a LQT3 model[2], mitigate conduction slowing during metabolic ischemia[3], global ischemia[4], and hyperkalemia[5], and finally, exacerbate conduction slowing during pharmacological sodium channel inhibition[6]. These are all accomplished by simple interventions in extracellular ion composition or modulation of the perinexus, a nanodomain of the intercalated disc. In chapter 2, we aimed to evaluate two mechanisms for reducing EpC as alternative diagnostic techniques for Brugada Syndrome, a disease which is commonly asympotomatic until the fourth decade of life[7]. The aforementioned prior work from our lab, combined with evidence from clinical case reports[8–11], presents both hyponatremia and mannitol as viable options for novel diagnostics.

The results of this project suggest that mice with a 50% loss in Nav1.5 expression (Scn5a+/-) are more sensitive to reductions in EpC by either hyponatremia or mannitol, as indicated by significantly greater reductions in conduction velocity relative to WT littermates. This suggests each of the two treatments may be viable mechanisms for unmasking arrhythmogenic substrates of BrS. Importantly, when combined, these treatments do not produce an additive

response. Instead, perfusion with mannitol appears to recover conduction deficits induced by hyponatremia alone. Results from this final experiment are more difficult to interpret in terms of translating to patient care, but they do inform us of the nonlinear relationship between perinexal width, conduction velocity, and functional sodium channel availability.

From here, there are multiple avenues of research to pursue. Regarding investigation of novel diagnostics for Scn5a LOF diseases, the next series of experiment to pursue would be *in vivo* mannitol and hyponatremia challenge via tail vein injection in the Scn5a+/- mouse, with conduction measured by QRS duration on ECG. Evidence of exacerbated QRS widening in the intact heterozygous animal would further support the theory that low serum sodium or extracellular edema may be dangerous conditions for BrS-diagnosed patients. The corollary to this theory would be that increased serum sodium should be protective of BrS-associated arrhythmogenic events. Therefore, a long-term goal of this work could be an early clinical trial of normal saline administration during BrS symptom presentation. As normal saline is hypernatremic relative to average human serum sodium, but is commonly administered in emergency care settings for a variety of cardiac disorders, the implementation of this trial could be relatively simple and yet yield important insight to potential BrS therapies.

It would also be worth pursuing both *ex vivo* and computational experiments in order to elucidate the mechanism behind the unexpected results of combined mannitol and hyponatremia treatment on conduction velocity. For example, our lab has previously shown that, under specific conditions, inhibition of hERG (IKr), though a repolarizing current, may actually be able to modulate ventricular conduction[12]. Because mannitol is reported to have off target effects on hERG (resulting in inhibition), it's possible that this function is contributing to the interesting conduction changes reported here. Application of a hERG inhibitor (E4031, for example) combined with hyponatremia in an *ex vivo* guinea pig heart model may yield insight to this phenomenon. Computational models of cardiac conduction that account for the intricate

morphology of the intercalated disc and perinexus may also yield insight to the effects of hyponatremia and mannitol together on conduction. For example, it would be fascinating to assess whether the "sodium transfer" theory proposed by Ianovic and Kucera in 2022 may be mediating this effect[13]. "Sodium transfer" was coined in response to their identification of an *outward* flow of sodium current into the perinexal cleft during the depolarization of the downstream cell in their two cell model of conduction. If this current is present under baseline conditions, perhaps it is reduced during sodium channel loss of function and then further limited by hyponatremia, but later resolved due to influx of extracellular sodium during perinexal widening by mannitol.

In summary, this series of experiments have provided valuable insight to a novel mechanism of arrhythmogenesis in BrS disease, though further investigation is warranted to explore how the combination of mannitol and hyponatremia attenuate conduction slowing.

Modulation of APD-K by Na^+ and Ca^{2+}

Hyperkalemia is another disease state associated with sodium channel loss of function that we have previously shown can be modulated by extracellular ion composition in the *ex vivo* guinea pig heart[5]. Specifically, the well-established inverse relationship between conduction slowing and severe hyperkalemia was mitigated by concurrent elevation of Na^+ and Ca^{2+}. In chapter 3 of the present dissertation, we therefore investigated whether the established inverse relationship between action potential duration (APD) and hyperkalemia could similarly be manipulated. While initial results indicated that APD may be prolonged during severe hyperkalemia during perfusion with 145mM Na^+, these findings were discovered to be confounded by changes in ECG rhythm during the perfusion protocol. Long periods of electrical quiescence likely resulted in accumulation of intracellular calcium and ultimately very long APD upon application of external pacing[14]. When rhythm changes were accounted for in a subsequent protocol, we found that steady state pacing after asystole onset significantly shortened APD, and,

interestingly, hearts perfused with higher Ca^{2+} (2.0mM) displayed greater APD shortening than those with lower Ca^{2+} (1.25mM). Additionally, we observed that APD adaptation to pacing rate during perfusion with 145mM Na^{+} was dependent on Ca^{2+} concentration.

While this study evaluates changes in APD in the context of prolonged asystole and severe hyperkalemia, two relatively unique and extreme conditions, it may still shed light on repolarization behaviors in the context of resuscitation and/or in the case of interstitial hyperkalemia, in which a local region of tissue may experience severe hyperkalemia due to trauma or ischemic disease. This study focused on changes in APD due to altered extracellular Na^{+} and Ca^{2+}, but future work could directly evaluate arrythmogenic propensity in models of hyperkalemia under these varied conditions.

Additionally, while this investigation was not designed to investigate the role of calcium gluconate in hyperkalemia, it does bring up some interesting observations about calcium treatment during hyperkalemia, a gold standard in in prevention of hyperkalemia-associated arrhythmias[15]. Calcium's anti-arrhythmic effects in the context of hyperkalemia are attributed to its recovery of reduced excitability via increasing the threshold potential[16]. But calcium has also been shown to activate I_{K1} via CamKII in cardiomyocytes of rabbit and dog, and subsequently reduce APD[17]. Future work may be able to assess whether this calcium-mediated enhancement of repolarization reserve is responsible for our APD results presented in Chapter 3.

Sequence-dependent Repolarization in the Ventricular Myocardium

The final work presented in this dissertation investigated the nuanced relationship between conduction and repolarization in the guinea pig epicardium. An inverse relationship has been regularly observed between activation time (AT) and action potential duration (APD) in the myocardium of a variety of species[18–23]. This relationship is thought to be biologically beneficial as it synchronizes repolarization time (calculated as AT + APD) across the surface of the heart, minimizing potentially arrhythmogenic dispersions of repolarization times[24,25]. This phenomenon

is commonly attributed to electrotonic coupling via gap junctions, but, up to this point, that had not been directly evaluated.

In chapter 4, we found that inhibiting gap junctional coupling did not significantly change the AT-APD relationship, as measured by R^2 and slope of AT-APD. We were surprised to observe that changes in conduction velocity, APD, or standard deviation of APD induced by each of these interventions did not consistently correlate with changes in R^2. Instead, mathematical simulations predict that the endogenous APD gradient is a stronger determinant of the AT-APD relationship.

Future *ex vivo* work could elaborate on the experimental findings presented here by complementing the carbenoxolone investigation with a treatment that would enhance gap junctional coupling. For example, the ACT1 peptide has been shown to increase gap junctional communication, and may shed further insight on the role of gap junctional coupling in the AT-APD relationship.

Biologically, the present findings highlight the resilience of the myocardium in response to acute electrical distress. Though cardiac memory studies suggest that AT-APD can be manipulated and become proarrhythmic after chronic modulation, the independence that we observe between AT-APD and acute changes to cell-cell uncoupling makes the epicardium a robust electrical network.

Limitations

While the limitations specific to each project are previously outlined in the preceding chapters, the following are general limitations to this work that are worth consideration.

The evaluation of perinexal width is a relatively new technique by which to evaluate ephaptic coupling within a given tissue[26,27]. As a three dimensional structure, the volume and morphology may not be perfectly represented in our two dimensional TEM images. While measuring

perinexal cross sections from a variety of planes across the tissue samples may be sufficient to account for this discrepancy, it is likely that future techniques will allow for even more precise evaluation of this nanodomain. In particular, developments in fast-frozen EM preparations have enabled the development of high resolution 3D reconstruction of microdomains such as t-tubules[28]. Interestingly, this technique can also be used to assess contraction-induced deformations of microdomains and organelles. While this tool has not been optimized for paired cells and is therefore not currently able to evaluate intact structures within the intercalated disc, it will likely be a possibility in the near future.

A second general limitation regards the use of mannitol. While we have validated the use of mannitol as a perinexal-widening agent[29], it is worth noting that the compound also has well-documented effects on the immune system, and is in fact being investigated as a potential diagnostic tool for asthma[30–32]. Mannitol has repeatedly been shown to activate mast cells and leukotrienes, though largely in pulmonary tissue[30–32]. The consequence of this immune response in the *ex vivo* heart preparation is unclear, though prior work from our lab with the cytokine TNFα suggests this kind of immune response may play a role in electrophysiology of even the *ex vivo* heart[33].

Conclusion

The work presented in this dissertation demonstrates how the ionic and osmotic composition of extracellular fluid in the heart can be used to both elucidate fundamental mechanisms of cardiac electrophysiology and potentially diagnose or mitigate electrophysiological disease. In particular, we explore the use of hyponatremia and mannitol as novel diagnostics for sodium channel loss of function, and evaluate the role of sodium and calcium on APD-shortening during hyperkalemia. Finally, we demonstrate how loss of cell-cell coupling does not consistently alter the relationship between AT and APD, and conclude that this tissue is very electrophysiologically stable in the face of acute stress.

Together, these investigations deepen our understanding of cardiac electrophysiology in *ex vivo* models, and clarify ways in which the epicardium is uniquely susceptible (Nav1.5 LOF) or uniquely resilient (AT-APD) to stress in the form of electrical uncoupling.

References

1. George, S. A. *et al.* Extracellular sodium and potassium levels modulate cardiac conduction in mice heterozygous null for the Connexin43 gene. *Pflugers Arch.* (2015) doi:10.1007/s00424-015-1698-0.
2. Wu, X. *et al.* Hypernatremia and intercalated disc edema synergistically exacerbate long-QT syndrome type 3 phenotype. *Am. J. Physiol. Heart Circ. Physiol.* **321**, H1042–H1055 (2021).
3. George, S. A. *et al.* Modulating cardiac conduction during metabolic ischemia with perfusate sodium and calcium in guinea pig hearts. *American Journal of Physiology-Heart and Circulatory Physiology* **316**, H849–H861 (2019).
4. Hoeker, G. S. *et al.* Attenuating loss of cardiac conduction during no-flow ischemia through changes in perfusate sodium and calcium. *Am. J. Physiol. Heart Circ. Physiol.* **319**, H396–H409 (2020).
5. King, D. R. *et al.* The conduction velocity-potassium relationship in the heart is modulated by sodium and calcium. *Pflugers Arch.* **473**, 557–571 (2021).
6. Veeraraghavan, R. *et al.* Sodium channels in the Cx43 gap junction perinexus may constitute a cardiac ephapse: an experimental and modeling study. *Pflugers Arch.* **467**, 2093–2105 (2015).
7. Milman, A. *et al.* Age of First Arrhythmic Event in Brugada Syndrome. *Circ. Arrhythm. Electrophysiol.* **10**, e005222 (2017).

8. Amusina, O., Mehta, S. & Nelson, M. E. Brugada phenocopy secondary to hyperkalemia and hyponatremia in primary adrenal insufficiency. *J Am Coll Emerg Physicians Open* **3**, e12800 (2022).
9. Ayad, S. *et al.* Fever and Hyponatremia Unmasking Brugada Pattern Electrocardiogram in a Patient With SARS-CoV-2 Infection. *Cureus* **13**, e18578 (2021).
10. Rattanawong Pattara ; Ungprasert Jitrada ; Senthong, V. Hyponatremia-Induced Symptomatic Brugada Syndrome Mimicking St Segment Elevation Myocardial Infarction | Ovid. *Circulation* https://oce-ovid-com.ezproxy.lib.vt.edu/article/00003017-201811061-02729 (2018).
11. Agrawal, Y., Aggarwal, S., Kalavakunta, J. K. & Gupta, V. All that looks like “Brugada” is not “Brugada”: Case series of Brugada phenocopy caused by hyponatremia. *Journal of the Saudi Heart Association* **28**, 274–277 (2016).
12. Larsen, A. P., Olesen, S.-P., Grunnet, M. & Poelzing, S. Pharmacological activation of IKr impairs conduction in guinea pig hearts. *J. Cardiovasc. Electrophysiol.* **21**, 923–929 (2010).
13. Ivanovic, E. & Kucera, J. P. Localization of Na+ channel clusters in narrowed perinexi of gap junctions enhances cardiac impulse transmission via ephaptic coupling: a model study. *J. Physiol.* **599**, 4779–4811 (2021).
14. Suto, F. *et al.* Ventricular rate determines early bradycardic electrical remodeling. *Heart Rhythm* **2**, 293–300 (2005).
15. Mahoney, B. A. *et al.* Emergency interventions for hyperkalaemia. *Cochrane Database Syst. Rev.* **2005**, CD003235 (2005).
16. Parham, W. A., Mehdirad, A. A., Biermann, K. M. & Fredman, C. S. Hyperkalemia revisited. *Tex. Heart Inst. J.* **33**, 40–47 (2006).
17. Mustroph, J., Maier, L. S. & Wagner, S. CaMKII regulation of cardiac K channels. *Front. Pharmacol.* **5**, 20 (2014).

18. Costard-Jäckle, A., Goetsch, B., Antz, M. & Franz, M. R. Slow and long-lasting modulation of myocardial repolarization produced by ectopic activation in isolated rabbit hearts. Evidence for cardiac “memory.” *Circulation* **80**, 1412–1420 (1989).
19. Chan, Y.-H. *et al.* Small-Conductance Calcium-Activated Potassium Current Is Activated During Hypokalemia and Masks Short-Term Cardiac Memory Induced by Ventricular Pacing. *Circulation* **132**, 1377–1386 (2015).
20. Osaka, T., Kodama, I., Tsuboi, N., Toyama, J. & Yamada, K. Effects of activation sequence and anisotropic cellular geometry on the repolarization phase of action potential of dog ventricular muscles. *Circulation* **76**, 226–236 (1987).
21. Jeyaraj, D. *et al.* Ionic bases for electrical remodeling of the canine cardiac ventricle. *Am. J. Physiol. Heart Circ. Physiol.* **305**, H410-9 (2013).
22. Cowan, J. C. *et al.* Sequence of epicardial repolarisation and configuration of the T wave. *Br. Heart J.* **60**, 424–433 (1988).
23. Franz, M. R., Bargheer, K., Rafflenbeul, W., Haverich, A. & Lichtlen, P. R. Monophasic action potential mapping in human subjects with normal electrocardiograms: direct evidence for the genesis of the T wave. *Circulation* **75**, 379–386 (1987).
24. Kuo, C. S., Munakata, K., Reddy, C. P. & Surawicz, B. Characteristics and possible mechanism of ventricular arrhythmia dependent on the dispersion of action potential durations. *Circulation* **67**, 1356–1367 (1983).
25. Janse, M. J. & Wit, A. L. Electrophysiological mechanisms of ventricular arrhythmias resulting from myocardial ischemia and infarction. *Physiol. Rev.* **69**, 1049–1169 (1989).
26. Raisch, T., Khan, M. & Poelzing, S. Quantifying Intermembrane Distances with Serial Image Dilations. *J. Vis. Exp.* (2018) doi:10.3791/58311.
27. Rhett, J. M. & Gourdie, R. G. The perinexus: a new feature of Cx43 gap junction organization. *Heart Rhythm* **9**, 619–623 (2012).

28. Kohl, P., Greiner, J. & Rog-Zielinska, E. A. Electron microscopy of cardiac 3D nanodynamics: form, function, future. *Nat. Rev. Cardiol.* **19**, 607–619 (2022).
29. Raisch, T. & Poelzing, S. Abstract 12147: Osmotically Narrowing the Perinexus Improves Cardiac Conduction. *Circulation* **138**, A12147–A12147 (2018).
30. Brannan, J. D. *et al.* Inhibition of mast cell PGD2 release protects against mannitol-induced airway narrowing. *Eur. Respir. J.* **27**, 944–950 (2006).
31. Brannan, J. D., Gulliksson, M., Anderson, S. D., Chew, N. & Kumlin, M. Evidence of mast cell activation and leukotriene release after mannitol inhalation. *Eur. Respir. J.* **22**, 491–496 (2003).
32. Sverrild, A. *et al.* Airway responsiveness to mannitol in asthma is associated with chymase-positive mast cells and eosinophilic airway inflammation. *Clin. Exp. Allergy* **46**, 288–297 (2016).
33. George, S. A., Calhoun, P. J., Gourdie, R. G., Smyth, J. W. & Poelzing, S. TNFα modulates cardiac conduction by altering electrical coupling between myocytes. *Front. Physiol.* (2017) doi:10.3389/fphys.2017.00334.